Miniature, High Efficiency Transducers For Use IN Ultrasonic Flow Meters

Meghna Saikia
Marquette University

MINIATURE, HIGH EFFICIENCY TRANSDUCERS FOR USE IN ULTRASONIC FLOW METERS

by

Meghna Saikia

A Thesis submitted to the Faculty of the Graduate School,

Marquette University,

in partial Fulfillment of the Requirements for the

Degree of Master of Science

Milwaukee, Wisconsin

August 2013

ABSTRACT
MINIATURE, HIGH EFFICIENCY TRANSDUCERS FOR USE IN ULTRASONIC FLOW METERS

Meghna Saikia

Marquette University, 2013

This thesis is concerned with the development of a new type of miniature, high efficiency transducer for use in ultrasonic flow meters. The proposed transducer consists of a thin plate of a suitable piezoelectric material on which an inter-digital transducer is fabricated for the generation and detection of plate acoustic waves. When immersed in a fluid medium, this device can convert energy from plate acoustic waves (PAWs) into bulk acoustic waves (BAWs) and vice versa. It is shown that this mode coupling principle can be used to realize efficient transducers for use in ultrasonic flow meters. This transducer can be mounted flush with the walls of the pipe through which fluid is flowing, resulting in minimal disturbance of fluid flow. A prototype flow cell using these transducers has been designed and fabricated. The characteristics of this device have been measured over water flow rates varying from 0 to 7.5 liters per minute and found to be in good agreement with theory. Another attractive property of the new transducers is that they can be used to realize remotely read, passive, wireless flow meters. Details of methods that can be used to develop this wireless capability are described. The research carried out in this thesis has applications in several other areas such as ultrasonic nondestructive evaluation (NDE), noncontact or air coupled ultrasonics, and for developing wireless capability in a variety of other acoustic wave sensors.

TABLE OF CONTENTS

LIST OF TABLES

LIST OF FIGURES

Chapter 1

Introduction

The characteristics of acoustic waves propagating in a piezoelectric material which is in contact with a fluid medium were recently investigated in our laboratory [1]. Analysis showed that, under suitable conditions, a plate acoustic wave (PAW) traveling in the piezoelectric material can efficiently radiate a bulk acoustic wave (BAW) in the fluid. It was recognized that this effect can potentially be used to develop transducers for use in ultrasonic flow meters. This thesis started out with three main tasks in mind. (1) To carry out detailed experiments to see if the theoretical results predicted in reference [1] are true, that is, whether one can indeed convert energy effectively from plate acoustic waves into bulk acoustic waves. (2) In order to use this effect in a flow meter, then one needs to convert energy from PAW into BAW on one wall of the flow pipe, and back from BAW into PAW on the opposite wall of the pipe. So the second task was to investigate the coupling of energy back from BAW into PAW. (3) The third task was to use the results obtained from the first two tasks above to develop transducers suitable for use in ultrasonic flow meters. As will be seen from the work that follows, we were able to obtain very good results for all the above tasks. In particular, the work done in task number 3 has resulted in the development of miniature, high efficiency transducers which have many attractive properties for use in ultrasonic flow meters. While working on the above tasks, we recognized that our transducers have another interesting property,

namely that they can be used to realize flow meters with passive, wireless capability. So the scope of the thesis was expanded to include work on developing this capability.

This thesis is organized as follows. The first chapter provides a brief introduction to the subject of plate acoustic waves and discusses the prior theoretical work on the radiation of energy from plate acoustic waves in to bulk acoustic waves. The next chapter presents a detailed investigation of the coupling of energy between PAWs and BAWs. It is shown that, with proper design, one can convert energy efficiently from a PAW into a BAW and back from a BAW into a PAW. Chapter 3 discusses the use of this coupling to realize transducers for use in ultrasonic flow meters. It is shown that one can use this principle to develop miniature, high efficiency transducers that have many attractive properties. Chapter 4 is concerned with the use of our transducers to realize remotely read ultrasonic flow meters with wireless capability. The last chapter provides a summary of the work done in this thesis, the main results obtained, and suggestions for further work in this area.

1.1 Plate acoustic waves

Acoustic waves propagate in solid materials can be divided into three main types of waves. These are: bulk acoustic wave (BAWs), surface acoustic wave (SAWs) and plate acoustic wave (PAWs). Bulk acoustic waves are elastic waves propagating in unbounded elastic media. Surface acoustic waves are elastic waves propagating in a semi-infinite elastic medium. Plate acoustic waves are elastic waves propagating in plates of finite thickness. A given plate can support a number of plate wave modes depending on the value of the ratio h/λ, where h is the plate thickness and λ is the acoustic

wavelength [2-3]. A typical plot of the dispersion characteristics for the first few modes is shown in Fig. 1. This figure refers to waves propagating along the X-axis of a 128 degrees rotated Y cut lithium niobate plate [4]. The waves can be divided into three families of modes. These are the anti-symmetric (A), symmetric (S), and shear horizontal (SH) modes. The modes have these names for the following reasons. The particle displacement of the A mode is anti-symmetric about the mid plane of the plate. The particle displacement of the S mode are symmetric about the mid plane and the particle displacement of the SH mode is predominately in the shear horizontal direction. There are three all pass modes, A_0, SH_0, and S_0, that have no cut off frequency and propagate all the way down to $h/\lambda = 0$. From Fig. 1 it can be seen that if h/λ is less than 0.3, then only these three modes will propagate while the higher order modes will be cut off. This is the region that is of interest in this thesis.

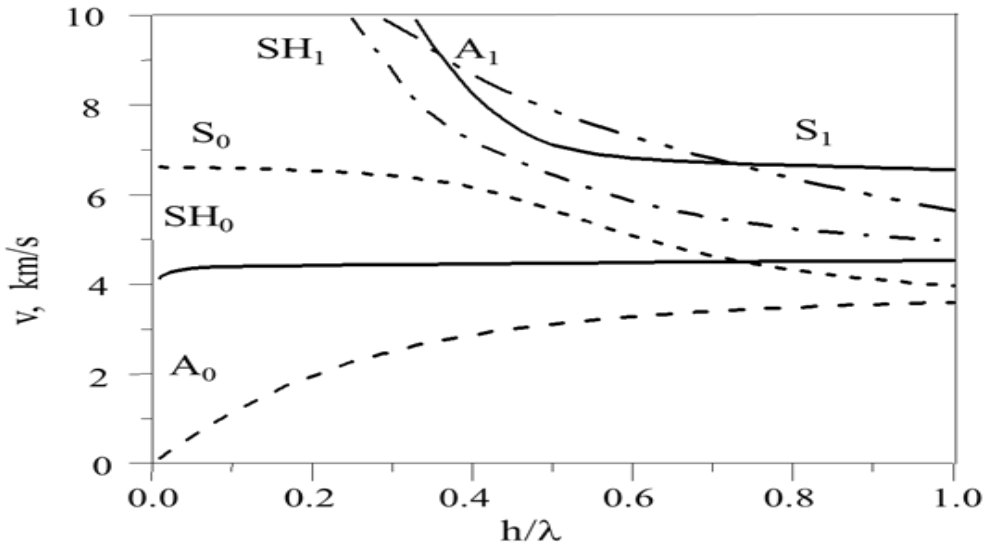

Figure 1: Dispersion characteristics for acoustic waves in a thin piezoelectric plate

1.2 Prior theoretical work

The problem that is of interest in this thesis is that of plate acoustic waves propagating in a piezoelectric material which is in contact with a fluid medium. The cross sectional view of the geometry of interest is shown in Fig. 2. It can be shown here that if v_p, velocity of plate acoustic wave in the substrate is less than v_B, velocity of bulk acoustic wave in the fluid, then the plate wave will not radiate any bulk wave in the fluid. On the other hand, if v_p is greater than v_B, then the plate wave will radiate a bulk wave in the fluid at an angle θ, where θ is given by the equation $\theta = \cos^{-1}(v_B/v_p)$.

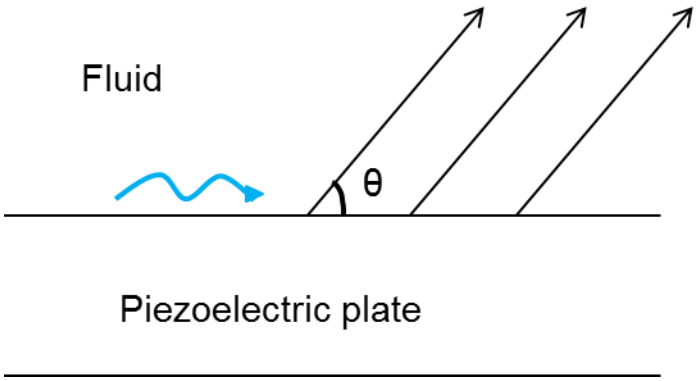

Figure 2: Cross-sectional view of a piezoelectric plate in contact with a fluid medium.

In order to determine as to which plate wave mode will be most efficient in radiating its energy in to a bulk wave in the fluid, we note that the particle displacement of the A_0 mode is predominantly normal to the plate surface, that of the S_0 mode is along the direction of propagation, and that of the SH_0 mode is in the shear horizontal direction. A non-viscous fluid can support only a compressional (longitudinal) wave. A plate wave

with particle displacement along the direction of propagation or in the shear horizontal direction cannot launch a compressional wave in the surrounding fluid. On the other hand, the component of particle displacement normal to the plate surface can generate longitudinal acoustic wave in the surrounding fluid. This indicates that the strongest coupling to bulk waves will be provided by the A_0 plate wave mode.

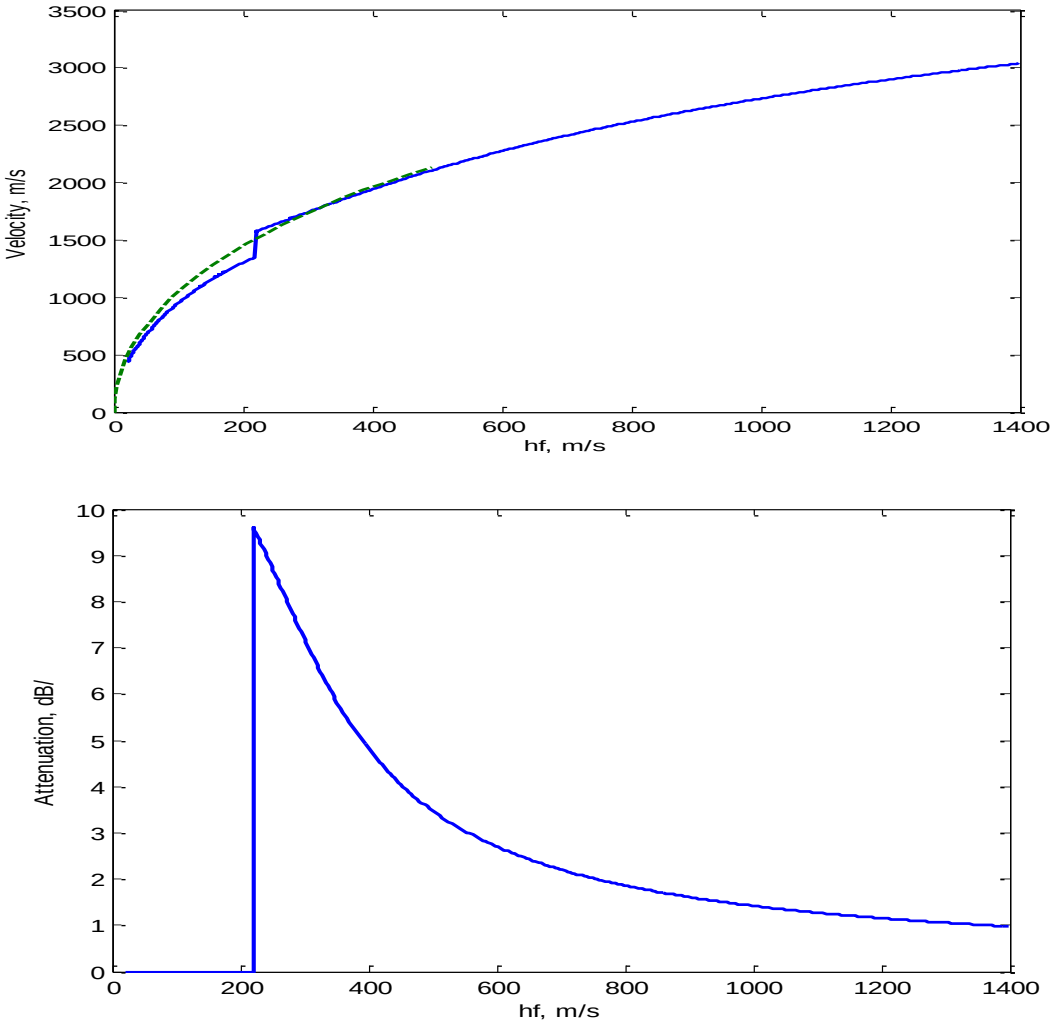

Figure 3: Velocity (a) and attenuation per wavelength (b) for A_0 plate waves propagating in a 128 Y-X lithium niobate plate in the presence of water contacting one of the plate surfaces. Dashed line in the velocity plot shows wave velocity in the absence of water loading [1].

In order to determine the effectiveness of converting PAW energy into BAW energy the problem of plate acoustic waves propagating in a piezoelectric substrate which is in contact with a fluid medium has been investigated. Details of the method used to analyze the generation of BAW by means of PAW have been described in [1]. Fig. 3 shows the results for the velocity and attenuation of the A_0 mode propagating in a 128 Y-X lithium niobate plate which is in contact with water on one of its surfaces. The horizontal axis here is the product hf where h is the plate thickness and f is the acoustic wave frequency. The velocity of bulk acoustic waves in water v_B is approximately 1500 m/s. In the absence of water loading, the velocity v_p of the A_0 wave becomes equal to v_B at $hf \approx 220$ m/s. The presence of water loading causes the velocity plot to have a discontinuity at this value of hf. For hf less than 220 m/s, v_p is less than v_B, whereas for hf greater than 220 m/s, v_p becomes greater than v_B. The plate wave will not radiate energy in the liquid, and hence not suffer any attenuation, when its velocity is less than v_B ($hf \leq 220$ m/s). On the other hand when v_p becomes greater than v_B ($hf \geq 220$ m/s), then the plate wave will radiate bulk wave in the fluid and therefore suffer attenuation. The attenuation coefficient is a measure of effectiveness of converting energy from PAW into BAW. Fig. 3 shows that values of attenuation coefficient greater than 2 dB per wavelength can be obtained for values of hf lying between 220 and 750 m/s. Values of attenuation coefficient greater than 2 dB per wavelength indicate that there is strong coupling between the A_0 plate wave mode and bulk acoustic wave propagating in water.

The theoretical results presented in Fig. 3 form the starting point for this thesis. The next chapter will carry out detailed investigation of the coupling of energy from plate waves in to bulk waves and back from bulk waves in to plate waves.

Chapter 2

Coupling of Energy between Plate Waves and Bulk Waves

The aim of this chapter is to investigate the coupling of energy between plate acoustic waves and bulk acoustic waves. In order to study this topic we designed and fabricated a suitable delay line for the generation and detection of plate acoustic waves. The electrode structure of the delay line can be seen in Fig. 4 . It consists of two identical interdigital transducers T_1 and T_2 with period p, aperture W, and number of finger pairs N.

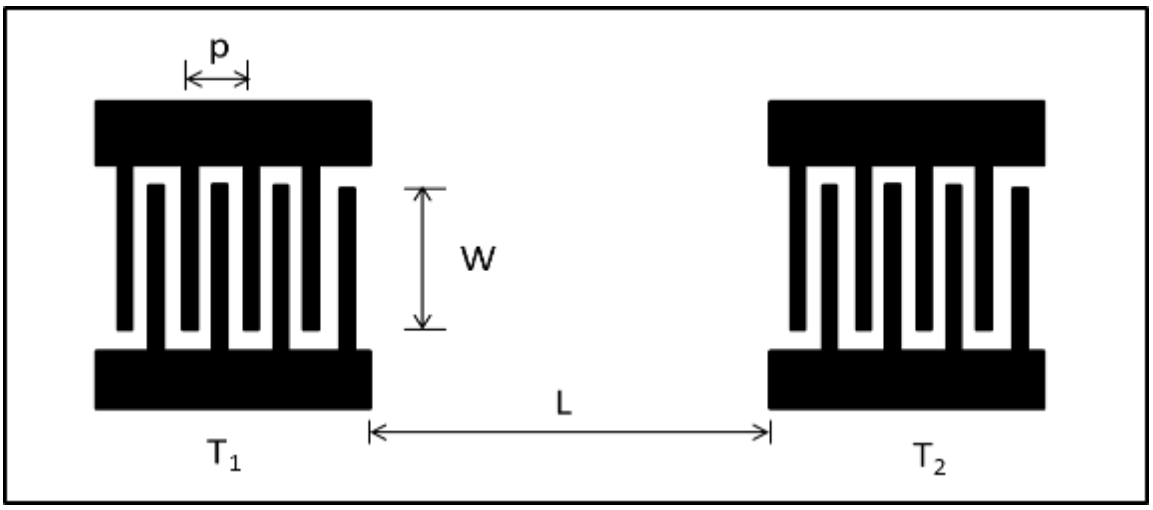

Figure 4: Electrode structure of a plate acoustic wave delay line.

It will be shown in chapter 3(a) that for flow meter applications, the optimum value of angle θ at which the bulk wave should be launched into the fluid is θ = 45°. So we designed the delay line to obtain this value of θ. Assuming that the fluid is water, the value of v_B is approximately 1500 m/s. Then from equation $\theta = \cos^{-1}(v_B/v_p)$, the velocity

of plate acoustic waves should be $v_p = (v_B/\cos\theta) = 2120$ m/s. Then Fig. 3 shows that to obtain $v_p = 2120$ m/s we should use hf = 500 m/s. The thickness of the lithium niobate plate available to us was h = 0.5 mm. So to operate at hf = 500 m/s, we get f = 1 MHz. Hence the period of the IDT was found as $p = v_p /f = 2.12$ mm. The number of finger pairs N in the IDT was decided based on two considerations. If the finger pairs are very few the IDT is very inefficient and if the finger pairs are too many then the IDT takes up a lot of space on the crystal. Therefore a moderate number was chosen as N = 4. The aperture W was also chosen based on two considerations: too small an aperture leads to significant diffraction spreading and if it is too large, then it occupies too much space on the crystal. Therefore W was chosen to be 10 mm, which is approximately 5λ. The spacing between the IDTs is a crucial factor as well. There needs to be enough space between the IDTs for the plate and bulk waves to interact with each other but also we are limited by the length of the crystal. The crystal length that was available to us was between 40 to 45 mm. Therefore the spacing between the IDTs was chosen to be 15 mm. So, the distance between the outer edges of the IDT will be approximately 31 mm.

The delay line was fabricated on a 128° rotated Y-cut lithium niobate substrate. Lithium niobate wafers of diameter 100 mm and thickness 0.5 mm were purchased from two different vendors. The wafers from Crystal Technology, Inc., had one surface polished optically flat and the other surface was lapped. The wafers from Precision Micro Optics were polished on both sides. The wafers were cut by outside companies to provide us rectangular plates of width 20 mm. The length of the plates varied between 40 to 45 mm.

The delay line was fabricated using thin film and photo lithographic techniques. The main steps in the fabrication process are shown in Fig. 5. First a thin film of aluminum approximately 200 nm thick was deposited on the crystal. This was done either in house (in Dr. Lee's lab) or obtained from outside vendor (LGA thin films, Santa Clara, CA). After Aluminum deposition the substrate was coated with a thin film of AZ 5214-E IR photo resist. This was done by spinning the wafer using Headway Research Inc., model PM101D photo resist spinner. The wafer was spun at 1500 rpm for one minute. The wafer was then soft baked in an oven for one minute at 100° C. The substrate was then exposed to ultra violet light through a photo mask. The photo mask pattern was designed using the software L-edit and then sent to Valley Type Design Inc, Fresno, CA for fabrication. The exposure time used was 8 minutes. The cross-sectional view of this step is shown in Fig. 5(d). Positive photo resist was used therefore the region exposed will dissolve in the photoresist. The photo resist pattern was then developed by dipping the plate in AZ 400K developer. The thin film of aluminum was then etched with 95% phosphoric acid + 5% nitric acid solution. The cross-sectional view of the wafer after this step is shown in Fig.5(e). Residual photo resist was then removed with Microposit remover 1165 stripper. The final IDT pattern is then obtained and this is shown in Fig. 5(f). The delay line was then mounted on a suitable test fixture. Electrical connections were made to the IDTs by means of thin gold or copper wires bonded to the transducer contact pads using a conducting silver paint.

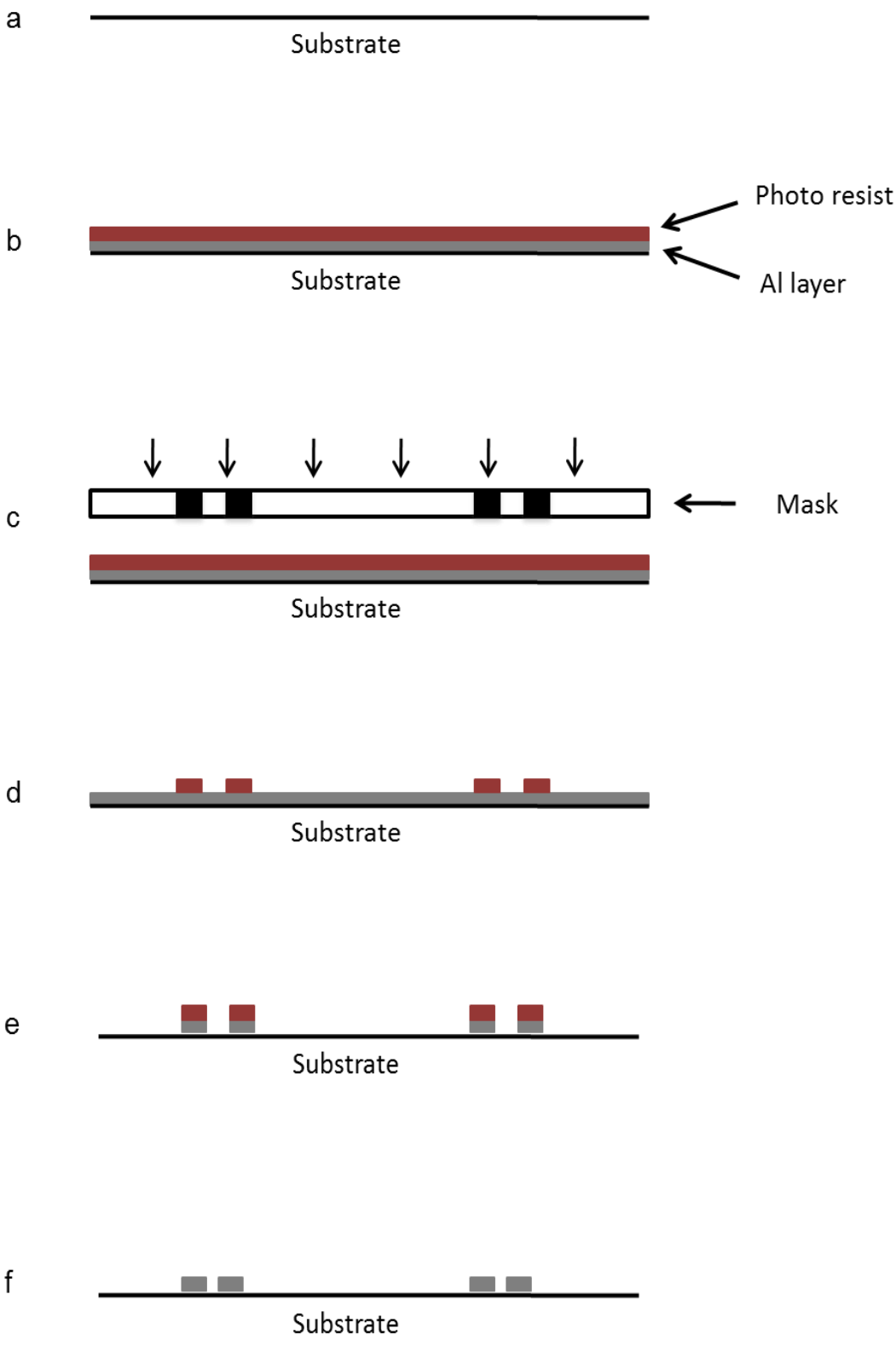

Figure 5: Basic steps in the lithographic process.

2.1 Electrical characteristics of delay line

The response of the delay line in the time domain can be studied by applying a radio frequency (r.f.) pulse to the input transducer. The block diagram of the experimental arrangement is shown in Fig. 6. A continuous wave is generated from the signal generator which is sent to the mixer. A rectangular pulse from the pulse generator is also sent to the mixer. The output of the mixer is the modulated signal which is sent to the amplifier. This is then sent to the input of the device for excitation of the transducer. The output of the amplifier is also sent to channel A of the oscilloscope. The output of the device goes to channel B of the oscilloscope. The response of one of our delay lines is shown in Fig. 7. Here the upper trace is the input rf pulse applied to the delay line, while the lower trace is the output of the device. The delayed acoustic output is the signal labeled b. The delayed acoustic signal has a trapezoidal envelope. It starts at a time delay of approximately 8 μs after the application of the input r.f. pulse and it reaches its maximum value at approximately 14 μs after the input pulse.. It can be seen that the device shows several unwanted (spurious) responses in addition to the desired response. The signal labeled a is the direct rf leakage, which occurs due to direct radiation of electromagnetic energy by the IDT, the connecting wires, etc. This signal can be reduced by the following methods. (1) Keeping the connecting wires as short as possible, (2) Minimizing resistance between the IDT contact pad and ground and (3) Shielding transducer T_1 from T_2. The signals appearing after the desired acoustic signal occur due to reflections from crystal edges, generation of other plate wave modes, etc. The

reflections from crystal edges can be reduced by putting suitable acoustic wave absorbers such as two-part epoxy on the crystal edges.

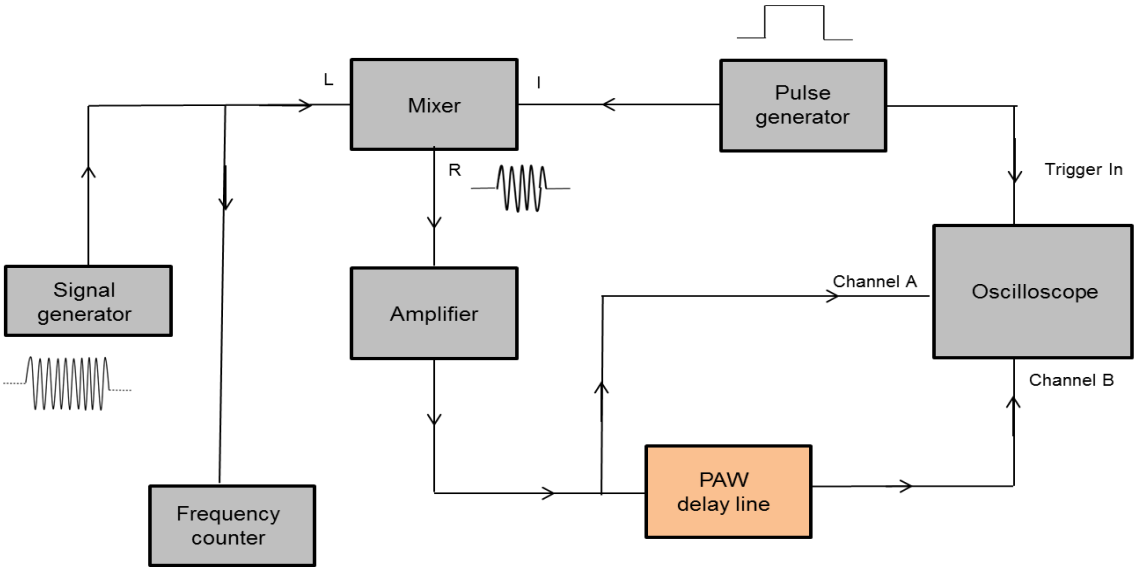

Figure 6: Block diagram of the experimental set up used for testing PAW delay line.

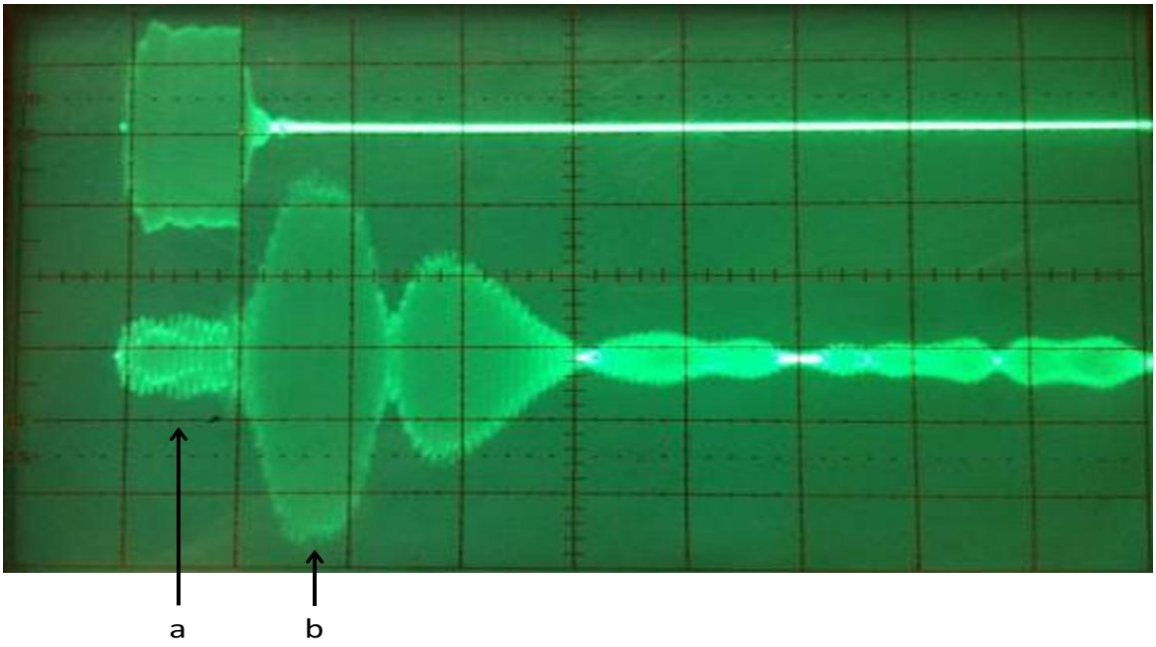

Figure 7: Pulse response of a PAW delay line. Upper trace: input 5 V/div, lower trace: output 20 mV/div. Horizontal axis = 10 μs/div.

For the first device made, the resonant frequency of the IDTs was found to be 0.94 MHz as compared to the design frequency of 1.0 MHz. So it seems that the actual value of v_p is somewhat lower than the theoretical value shown in Fig. 3. So we made a new photo mask with IDT period p = 2.014 mm. The resonant frequency of the new device was found to be 1.01MHz. Since a resonant frequency of exactly 1.0 MHz is not critical in our application, we have used either of these devices, that is, those with p = 2.12 mm and p = 2.014 mm in our work.

In order to calculate electrical characteristics of the delay line we first look at the characteristic of the individual IDTs. The electrical equivalent circuit of the IDT valid at frequencies in the vicinity of the fundamental resonant frequency is shown in Fig. 8. Here C_T is the electrostatic capacitance of the IDT, G_a is the acoustic conductance, and Ba is the acoustic susceptance. The equations to calculate these parameters are as follows [5].

$$C_T = C_O \; N \; W \tag{1}$$

where C_o is capacitance per pair per unit width of the IDT, N is the number of finger pairs, and W is the aperture of the IDT.

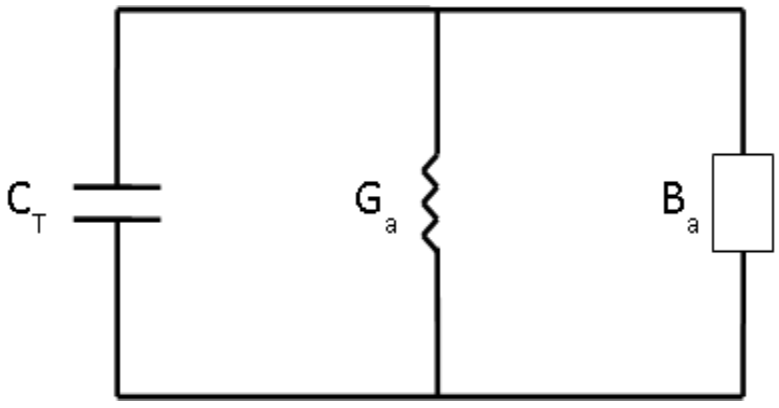

Figure 8: Shunt equivalent circuit of the IDT.

The radiation conductance G_a varies with frequency and is given by

$$G_a(f) = G_{ao}\left(\frac{\sin(N\pi\delta)}{N\pi\delta}\right)^2 \tag{2}$$

Here G_{a0} is the value of G_a at $f = f_0$ and δ is the fractional frequency deviation given by

$$\delta = \frac{f-f_o}{f_o} \tag{3}$$

Here f_0 is the resonant frequency of the IDT given by $f_0 = v/p$ and $\omega_0 = 2\pi f_0$

The value of G_{a0} can be calculated from the equation

$$G_{ao} = \frac{\omega_o C_T}{Q_e} \tag{4}$$

where electrical quality factor Q_e is given by

$$Q_e = \frac{\pi}{4K^2N} \tag{5}$$

Here K^2 is the electromechanical coupling coefficient. For 128 Y-X lithium niobate, the value of C_0 is 4.54 x 10^{-10} F/m [6] and the value of K^2 for the A_0 plate wave mode at hf = 500 m/s is 0.07 [7]. Using the above values for our IDTs, we get C_T = 18.15 pF and G_{a0} = 42.8μS. The acoustic susceptance B_a is also a function of frequency and is given by

$$B_a(f) = G_{ao}\left(\frac{\sin(2N\pi\delta) - 2N\pi\delta}{2(N\pi\delta)^2}\right) \tag{6}$$

The equation of $B_a(f)$ is of the form $(\sin(2x) - (2x))/(2x^2)$ where x is $N\pi\delta$. By Taylor series expansion of sin(2x), we get $\sin(2x) = [2x - (2x)^3/3! + (2x)^5/5! - \ldots.]$

Thus we get $B_a(f) = G_{ao}[(2x - (2x)^3/3! + (2x)^5/5! \ldots. - 2x) / (2x^2)] = G_{ao}[(1/6)x + \ldots]$

Substituting the value of x we get $B_a(f) = G_{ao}[(1/6) N\pi\delta +...]$.

Therefore, at the resonant frequency f_0, $B_a = 0$ from above. Therefore the equivalent circuit of the IDT valid at $f = f_0$ becomes as shown in Fig. 9.

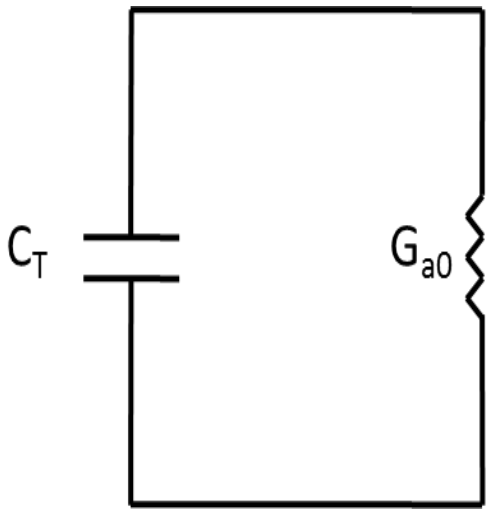

Figure 9: Equivalent circuit of the IDT valid at $f = f_0$.

The capacitance and conductance of the IDT were measured using an HP 4129A impedance analyzer. This analyzer has several measurement selections, one of which is to measure input capacitance C and conductance G of the device. This option was used in our measurements. The electrostatic capacitance C_T is a constant independent of frequency. In order to measure C_T we recognized at frequencies far below from resonance G_a and B_a vanish and the IDT acts like a simple capacitor of value C_T. So we determined C_T by measuring the value of IDT capacitance at a frequency of 10 kHz which is far below the value of f_0. The measured and calculated values of C_T and G_{ao} for the device having $f_0 = 1.01$ MHz are shown in Table 1 below.

Table 1: Measured and calculated values of IDT parameters.

Transducer	Capacitance CT, pF		Conductance G_{a0}, μS	
	Measured	Calculated	Measured	Calculated
T_1	27.2	18.15	58.0	42.8
T_2	25.4	18.15	47.0	42.8

The measured values of G_a versus frequency for the two IDTs are shown in Fig. 10 and Fig. 11. The general trend of measured values is in agreement with the theoretical plot. The theoretical plots of G are from Eq. (2). But there are significant ripples in the experimental plots. Also, the G_a versus frequency plots for the two IDTs are not identical. The theoretical plots shown in Fig. 10 and Fig. 11 are for the ideal case with no spurious signals. However in our device we have a number of spurious signals such as r.f. leakage, reflection form crystal edges etc. Under continuous wave (CW) conditions these spurious signals can combine with the direct acoustic signal to produce large peaks and values in the output. This can account for the large ripples that are seen in Fig. 10 and Fig. 11 below.

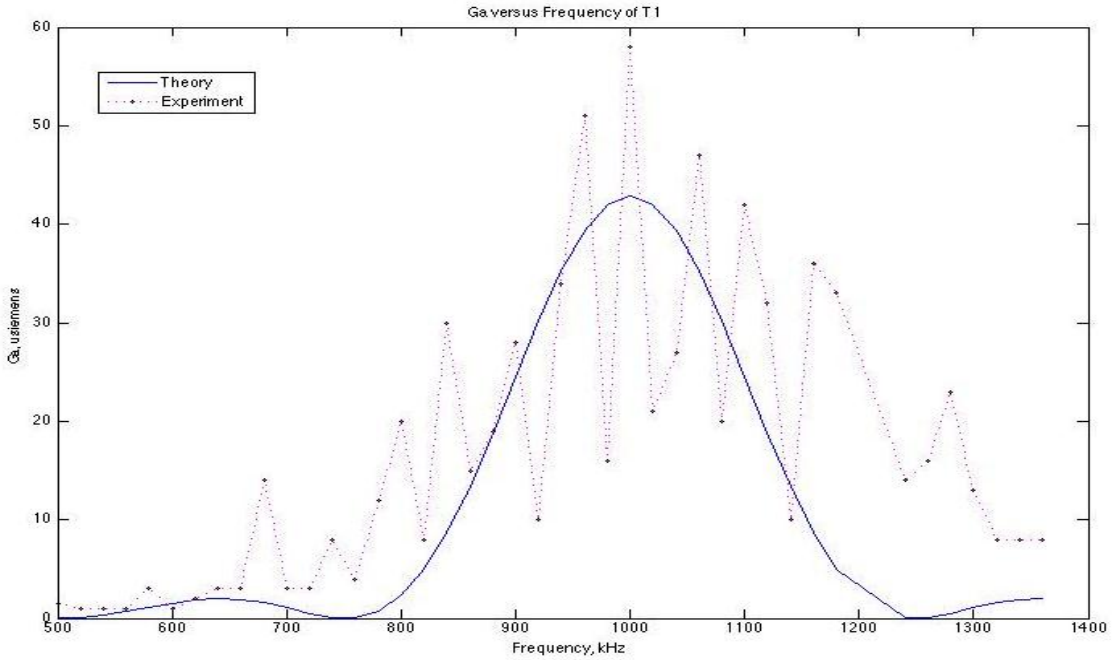

Figure 10: Plot of acoustic radiation conductance versus frequency for transducer $T_{1.}$

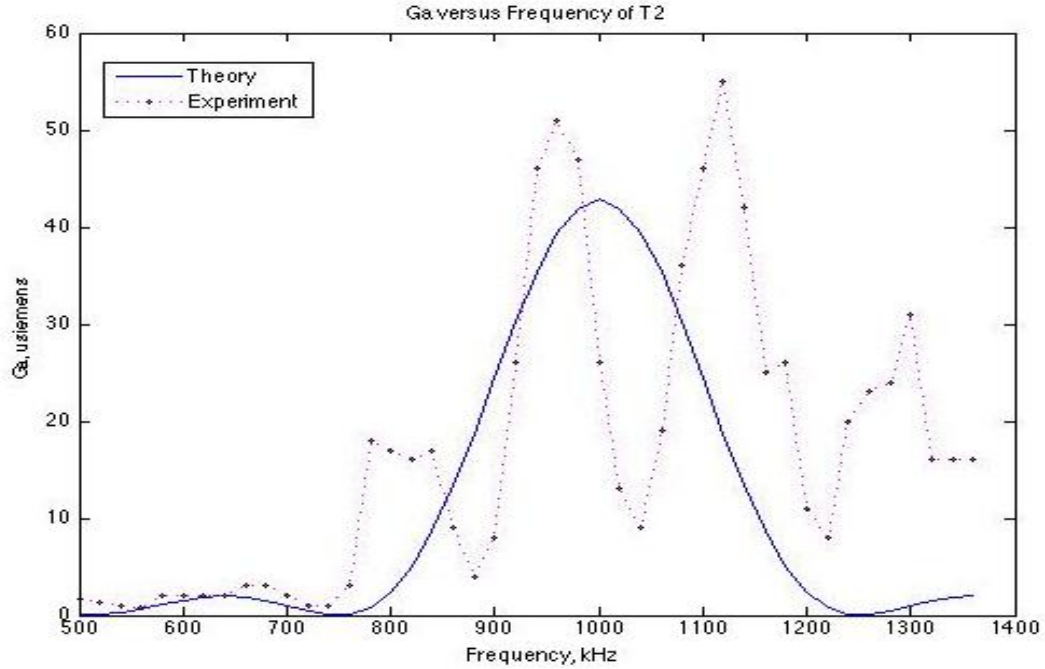

Figure 11: Plot of acoustic radiation conductance versus frequency for transducer $T_{2.}$

The equivalent circuit of the IDT can be used to calculate various parameters of the delay line such as output over input voltage ratios, insertion loss, etc. Consider the experimental set up shown in Fig. 12. Here the delay line is excited by a voltage source having internal resistance R_s. A load impedance Z_L is connected across the output of the delay line. To calculate the output to input voltage ratio and insertion loss we replace the IDTs with their equivalent circuits. The equivalent circuit for the generating transducer T_1 has already been discussed in Fig. 8. The equivalent circuit for the receiving transducer T_2 is slightly different and is shown in Fig. 13. Here the current source I_2 accounts for the conversion of acoustic energy into electrical energy. It can be shown that if the transducers are identical, then $I_2 = I_1$, where I_1 is the current flowing through the radiation conductance of T_1 [6,8]. Replacing the transducers by their appropriate equivalent circuits we get the following circuit shown in Fig. 14.

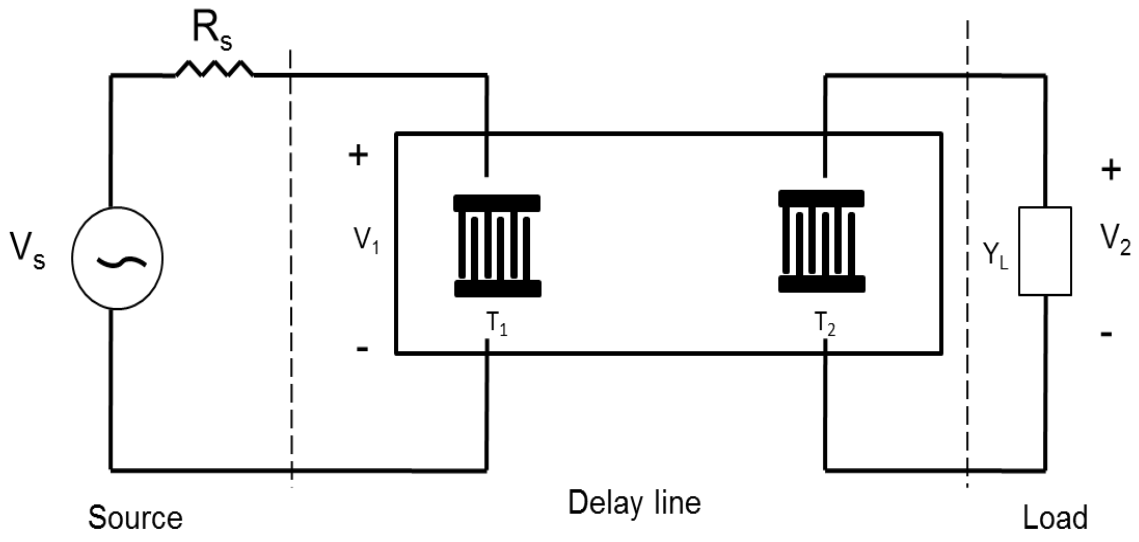

Figure 12: Circuit used to measure performance of delay line.

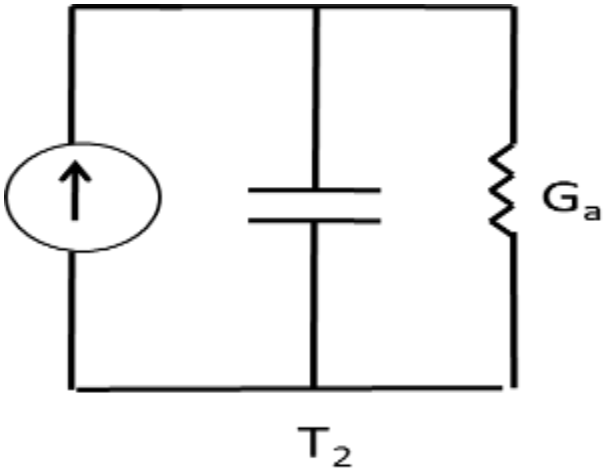

Figure 13: Equivalent circuit of receiving transducer T_2.

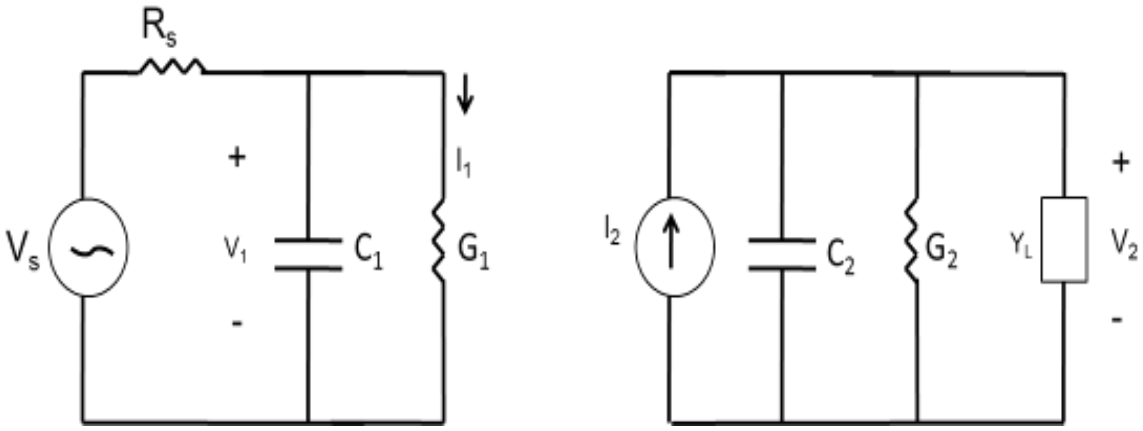

Figure 14: Circuit used to calculate output to input voltage ratio.

This figure can now be used for calculating the voltage ratios and insertion loss. The equations used are as follows.

$$I_1 = V_1 G_1 \quad (7)$$

$$V_2 = I_2 / Y_{total} = I_1 / Y_{total}, \text{ where} \quad (8)$$

$$Y_{total} = G_2 + j\omega C_2 + Y_L \quad (9)$$

Therefore we get

$$|V_2/V_1| = G_1/|Y_{total}| \quad (10)$$

In our work the voltage ratio $|V_2/V_1|$ was measured for two different cases. In the first case the output was connected to the oscilloscope by means of a coaxial cable about 1 m long. The capacitance of the cable was measured to be 88 pF. The input capacitance of the oscilloscope is 20 pF. So the total load on the transducer is a capacitance of value 108 pF. In the second case, the cable was terminated in its characteristic impedance of 50 Ω. In this case, the effective load on the transducer is a resistive load of 50 Ω. The measured and calculated values of V_2/V_1 for these two cases are shown in Table 2 below. The calculated values shown below are obtained using the calculated values of parameters shown in Table 1.

Table 2: Measured and calculated values of voltage ratio.

Load	Measured (V/V)	Calculated (S/S)
Capacitive load of 108 pF	3.6×10^{-2}	5.39×10^{-2}
Resistive load of 50 Ω	1.67×10^{-3}	2.13×10^{-3}

The insertion loss of the delay line is given by the equation

$$IL = 10\log_{10}(P_{max}/P_L)\ dB \quad (11)$$

where P_{max} = maximum power available from the source and P_L = power delivered to the load. To calculate the insertion loss it is convenient to replace the voltage source by its equivalent current source as shown in Fig. 15. Consider the case where the load on

transducer T_2 is a resistive load R_L. Then to calculate P_L, we do the following. From the input circuit we get

$$I_1 = I_s\, G_1/(G_s+G_1+jwC_1) \quad (12)$$

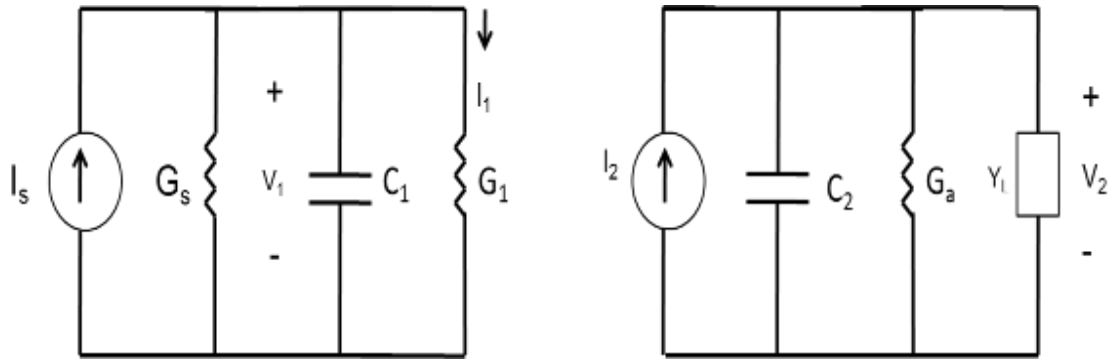

Figure 15: Circuit used to calculate insertion loss of delay line.

From the output circuit we get

$$V_2 = I_2/(G_2+G_L+jwC_2) \quad (13)$$

Here $I_1 = I_2$, therefore from Eq. (12) and Eq. (13), we get

$$V_2 = I_s\, G_1/((G_s+G_1+jwC_1)\,(G_2+G_L+jwC_2)) \quad (14)$$

$$P_L = |V_2|^2 G_L \quad (15)$$

$$= |I_s|^2\, G_1{}^2.\, G_L/\,(((G_1+G_s)^2 + (wC_1)^2)((G_2+G_L)^2+(wC_2)^2))$$

$$P_{max} = I_s{}^2/\,4G_s \quad (16)$$

Therefore,

$$P_{max}/P_L = (((G_1+G_s)^2+(wC_1)^2)((G_2+G_L)^2+(wC_2)^2))\,/\,4G_1{}^2G_s{}^2 \quad (17)$$

For insertion loss in a 50 Ohms system Rs = R_L = 50 Ω. Using the values for G_1, C_1, G_s etc. we get P_{max}/P_L = 30053.27. Therefore we get insertion loss IL = $10\log_{10}(P_{max}/P_L)$ dB = 44.7 dB.

The insertion loss was measured using the substitution method. The delay line was replaced by a variable attenuator and the attenuator setting was adjusted to get the same output as in the case of the delay line. The experimental arrangement is shown in Fig. 16 below. The measured value of insertion loss was found to be 51 dB, which is close to the calculated value of 44.7 dB.

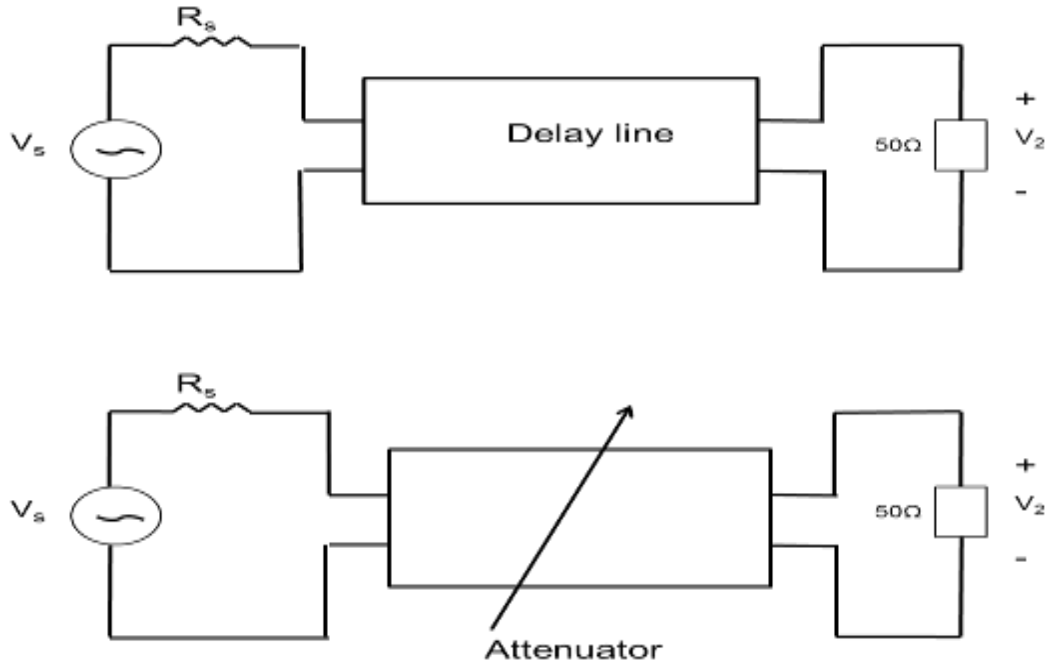

Figure 16: Experimental arrangements used to measure insertion loss.

We note that the measured values of IDT and delay line parameters differ somewhat from the calculated values. The reasons for these discrepancies are not investigated here, because they are outside the scope of this thesis. The function of plate wave delay line in this thesis is to generate and detect plate acoustic waves. The delay line designed here is adequate to serve that purpose.

2.2 Conversion of energy from plate waves into bulk waves

The theoretical analysis discussed in chapter 1 show that when a delay line is immersed in water, the plate wave will suffer attenuation due to radiation of energy in the form of bulk waves. To verify this we performed the following experiments. The first experiment performed is shown in Fig. 17(a). A part of propagation path of length d between the input and output transducers, was immersed in water. A suitable fixture was designed such that d could be varied by moving the delay line up and down. The photograph of the fixture is shown in Fig. 17(b). The insertion loss of the delay line was measured as d was varied from 0 to about 14 mm. The data is plotted in Fig. 18. It is seen that, as expected, the plate wave suffers attenuation as it comes in contact with water.

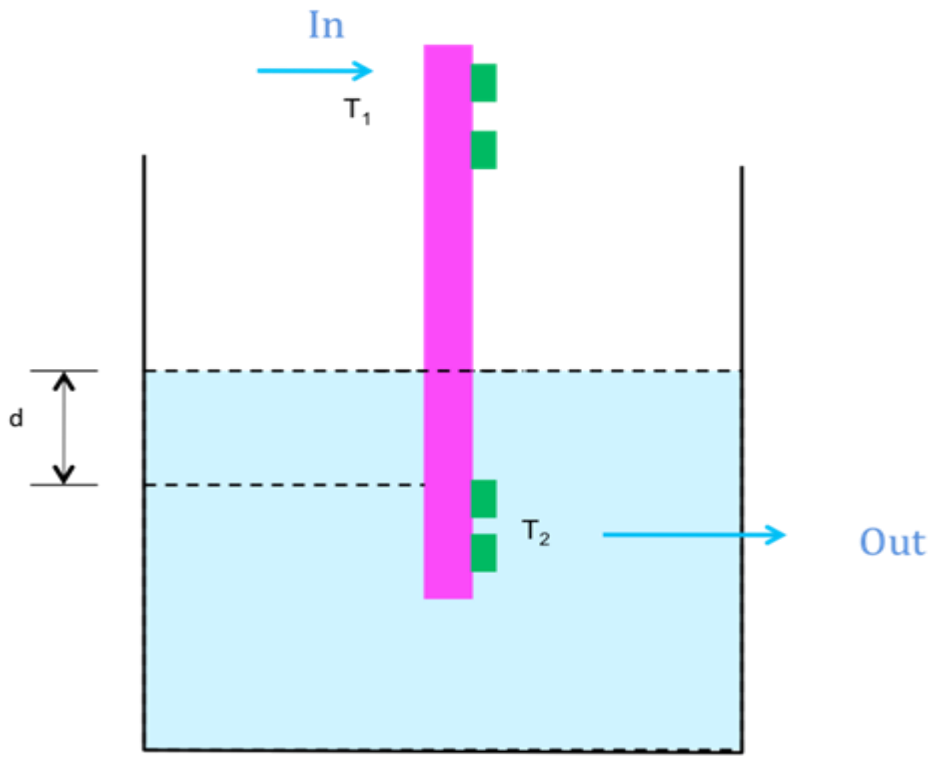

Figure 17(a): Experimental arrangement used to measure insertion loss of a PAW delay line as a function of d, length of propagation path immersed in water.

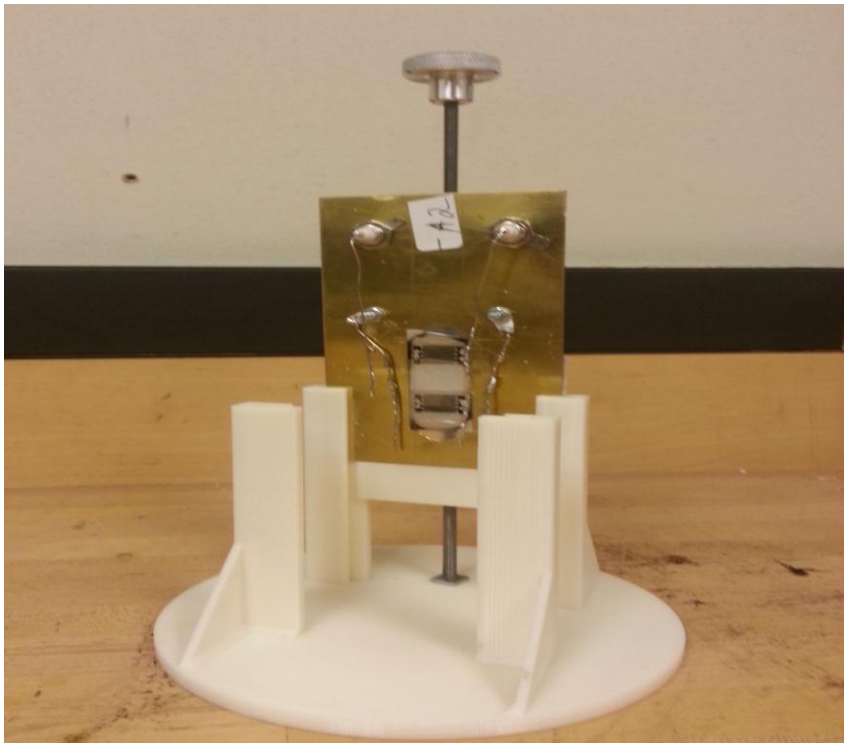

Figure 17(b): Photograph of experimental set up used to perform experiment shown in Fig. 17(a).

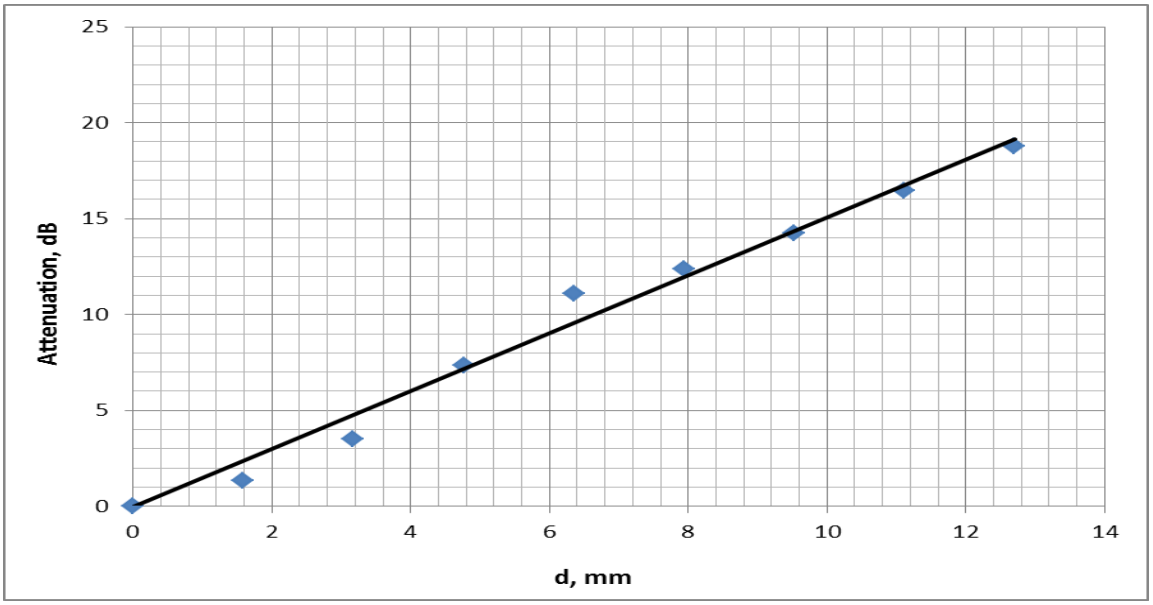

Figure 18: Plot of attenuation versus d, length of propagation path immersed in water.

From the slope of the plot in Fig. 18, the measured value of attenuation was found to be 1.68 dB/mm. The acoustic wavelength λ for our device is 2.12 mm. This means that the measured attenuation is 3.56 dB/λ. From Fig. 3 the calculated value of attenuation is 3.3 dB/λ. At first glance, it seemed that the measured and calculated values are in good agreement. However it was later recognized that the calculated value shown in Fig. 3 is for water only on one side of the device. In the actual experiment however it can be seen from Fig. 17(b) that water is on both sides of the device. We used de-ionized (DI) water having resistivity greater than 10^7 Ω-cm that prevented electrical shorting of the transducer immersed in water. For water on both sides, the calculated attenuation according to reference [1] is 6.6 dB/λ. So it seems that the experimental value is off from the calculated value by nearly a factor of two. More work is needed to investigate the reasons for this difference. Nevertheless, the experimentally observed attenuation is sufficiently large to indicate efficient conversion of energy from plate acoustic wave to bulk acoustic wave. To illustrate this point, suppose there was water only on 1 side of the device (this will be the case when the device is used in the flow meter) 1.68/2= 0.84 dB/mm. Then in a propagation path of say 20 mm, the plate wave will suffer attenuation greater than 16 dB. Therefore, we can write that 10 log (P_2/P_1) = 16 dB where P_1 is plate wave energy before attenuation P_2 is plate wave energy after attenuation. We get P_1/P_2 = 39.8, therefore P_2/P_1 = 0.025, which means P_2 = 0.025 P_1 or P_2 = 2.5% P_1. Assuming that this attenuation is due to radiation of bulk waves, we can thus say that more than 97 percent of plate wave energy will be converted into bulk wave energy.

In order to verify that plate wave energy is indeed converting into bulk acoustic wave energy, the following experiments were performed. The photograph of the fixture used is shown in Fig. 20 and the experimental set up is explained in Fig. 20. The fixture essentially consists of two tracks parallel to each other separated by a distance of 40 mm. The PAW delay line is mounted in one track and the BAW transducer in the other track. The bulk wave transducer used was a 1 MHz immersion transducer, model ICMF014 obtained from NDT Systems, Inc., Huntington Beach, CA. The diameter of the transducer was 12.5 mm. When input signal was applied to transducer T_1 of the PAW delay line, an output signal was observed on the BAW transducer as seen in Fig. 21(a). This shows that the plate acoustic wave is indeed generating a bulk acoustic wave. The bulk wave transducer was tilted to observe the output and it was noted that the output was maximum when the transducer surface was normal to the incoming bulk wave. The exact value of tilt angle θ shown in Fig. 20 could not be measured in this fixture. However, as expected, it was found that when the tilt angle was varied from its maximum value, the output decreased. This is shown in Fig. 21(b).

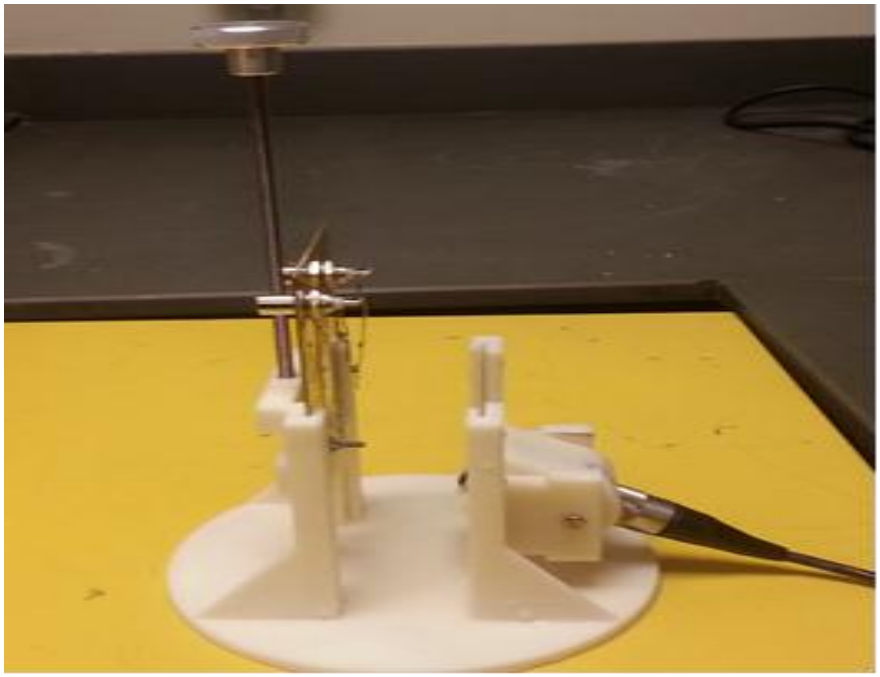

Figure 19: Photograph of fixture used to observe generation of bulk waves.

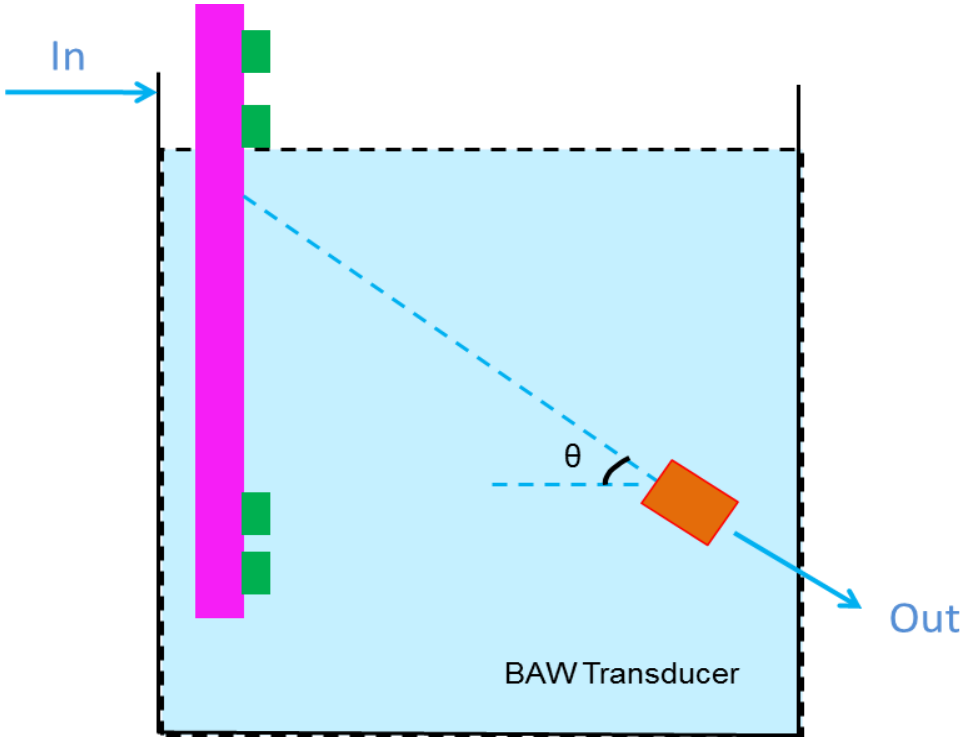

Figure 20: Set up of delay line and bulk acoustic wave transducer used to observe generation of bulk waves.

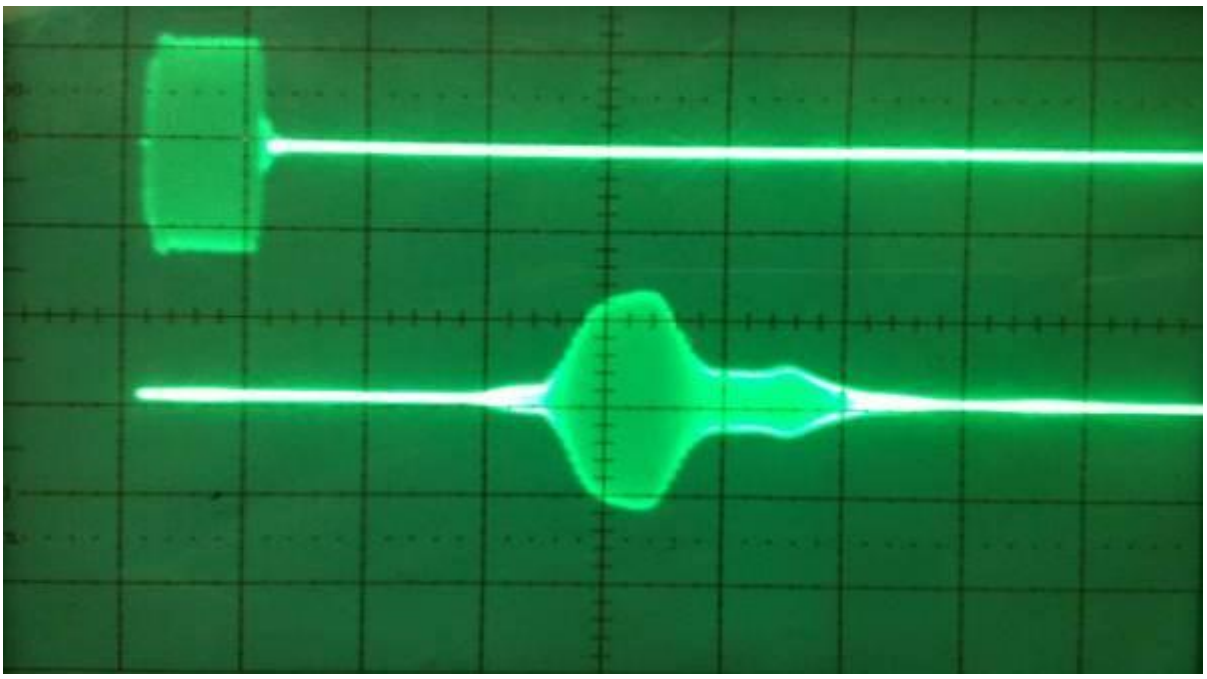

Figure 21(a): Oscilloscope picture of the output obtained at the bulk wave transducer. Upper trace: Input to applied to transducer T_1, 5 V/div; Lower trace: output of BAW transducer; 0.1 V/div; horizontal axis: 10 μs/div.

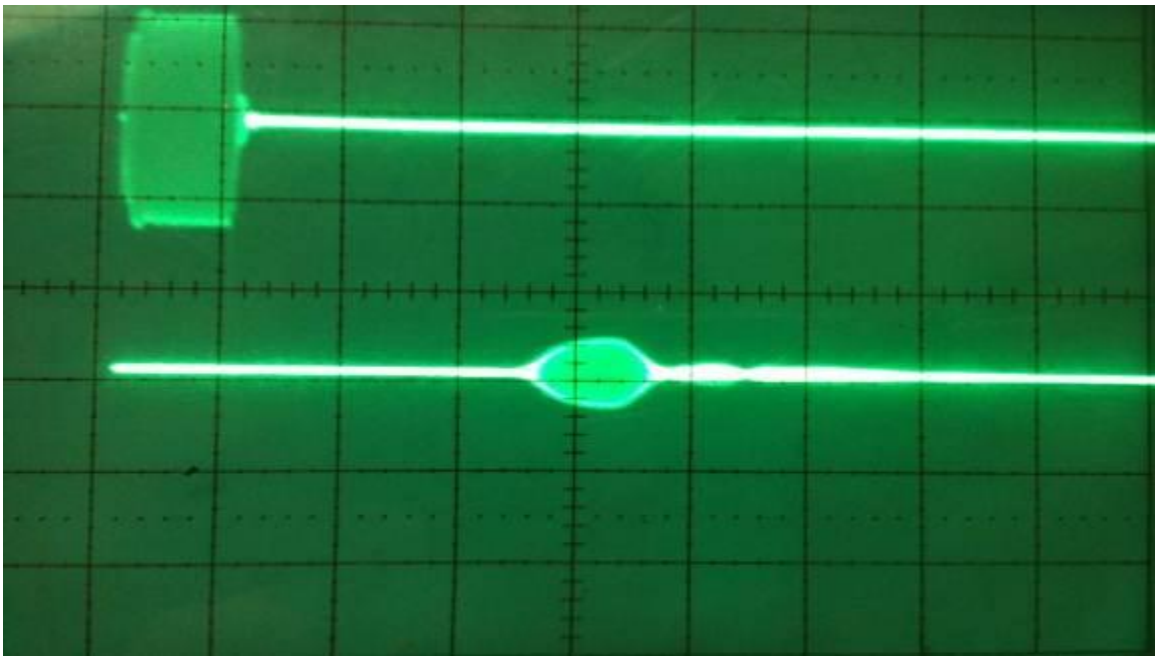

Figure 21(b): Oscilloscope picture when BAW transducer is tilted. Upper trace: Input to applied to transducer T_1; 5 V/div. Lower trace: output of BAW transducer; 0.1 V/div, horizontal axis: 5μs/div.

Next, an acoustic absorber was placed between the PAW delay line and the bulk wave transducer. It can be seen from Fig. 22(a) that the output has disappeared verifying that the bulk wave generated by the plate wave is no longer reaching the bulk wave transducer. When the absorber was removed the signal recovered as can be seen in Fig. 22(b). The above experiment confirms that the plate acoustic wave is indeed generating a bulk acoustic wave in the fluid.

Next, we wanted to observe how the amplitude of plate acoustic wave changes along the propagation path. For this purpose we proposed to perform the following experiment, the setup of which is shown in Fig. 23. We wanted to move the bulk wave transducer in the direction shown.

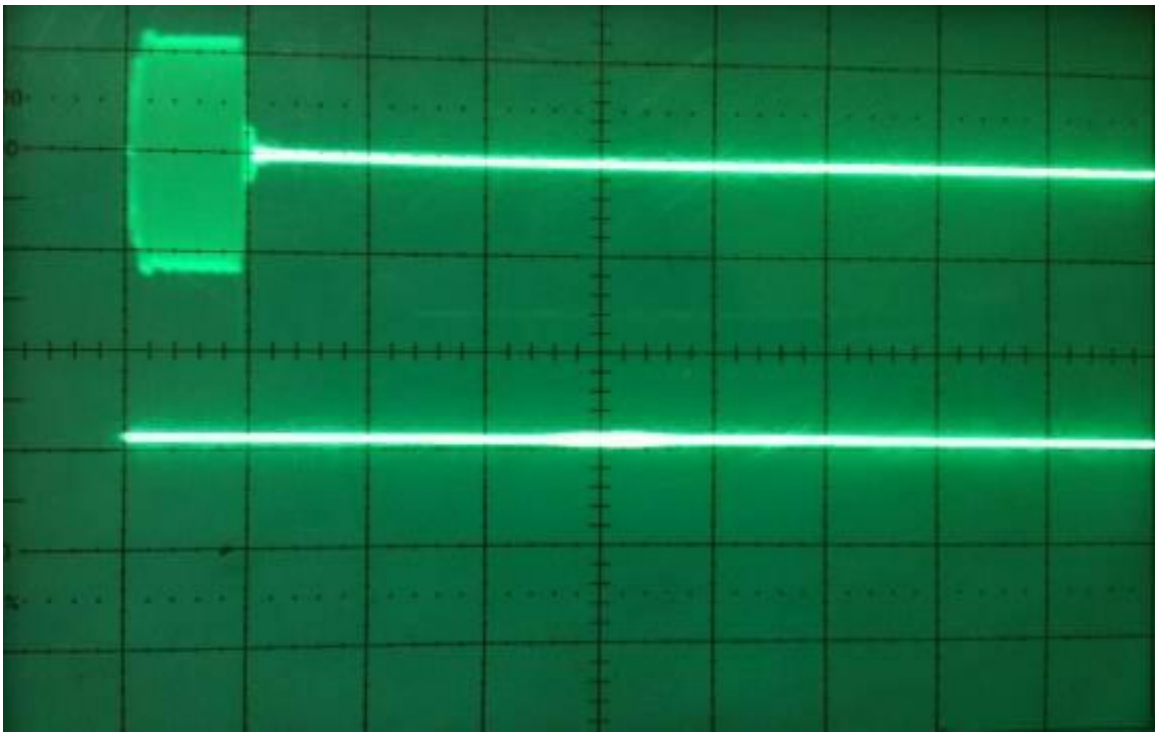

Figure 22(a): Oscilloscope picture when acoustic absorber is placed between bulk wave transducer and delay line. Upper trace: Input to applied to transducer T_1; 5 V/div. Lower trace: output of BAW transducer; 0.1 V/div, horizontal axis: 5μs/div.

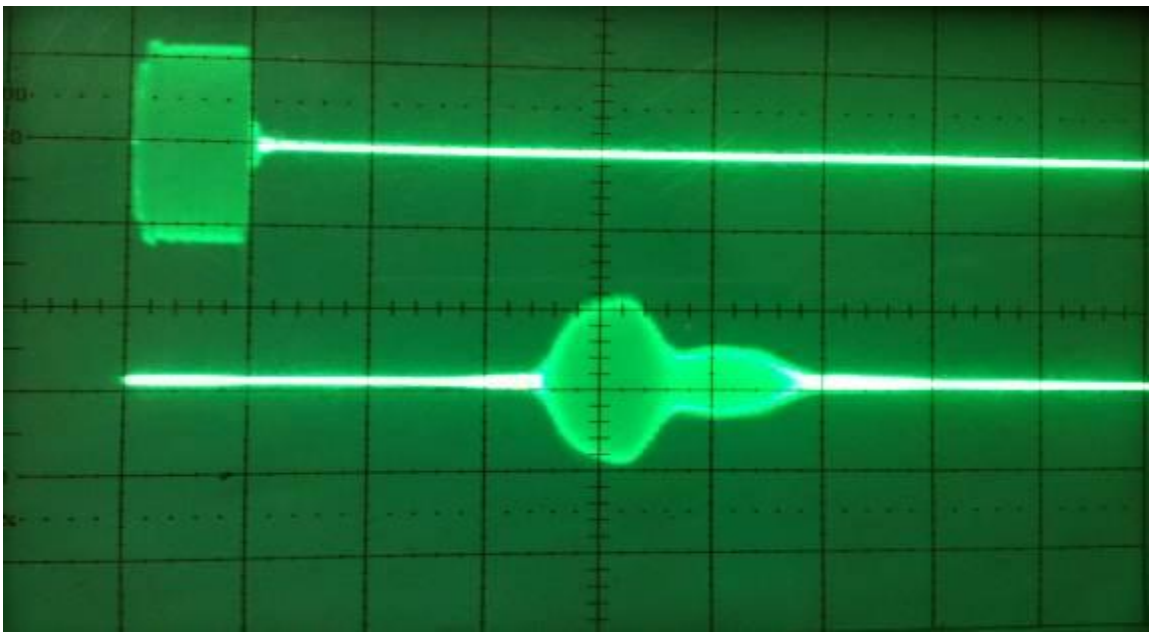

Figure 22(b): Oscilloscope picture when absorber is removed and output is recovered. Upper trace: Input to applied to transducer T_1; 5 V/div. Lower trace: output of BAW transducer; 0.1 V/div, horizontal axis: 5μs/div.

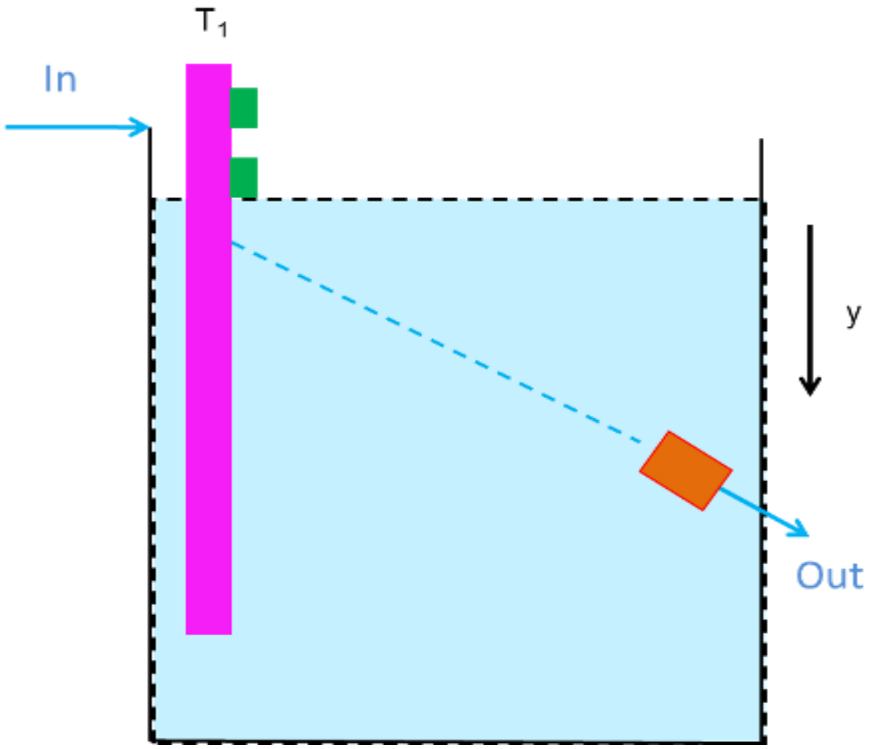

Figure 23: Proposed set up where bulk wave transducer moves in direction y.

However, it is difficult to move the BAW transducer because it is rather heavy, and also the tilt angle of the transducer could change as it is moved. On the other hand moving the plate wave delay line is relatively easy. Therefore an equivalent set up of the above experiment was performed. This was done by keeping the BAW transducer fixed and moving the PAW delay line and the level of water. This simulation is now discussed. Keeping the BAW transducer fixed at the bottom of the tank, the first measurement was obtained at the position shown in Fig. 24(a). In this case the BAW transducer receives the bulk wave generated from point A on the PAW delay line. Next, the delay line was moved up and the level of water in the tank was increased. In this case the BAW transducer receives the bulk wave generated from point B on the PAW delay line. This is shown in Fig. 24(b). In the third step, the delay line was moved still further up and water level was increased. In this case the BAW transducer receives the bulk wave generated from point C on the PAW delay line. Now since d_1 is less than d_2, and d_2 is less than d_3, the output in Fig. 24(a) will be greater than the one obtained in Fig. 24(b), and that in Fig. 24(b) will be greater than that in Fig. 24(c). The oscilloscope photos shown in Fig. 25(a) through (c) confirm this fact. Also as expected, the time delay increases as we move from Fig. 24(a) to Fig. 24(c) as expected. From Fig. 24(a) to Fig. 24(c) the path length traveled by the wave through water is the same but the path length traveled by the wave on the crystal will increase as we go from Fig. 24(a) to Fig. 24(c) therefore the time delay will increase. This is indeed what we observe in the pictures.

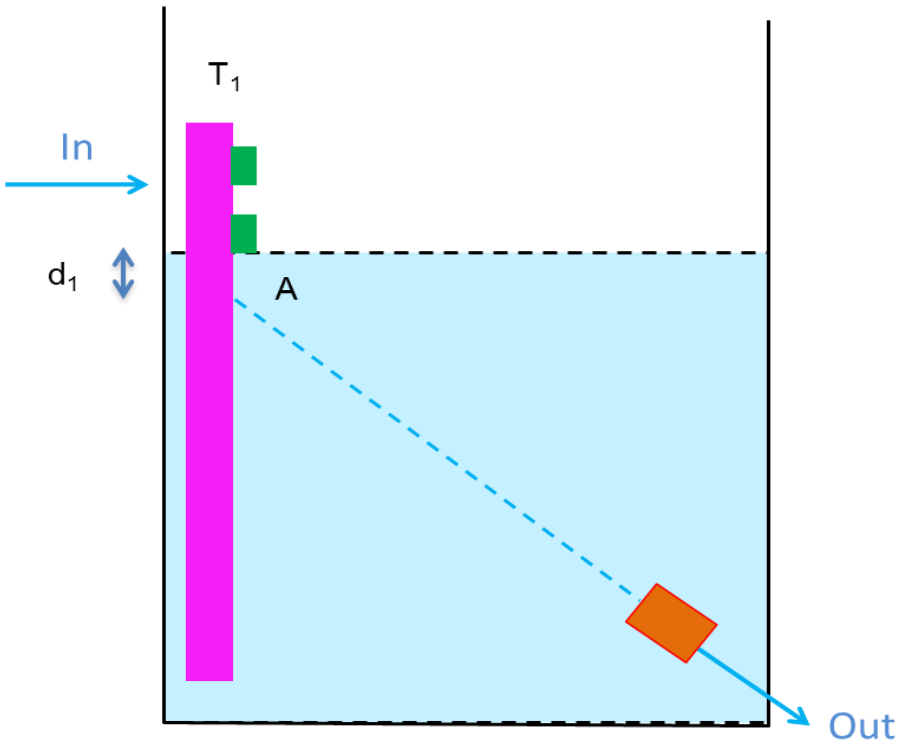

Figure 24(a): Simulation of set up where plate wave travels distance d_1.

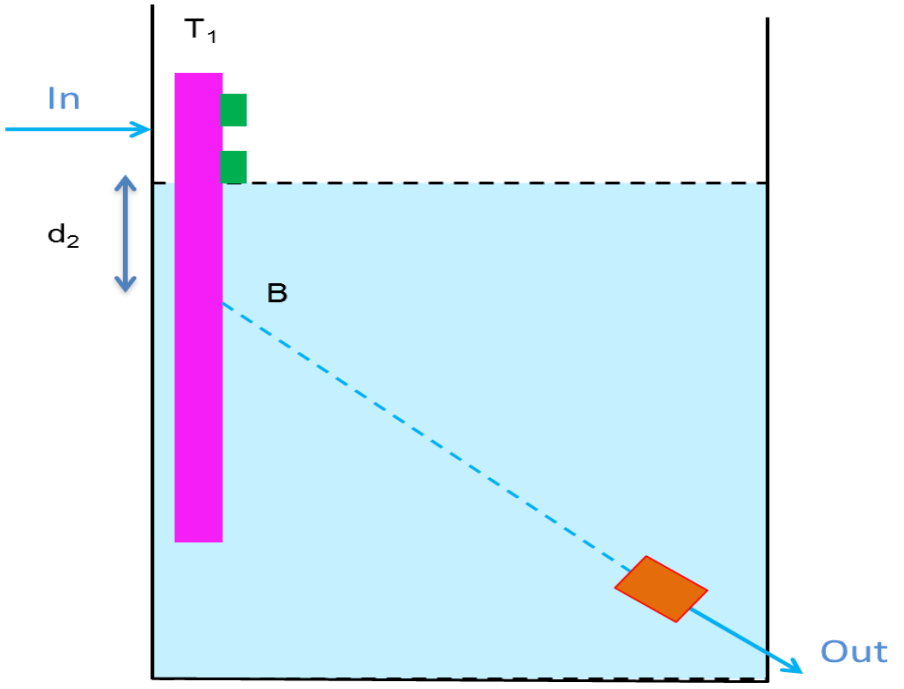

Figure 24(b): Simulation of set up where plate wave travels distance d_2.

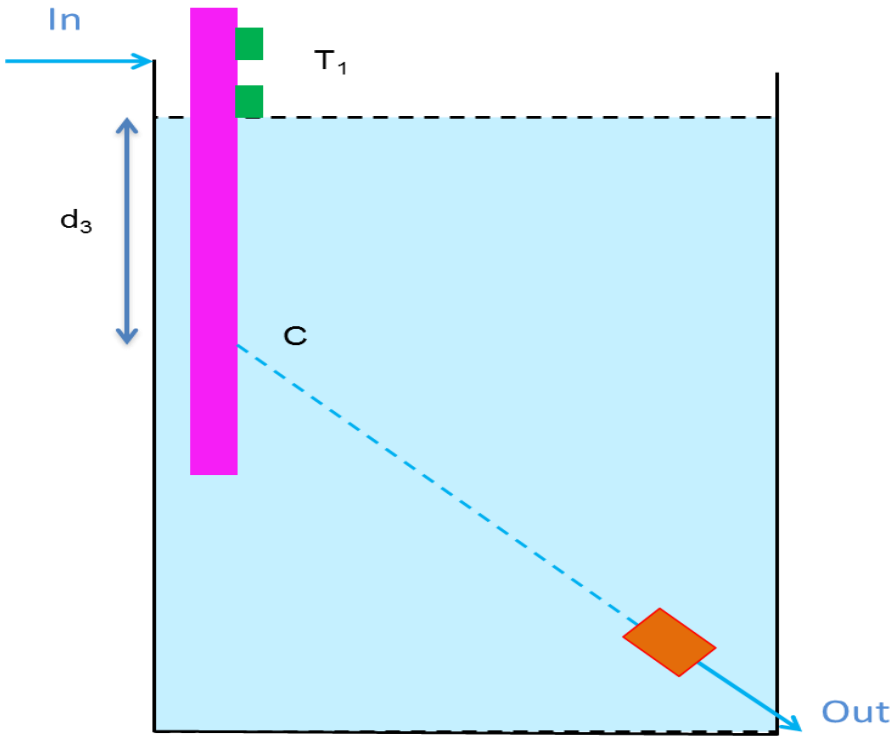

Figure 24(c): Simulation of set up where plate wave travels distance d_3.

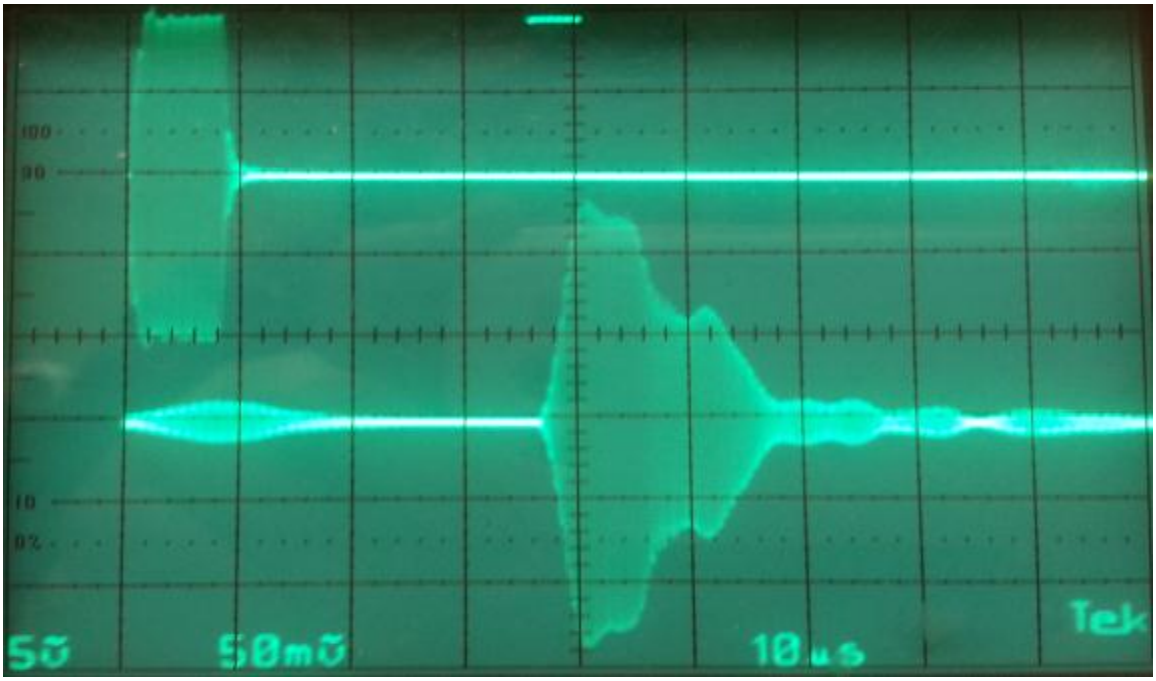

Figure 25(a): Oscilloscope picture of output obtained for set up shown in Fig. 24(a).

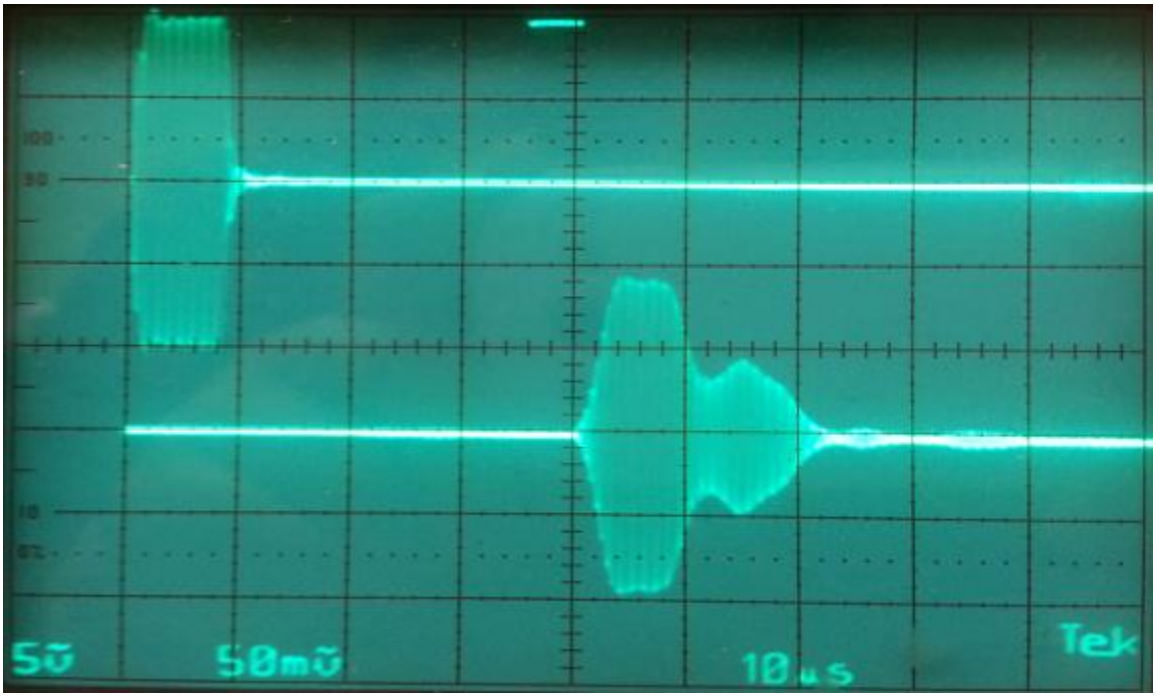

Figure 25(b): Oscilloscope picture of output obtained for set up shown in Fig. 24(b).

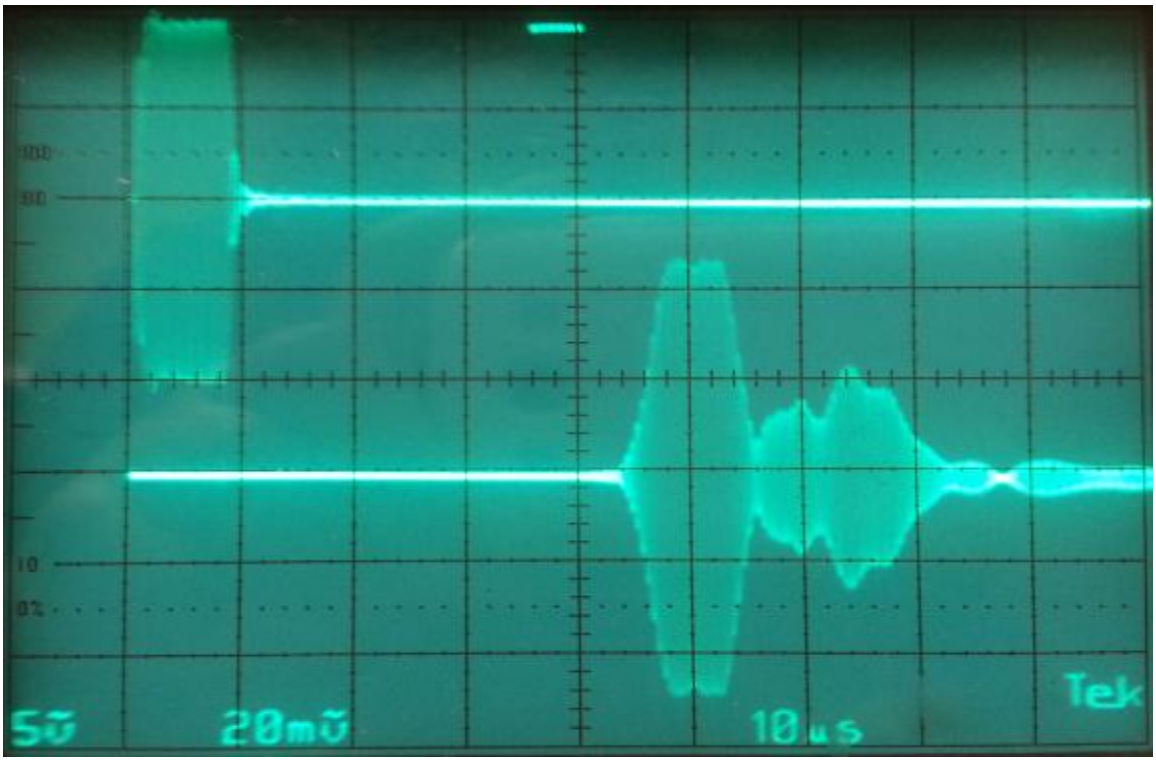

Figure 25(c): Oscilloscope picture of output obtained for set up shown in Fig. 24(c).

Table 3: Output of bulk wave transducer for different cases in Fig. 24

Case	Height of water in tank	Output, mV	Time delay, us
A	9.4 cm	140	36
B	10.3cm	90	40
C	11.3 cm	48	45

The output in case B is 3.84 dB below that in case A and the output in C is 5.46 dB below than that in case B. The difference in water height from A to B is 0.9 cm and that from B to C is 1 cm. From Fig. 18 the attenuation from A to B would have been 1.68 dB/mm x 9 mm = 15.12 dB and that from B to C is 1.68 dB/mm x 10 mm = 16.8 dB but the attenuation observed in table 3 is much less than these values. This is due to the diameter of the BAW transducer (12.5 mm) that was being used instead of a point receiver, therefore the output gets averaged.

2.3 Conversion of energy from bulk waves into plate waves

Now we turn our attention to the conversion of energy from bulk waves into plate waves. The photograph of the experimental arrangement that was used to observe this is shown in Fig. 19. Here input was applied to the BAW transducer and the output was taken from transducer T_1 of the PAW delay line. The oscilloscope output of this experiment is shown in Fig. 26. This confirms that the device is able to convert bulk acoustic wave back into plate acoustic wave.

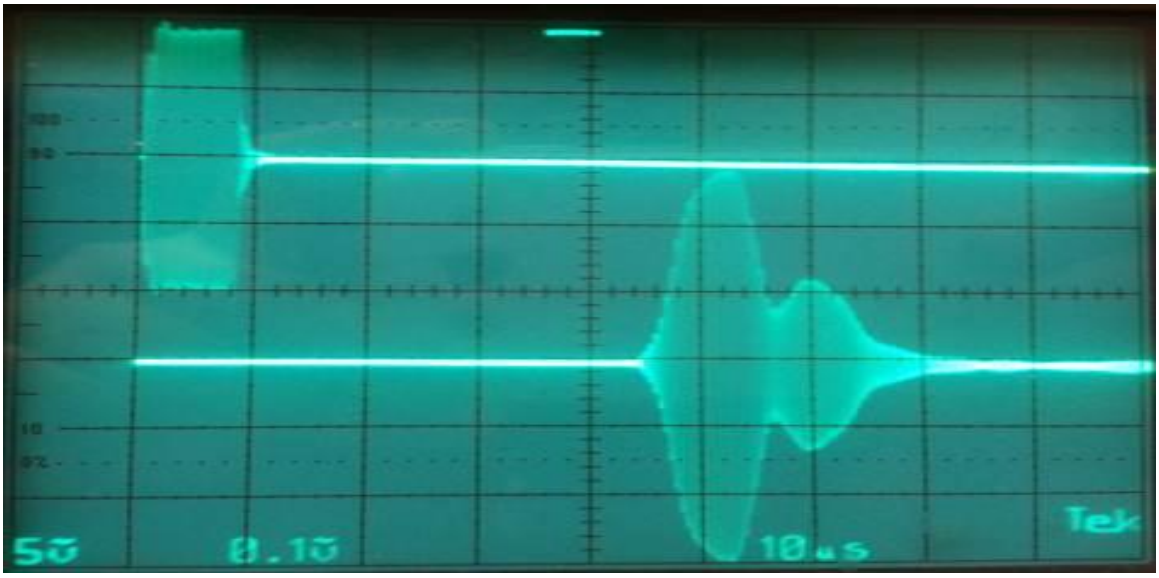

Figure 26: Oscilloscope photo showing generation of plate wave from bulk wave.

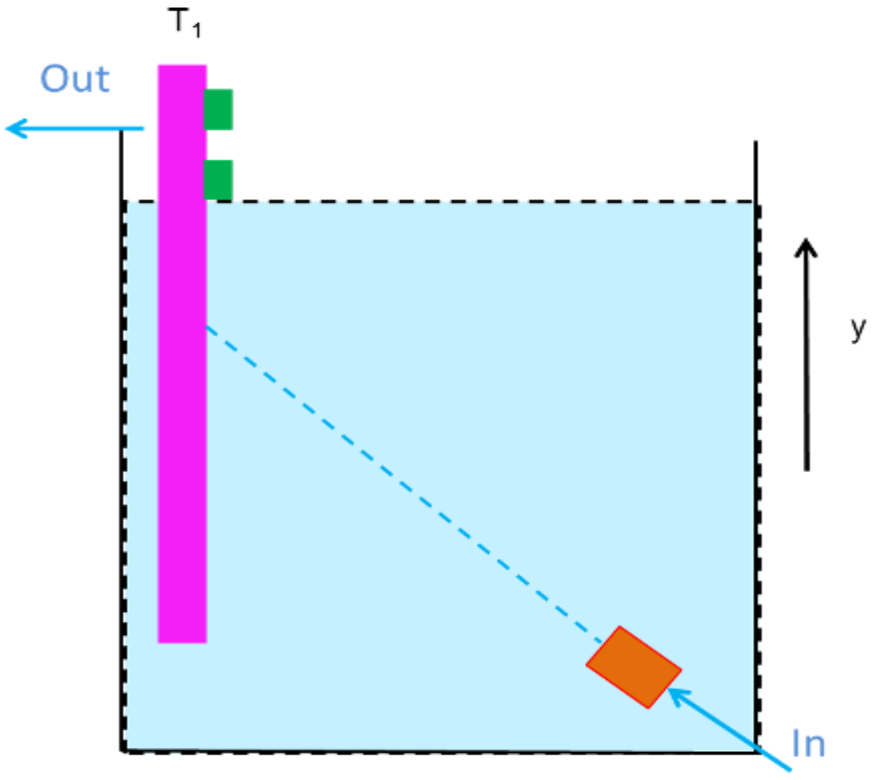

Figure 27: Proposed set up where bulk wave transducer moves in direction y.

Next, we wanted to observe as to how the amplitude of the generated plate wave varies as it travels along the surface of the crystal. For this purpose we wanted to perform an experiment in which the BAW transducer is moved up in the direction y as shown in Fig. 27. However, as mentioned previously moving the BAW transducer is difficult. Instead am equivalent set up of the experiment was performed. This was done by keeping both the BAW transducer and the PAW delay line fixed and varying the water level. Let us now consider the cases shown in Fig. 28 (a) through (c). In Fig. 28(a), the plate wave is generated and travels distance d_1 in water before reaching the output transducer T_1. In Fig. 28(b), the plate wave travels distance d_2 before it reaches the output transducer T_1, while in Fig. 28(c), the plate acoustic wave has to travel distance d_3 before reaching the output transducer T_1.

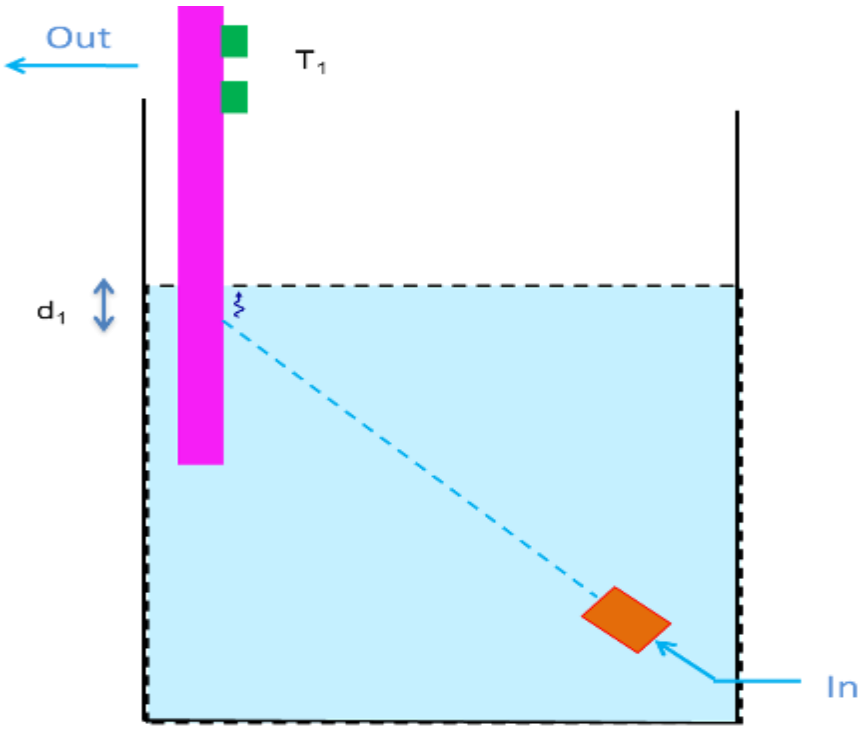

Figure 28(a): Simulation of set up where plate wave travels distance d_1.

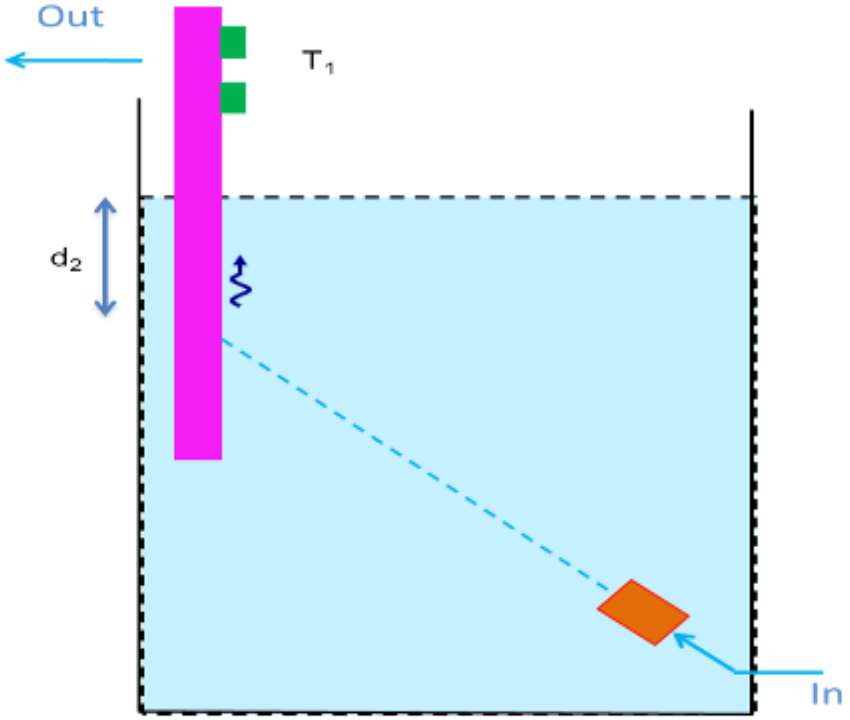

Figure 28(b): Simulation of set up where plate wave travels distance d_2.

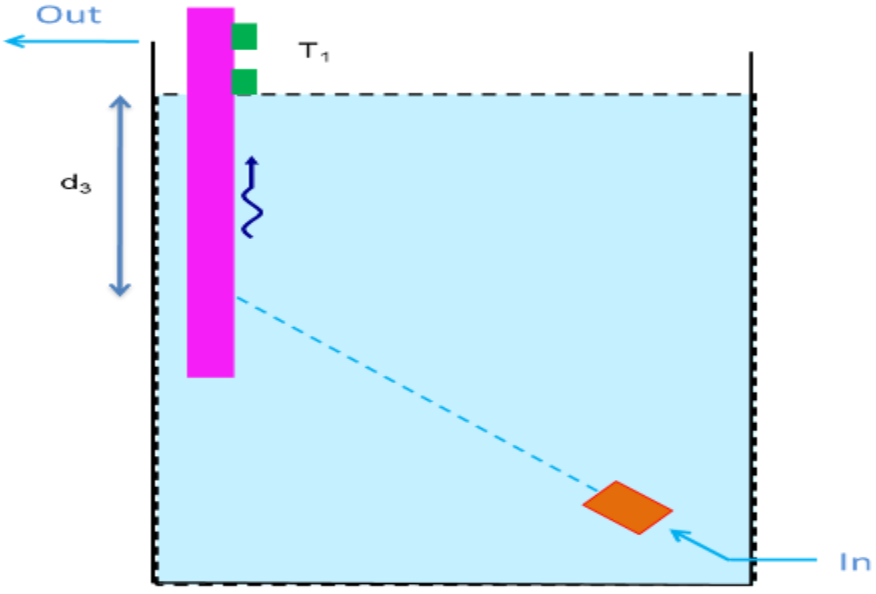

Figure 28(c): Simulation of set up where plate wave travels distance d_3.

The outputs for these three cases are shown in Fig. 29(a) through (c). We observe that the output for Fig. 28(b) is lower than that for 28(a) and that for Fig. 28(c) is further lower than that for 28(b). We wonder why does this happen? The explanation for this is as follows. In case of Fig. 28(b), as the plate wave travels through distance d_2, a part of it also gets converted into bulk waves, therefore some energy of plate wave is radiated into bulk waves before it reaches T_1 of the delay line. Therefore the output in Fig. 29(b) is less than that in Fig. 29(a). In case of Fig. 28(c), the plate acoustic wave has to travel a distance of d_3 where d_3 is greater than d_2 and hence more plate acoustic energy gets converted into bulk waves and therefore the output in case of Fig. 29(c) is even lower than that Fig. 29(b).

The oscilloscope photos shown below confirm that measurement. Unlike in Fig. 25 (a,b,c, - plate acoustic to bulk waves), the time delay stays constant as the water level changes. This is because the distance traveled by the wave in water and on the crystal remains the same in all three cases.

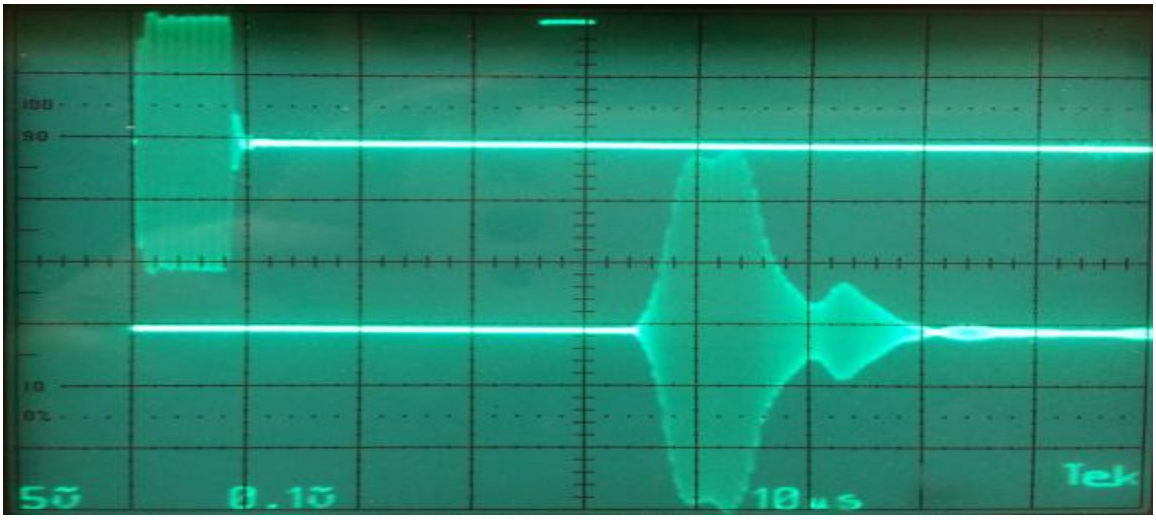

Figure 29(a): Oscilloscope picture of output obtained for set up shown in Fig. 28(a).

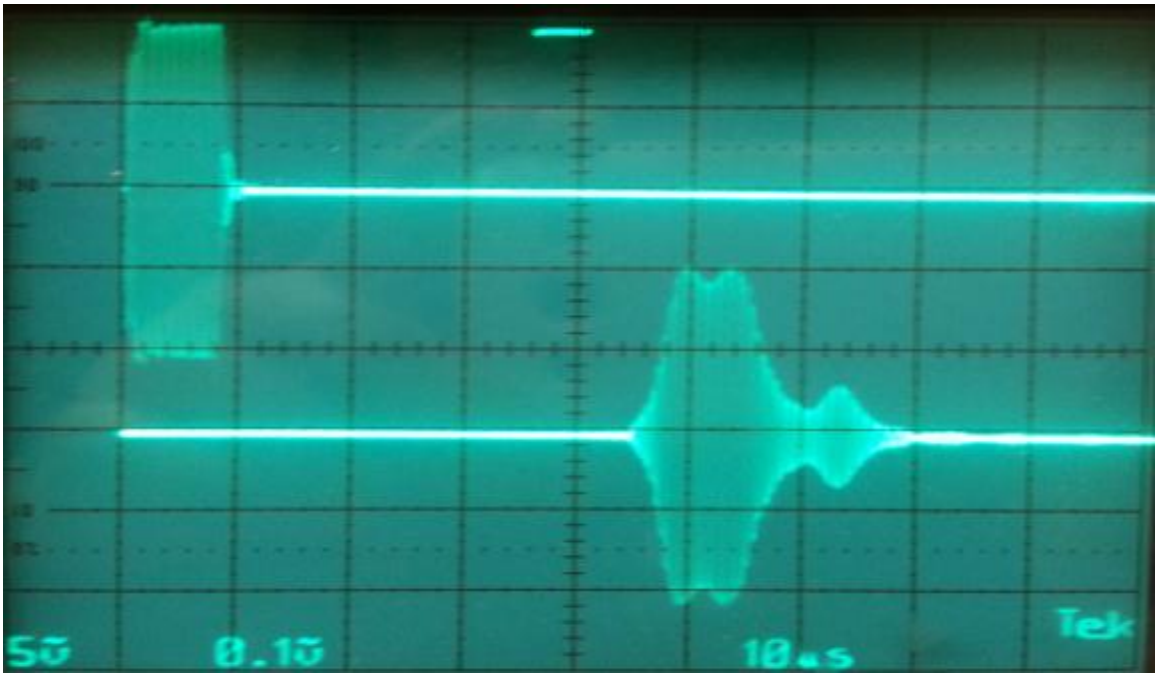

Figure 29(b): Oscilloscope picture of output obtained for set up shown in Fig. 28(b).

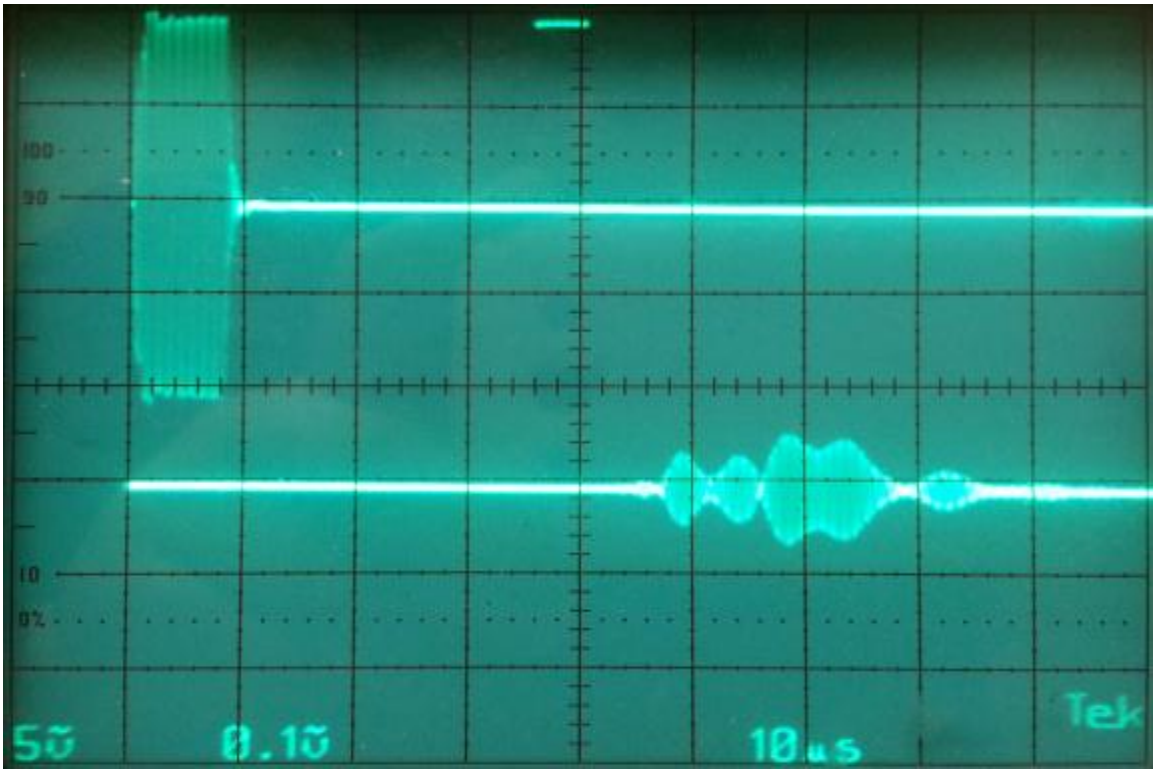

Figure 29(c): Oscilloscope picture of output obtained for set up shown in Fig. 28(c).

Table 4: Output of delay line for different cases in Fig. 28

Height of water in tank	Output, mV
10.3	300
10.7	200
11.4	20

The work described in this chapter shows that the mode coupling principle can be used to convert energy efficiently from plate wave into bulk wave and vice versa. This indicates that this principle can be used to realize efficient transducer for use in ultrasonic flow meters. This is topic that is investigated in the next chapter.

Chapter 3

Development of Transducers for Use in Ultrasonic Flow Meters

The aim of this chapter is to use the results obtained in the previous chapter to develop transducers for use in ultrasonic flow meter. The chapter will begin with a brief introduction to the subject of ultrasonic flow meters. An ultrasonic flow meter is an instrument that uses ultrasonic waves to measure flow rate of fluids [9]. It has no moving parts, does not produce any pressure loss, and provides maintenance free operation – important advantages over conventional mechanical meters such as positive displacement meters (PDs), turbines, vortex meters, etc. Moreover, ultrasonic flow meters are invariably more accurate and reliable than many traditional or non-ultrasonic methods such as venturi tubes, orifice plates, pitot tubes, turbine, magnetic, coriolis, thermal or target meters, etc [10-12]. Due to these advantages, ultrasonic flow meters are finding increasing use in various applications. Some of the conventional non-ultrasonic flow meters are described below.

There are various conventional non – ultrasonic flow meters available to measure flow. Some of the most common ones are turbine-type meters, thermal anemometer and magnetic flow meter. The turbine –type meter consists of rotating-wheel that is used to measure water flow in rivers and streams. Wheel motion proportional to flow rate is sensed by reluctance –type pick up coil. A permanent magnet is encased in the rotor body, and each time a wheel blade passes the pole of the coil, a change in the

permeability of the magnetic circuit produces a voltage pulse at the output terminal. Frequency converters are also available that convert flow meter pulses to a proportional d.c. output permitting use of simple meters for indication. Fig. 30 (a) shows a typical turbine-type flow meter [13].

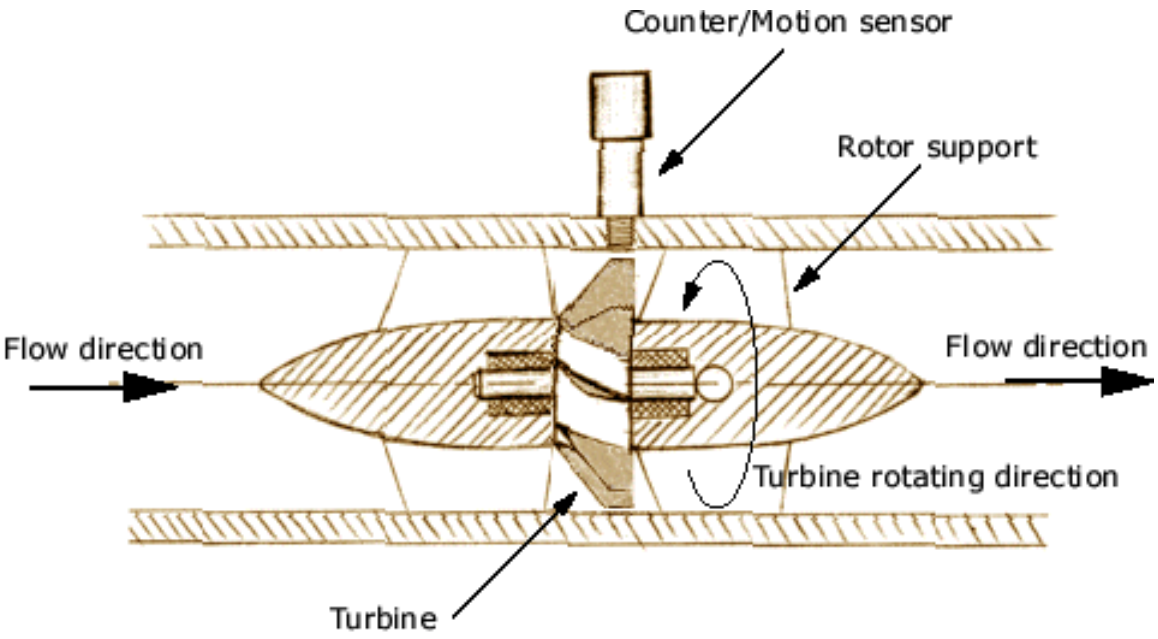

Figure 30 (a): Turbine type flow meter [14].

When an electrically heated wire is placed in a flowing stream, heat will be transferred between the two, depending on a number of factors, including flow rate. This is popularly known as the hot-wire anemometer. The instrument consists of a short length of fine wire stretched between two supports. Two methods are used to measure flow. The first technique consists of passing a constant current through the sensing wire. Variation in flow results in changed wire temperature and thus changed wire resistance, which thereby becomes a measure of flow. The second technique uses a servo system to maintain wire resistance, hence wire temperature. In this case, a change in the servo

system is then interpreted as a flow analog. The two methods are called constant-current and constant-temperature, respectively. When hot wire is placed in a flowing stream, heat will be transferred from the wire, primarily by convention. Radiation and conduction are normally negligible. Fig. 30(b) shows a typical hot wire anemometer [13].

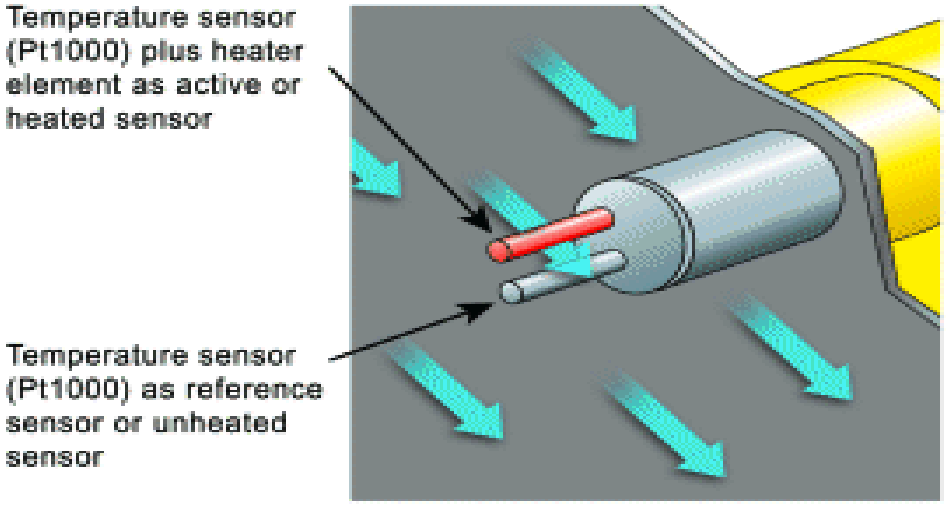

Figure 30(b): Hot-wire anemometer [14].

Another popular flow meter is the magnetic flow meter. The flowing fluid is passed through a pipe, a short section of which is subjected to a transverse magnetic flux. Fluid motion relative to the magnetic field causes a voltage to be induced proportional to the fluid velocity. The electromagnetic field is detected by electrodes placed in the conduit walls. Either an alternating or direct magnetic flux may be used. Two types of magnetic flow meter have been developed. In the first case, the fluid needs to be only slightly conductive, and the conduit must be of glass or some similar non-conducting material. The electrodes are placed flush with the under conduit surfaces making direct contact with the flowing fluid. Output voltage is quite low and an alternating magnetic field is used for amplification and to eliminate polarization problems. The second form of

magnetic flow meter is primarily intended for use with highly conductive fluids such as liquid metals. This meter operates on the same basic principle but may use electrically conducting materials for the conduit. Stainless steel is commonly used. A permanent magnet supplies the necessary flux, the electrodes may simply be attached to diametrically opposite points on the outside of the pipe. The output of this type is sufficient to drive ordinary commercial indicators or recorders and zero output for no flow conditions. Fig. 30(c) shows a magnetic flow meter [13].

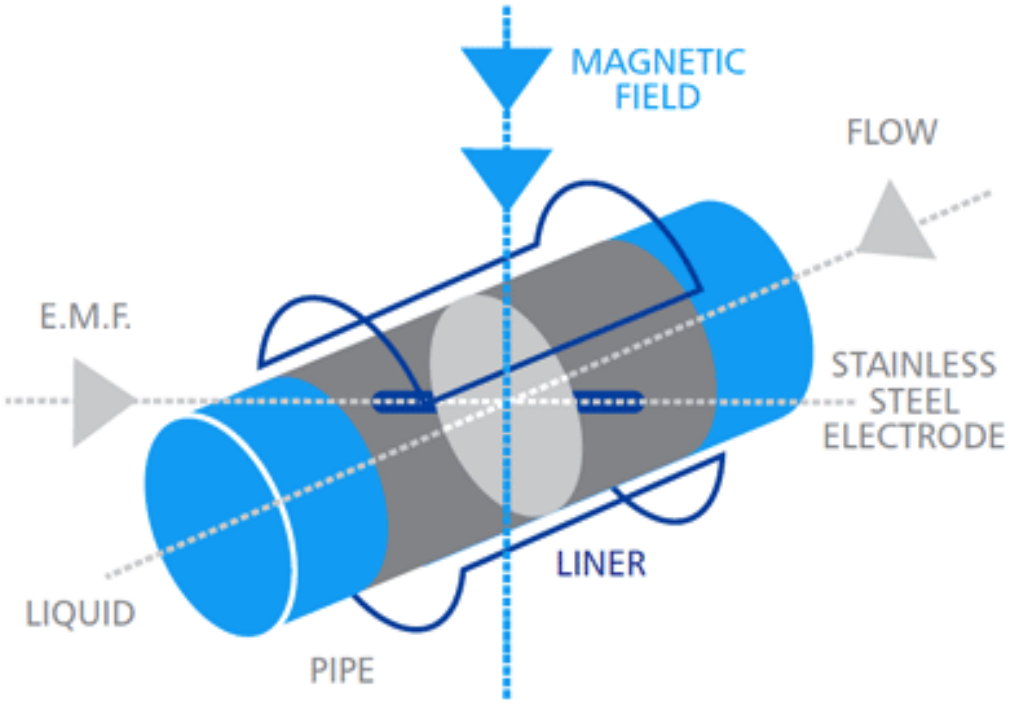

Figure 30(c) : Magnetic flow meter [15].

Next, we describe ultrasonic flow meters. There are two main types of ultrasonic flow meters: Doppler flow meter and transit time flow meter. Doppler flow meters are designed to measure the flow of liquids that contain sound reflectors- suspended solids or gas bubbles. In the Doppler flow meter, an ultrasonic transducer is used to generate a

sound wave in the flowing liquid. The wave is reflected by sonic reflectors suspended in the liquid, and the reflected wave is received by a second transducer. If the reflectors are moving within the sound transmission path, sound waves will be reflected at a frequency shifted from the transmitted frequency (Doppler shift). The difference between the reflected and transmitted frequencies is directly proportional to the speed of the sonic reflectors. Thus by measuring this frequency shift, one can determine the velocity of the flowing liquid and then use it to calculate other related flow parameters. Successful application of Doppler flow meter requires that the liquid contain sufficient concentration, typically 100 ppm or greater, of particulate matter or gas bubbles that can cause acoustic reflection. Note that dissolved solids do not generate reflections and are not useful for this purpose [9].

In the transit time ultrasonic flow meter, two transducers are placed on opposite walls of a pipe through which the fluid is flowing. Acoustic waves generated by one transducer travel through the fluid and reach the other transducer. The time taken by the acoustic wave to travel from one transducer to the other, the transit time, is a function of the flow velocity of the fluid. Thus by measuring this time, one can determine the fluid velocity and other relevant flow parameters. The basic principle can be understood by referring to Fig. 31(a) which shows transducers A and B placed on opposite walls of a pipe [9].

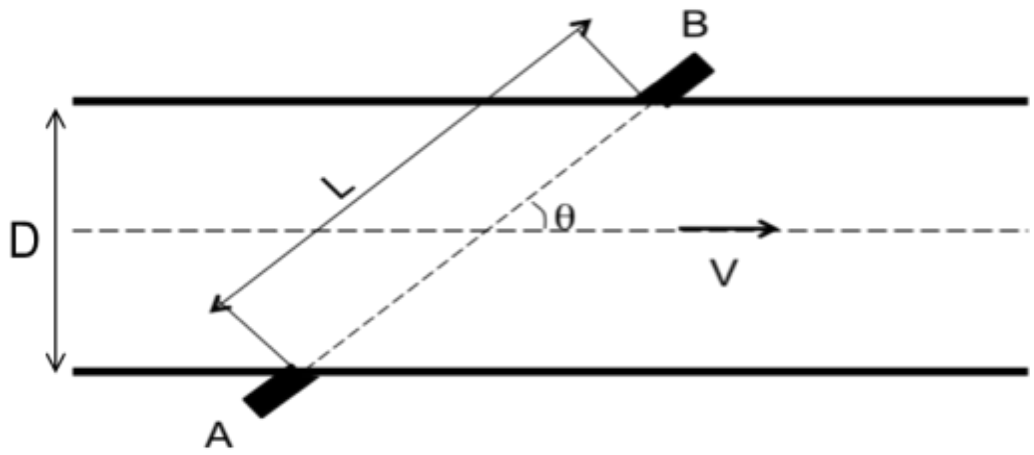

Figure 31 (a): Block diagram of ultrasonic flow meter using the transit time principle [9].

Let us assume that a fluid with velocity V is flowing through the pipe and let v_B denote the velocity of bulk acoustic waves in the fluid. From Fig. 31(a) it can be seen that effective velocity of the ultrasonic wave traveling from A to B will be equal to v_B +Vcosθ), whereas the effective velocity if the wave traveling from B to A will be v_B - Vcosθ), Therefore t_1, the transit time of acoustic waves to travel from A to B will be given by $t_1 = L/(v_B + V\cos\theta)$, where L = acoustic path length between transducers A and B, and θ is the angle between the direction of acoustic wave propagation and the direction of fluid flow. The transit time of acoustic waves to travel in the opposite direction, that is, from B to A, t_2 will be given by $t_2 = L/(v_B - V\cos\theta)$. If we define a parameter α by the Equation $\alpha = (1/t_1 - 1/t_2)$, we get

$$\alpha = (1/t_1 - 1/t_2) = 2V\cos\theta/L \qquad (18)$$

Eq. (18) shows that α is independent of v_B, and depends only on fluid velocity V, angle θ and distance L. Thus by measuring this quantity one can determine the flow velocity V of the fluid. This can then be used to find other flow related parameters. The fact that α is

independent of v_B is very advantageous because parameters that affect v_B such as density or temperature of the fluid, presence or absence of particulate matter in the fluid, will not affect the output of the flow meter.

In order to find the best possible value for angle θ, let us look at Eq. (18) again. We note that the acoustic path length L = D/sinθ, where D is the diameter of the pipe. Substituting for L into Eq. (18) we get

$$\alpha = 2V\cos\theta\sin\theta/D \quad (19)$$

$$\alpha = V\sin2\theta/D \quad (20)$$

Eq. (20) shows that α becomes maximum at θ = 45º. So the optimum angle to launch the acoustic wave in the fluid is θ = 45º.

In the transit time flow meter, the ultrasonic transducers can be mounted outside the pipe (clamp-on transducers) or inside the pipe (wetted transducers). Clamp-on method has the advantage that there is no need to cut the pipe or drill holes in it. This method is suitable for portable flow meters and in applications where the existing piping cannot be disturbed. However, the clamp-on method has certain limitations. The transducer is acoustically coupled to the outside of the pipe using grease or RTV couplant. Maintaining the integrity of this contact over long periods of time can be a challenge. Another limitation is that the pipe material must be such that acoustic waves can pass through the walls of the pipe without suffering significant attenuation. Most pipes constructed of solid, homogeneous materials can meet this qualification. Pipes that cause application

difficulty include concrete pressure pipes, Teflon coated pipes, and fiberglass reinforced pipes.

Transit time flow meters using transducers mounted inside the flow tube (wetted) are somewhat more expensive than clamp on flow meters. But they offer superior performance in terms of accuracy, long term reliability, zero maintenance, and tamper proof construction in which all the parts including the transducers are inside the pipe. In view of the characteristics, advantages, and limitations of the different types of flow meters considered above, the ultrasonic flow meter which is finding increasing applications today is the transit time flow meter using wetted transducers. This thesis will therefore focus on this type of flow meter. In the discussion that follows, unless stated otherwise, the term flow meter will mean transit time flow meter using wetted transducers.

3.1 Transducers for use in ultrasonic flow meters

The transducers that are used to generate and detect acoustic waves in the flowing liquid play an important role in the operation and performance of the flow meter. The structure of the conventional transducer used to generate acoustic waves in fluids is shown in Fig. 31(b). It consists of three main parts: the piezoelectric crystal element which generates/detects the acoustic wave, the impedance matching layer which is required in order to match the high acoustic impedance of the piezoelectric crystal to the low impedance of the liquid, and the acoustic damping layer which is required in order to obtain a reasonable frequency bandwidth for the transducer. The packaged transducer has the shape of a cylinder whose diameter and length depend on the operating

frequency, bandwidth, and aperture of the acoustic wave that is to be launched in the fluid. The cylindrical shape of the transducer and the fact that it has to be mounted at an angle to the pipe wall causes problems. This can be seen from Fig. 32. The transducers protrude a considerable distance inward from the pipe walls and into the path of the flowing fluid. This causes disturbance of the flow stream and can result in erroneous flow data. The use of the recessed arrangement shown in Fig. 33 reduces the severity of the problem, but does not eliminate it.

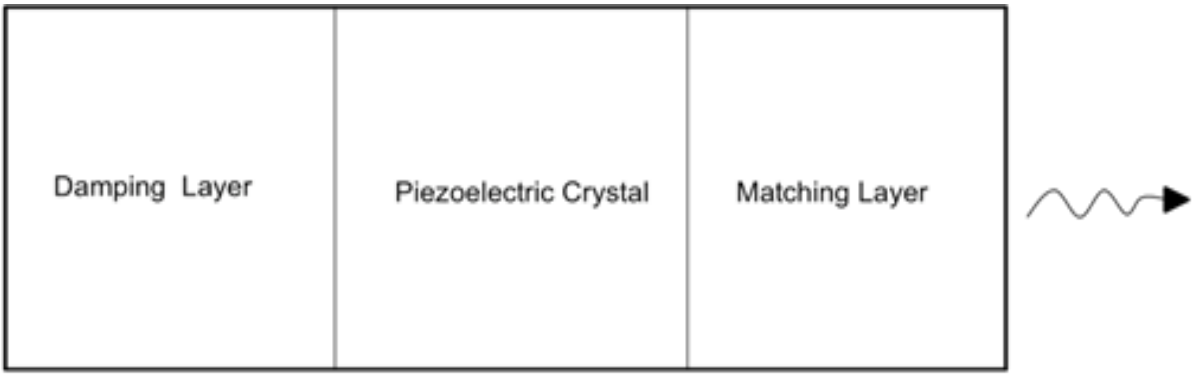

Figure 31(b) : Geometry of conventional transducer used to generate ultrasonic waves in fluids.

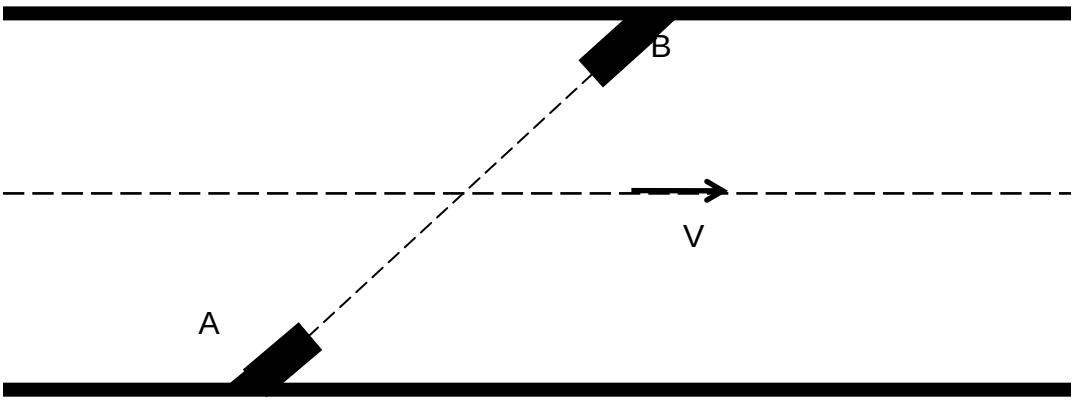

Figure 32: Use of conventional transducers in ultrasonic flow meter.

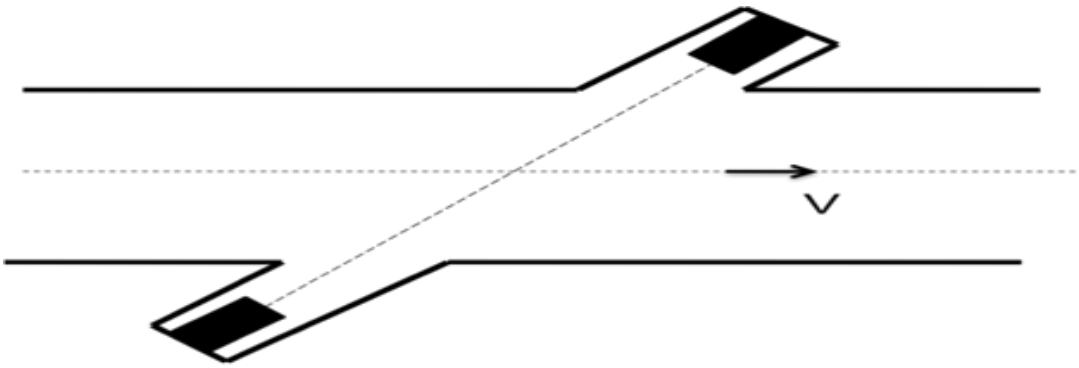

Figure 33: Recessed transducer arrangement used to minimize perturbation of fluid flow.

A novel approach to overcome the transducer protrusion problem mentioned above is provided by the theoretical and experimental work described in the previous chapter. That work has shown that one can couple energy from a plate acoustic wave into a bulk acoustic wave, and vice versa. This fact can be used to develop the transducer whose geometry is shown in Fig. 34. The proposed transducer consists of a thin plate of a suitable piezoelectric material on which inter digital transducer (IDT) is fabricated to generate plate acoustic waves. As shown previously, if the velocity of plate waves in the substrate v_p is greater than the velocity of bulk waves in the fluid v_B, then the plate wave propagating in the substrate will radiate a bulk wave in the fluid at an angle θ given by the equation $\theta = \cos^{-1}(v_B/v_p)$. A similar device can be used to convert energy back from bulk waves to plate waves. Here bulk wave incident from the fluid will generate plate acoustic wave on the substrate. We refer to this type of transducer, which depends on the coupling of energy between plate acoustic waves and bulk acoustic waves, as mode coupling transducer or mode conversion transducer (MCT).

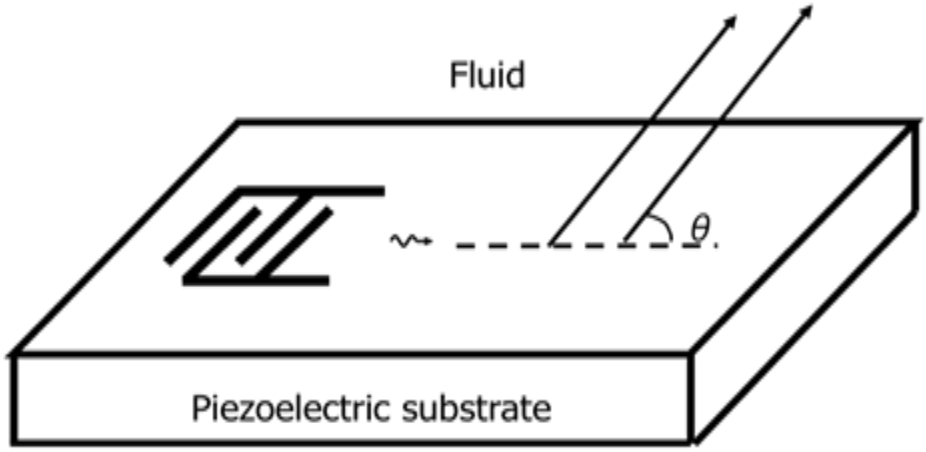

Figure 34: Geometry of the proposed mode coupling transducer (MCT).

One important point to note about the mode coupling transducer is the following. We note that the energy of a plate acoustic wave is available on both plate surfaces. So in Fig. 34, the IDT does not have to be on the top surface, but can be on the bottom surface of the plate. That is, the IDT can be located on the surface opposite from that which is in contact with the fluid. This has the advantage that transducer electrodes will not come in contact with the fluid, and so they will not be affected by it. It also simplifies the job of making electrical connections to the IDT.

3.2 Use of mode coupling transducers in a flow meter

In order to confirm that the proposed transducer arrangement can work in a flow meter, we fabricated a simple plastic box. The box was fabricated using a slab of acrylic plastic of dimensions 150 mm x 20 mm x 100 mm. A slot was milled in the center of the slab enabling us to pour water in the box. Fig. 35 shows the three-dimensional view of this box. There were two recessed slots cut in the opposite walls of the box where our transducers were mounted at an offset of 14.14 mm. A photograph of the box with the

transducers mounted is shown in Fig. 36. The box was then filled with water from the top opening. When electrical input was applied to one of the transducers, we were able to see output on the other transducer at the expected time delay. This is shown in Fig. 37. The output of the device shows very high rf leakage and many other spurious signals. But the fact that we are getting output on the other transducer is very promising and shows that the proposed transducers can indeed work in a flow meter arrangement.

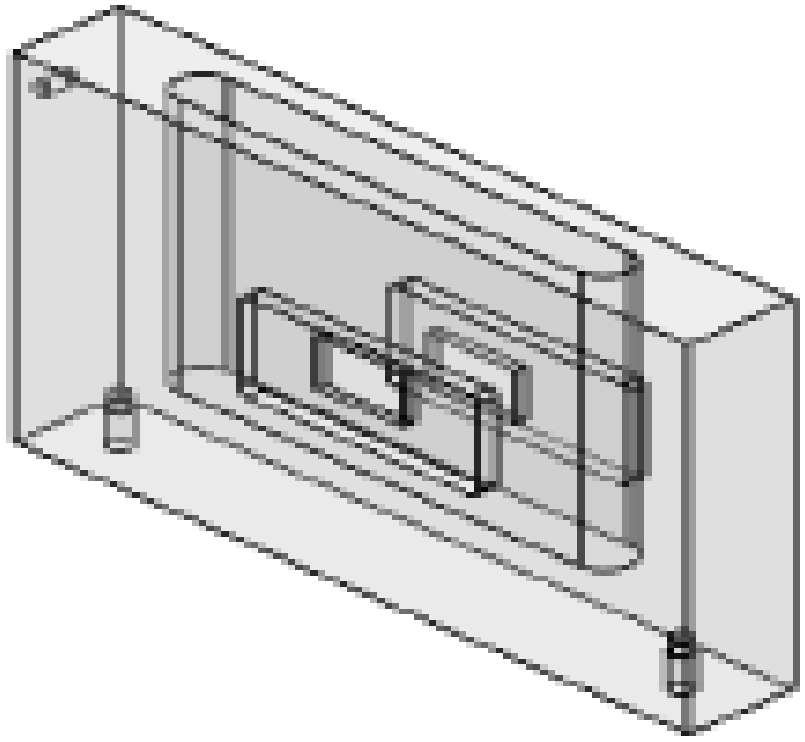

Figure 35: Three dimensional view of the plastic box used to test mode conversion transducers.

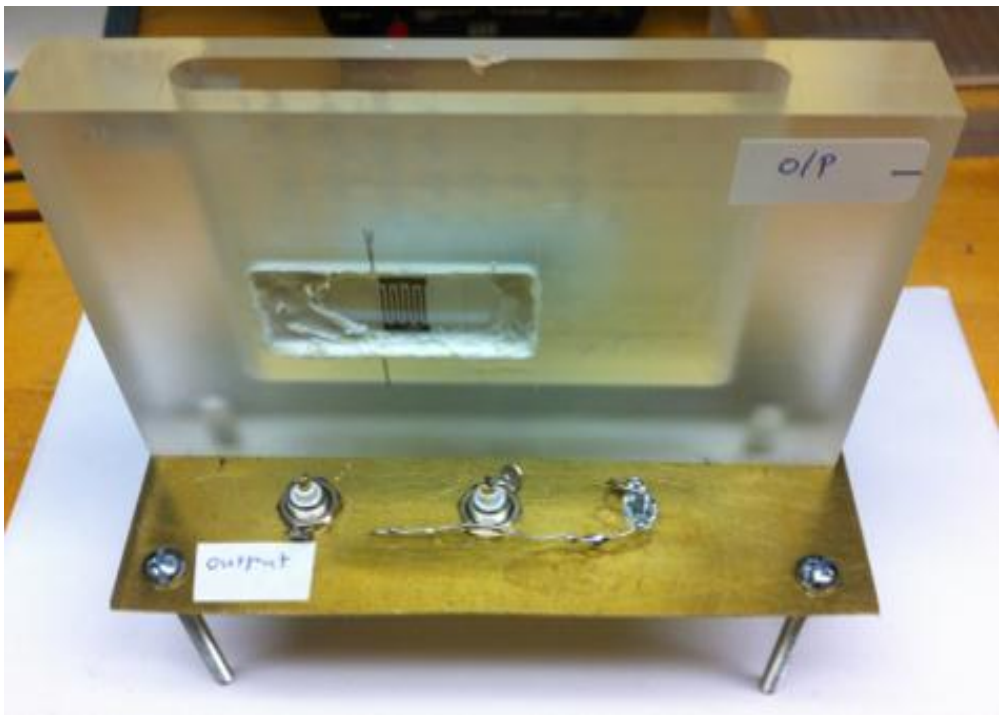

Figure 36: Photograph of plastic box with transducers mounted.

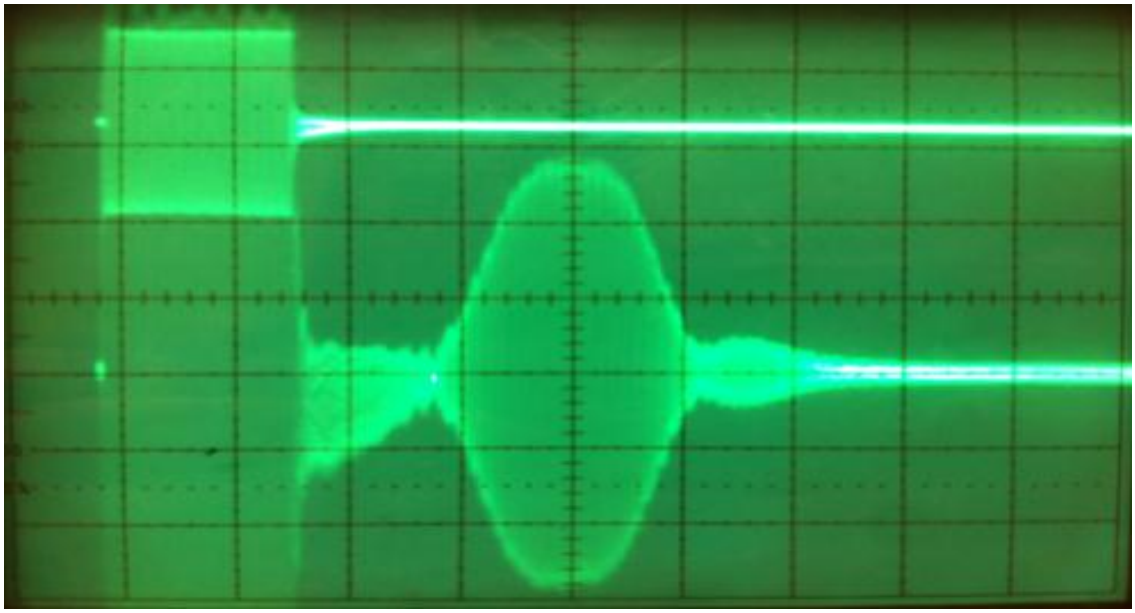

Figure 37: Oscilloscope picture showing input and output obtained from the box. Upper trace: Input to applied to transducer T_1; 5 V/div. Lower trace: output of BAW transducer; 50 mV/div, horizontal axis: 5μs/div.

Now we turn our attention to developing an arrangement that is close to what can be used in a practical flow meter. After several design iterations, we were able to develop a flow cell which is fairly close to what can be used in a practical flow meter. The cell was fabricated using a square aluminum tube having outside dimensions of 1" x 1". The tube has wall thickness of 3/16", so that the dimensions of the channel through which fluid can flow are 5/8" x 5/8". Mode coupling transducers were mounted on slots cut in opposite sidewalls of the cell. A photograph of the fabricated cell (referred to as device D5) is shown in Fig. 38. A detailed view of the region in which transducer action takes place is shown in Fig. 39. This figure shows thin piezoelectric plates A and B mounted on the slots. Inter digital transducers T_1 and T_2 are fabricated on these plates for the generation and detection of plate acoustic waves. Input signal applied to transducer T_1 generates a plate acoustic wave, which is converted in to a bulk acoustic wave which travels through the fluid and reaches plate B. There the bulk wave is converted back in to a plate wave and is then detected by transducer T_2. The plates A and B are mounted in recessed regions cut in the walls of the flow tube. The depth of the recessed region is 1/8". The dimensions D_1 through D_3 shown in Fig. 39 are as follows. D_1 = 1" = 25.4 mm, D_2 = 1 – 2 x (3/16) = 5/8" = 15.87 mm, and D_3 = 1 – 2 x (1/8) = 3/4" = 19.05 mm. The length of the slots is 20 mm and they are offset from each other by a distance equal to D_3.

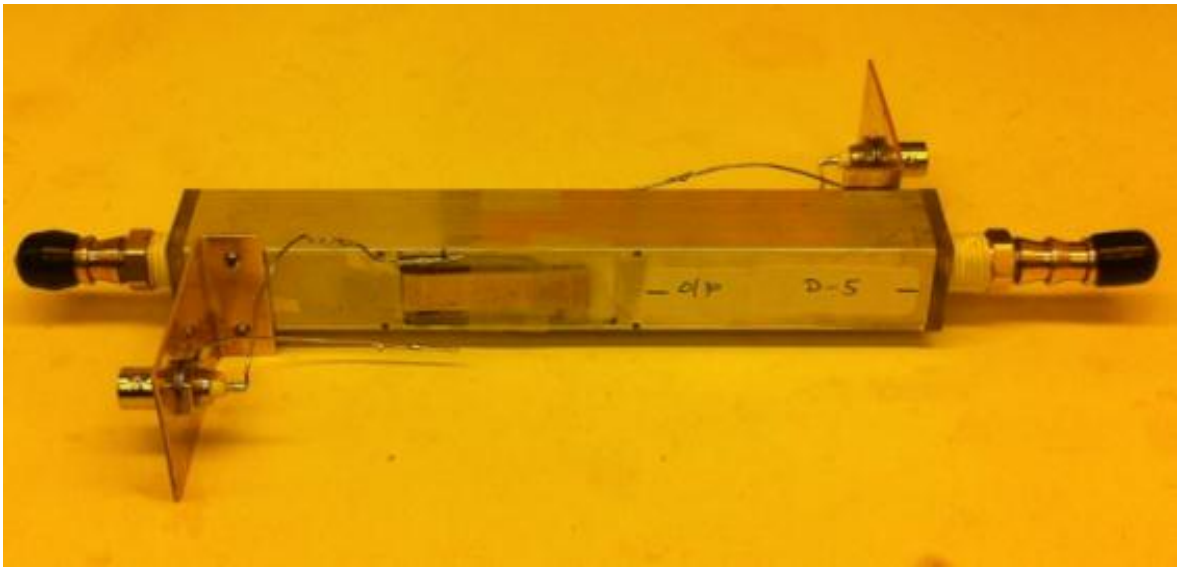

Figure 38: Photograph of flow cell.

The output has almost no rf leakage as seen in Fig. 40. There are a few spurious signals occurring after the main acoustic signal. More work will be needed to reduce the strength of these signals.

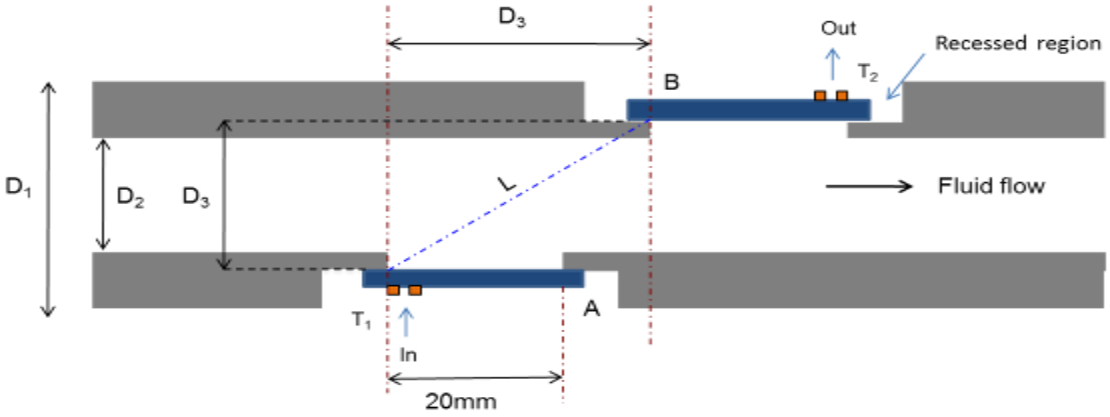

Figure 39: Top view of flow cell in the region where transducers are mounted.

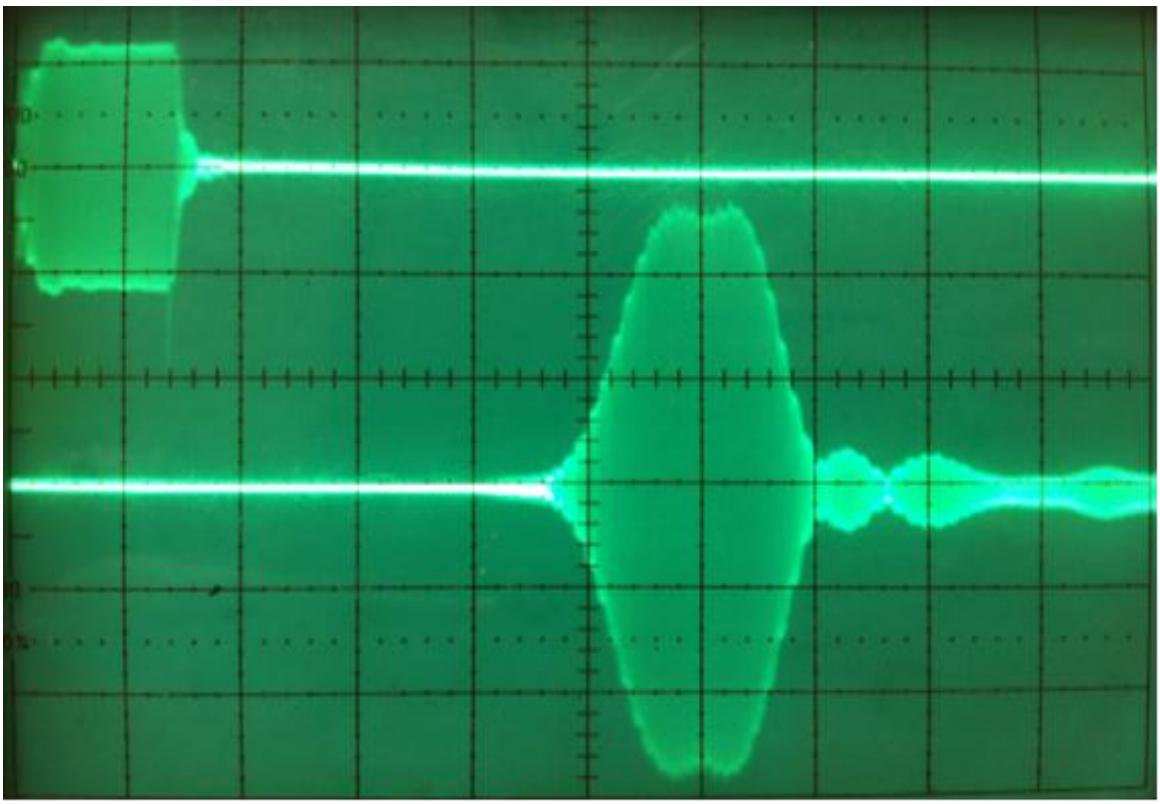

Figure 40: Oscilloscope picture showing response of the flow cell. Upper trace: Input to applied to transducer T_1; 5 V/div. Lower trace: output of BAW transducer; 50 mV/div, horizontal axis: 5μs/div.

Now let us consider the time delay of this device. If we consider the operation of this device, we recognize that the signal travels mostly as bulk acoustic wave through the fluid, but partly also as plate acoustic wave on the crystals. So the time delay t_d is given by

$$t_d = t_f + t_c \tag{21}$$

where t_f is the time delay through the fluid and t_c is the time delay on the crystal. Now

$$t_f = L/v_B \tag{22}$$

where L is the path length through the fluid. From Fig. 39, $L = D_3/\sin\theta$. Here D_3 = 19.05mm and $\theta = 45°$, therefore L = 26.9 mm. Using v_B = 1500m/s, we get t_f = 17.9 μs. Now let us look at t_c. Here t_c is given by

$$t_c = L_{eff}/v_p \tag{23}$$

where L_{eff} is the effective length the wave travels on the crystals. To calculate L_{eff}, we consider the following. The interdigital transducers T_1 and T_2 are actually distributed sources. We can replace each IDT by an effective source located at the geometric center of the IDT. Then the effective path length L_{eff}, will be equal to

$$L_{eff} = (20 - L_p) \tag{24}$$

where L_p is the length of the IDT along the propagation path. Here L_p = Np = 8.04mm, therefore L_{eff} = 11.96mm. Using v_p = 2120 m/s we get t_c = 5.64 μs. Thus the total time delay comes to $t_d = t_f + t_c$ = 23.54 μs.

To measure t_d the oscilloscope response in Fig. 40 gives us the approximate value, but is not suitable for accurate measurements. To get more precise results we have to use CW (continuous wave) method. The time delay equation is given by

$$td = -(1/2\pi)\left(\frac{\partial\phi}{\partial f}\right) \tag{25}$$

where ϕ is the phase shift through the device and f is the frequency. To use Eq. (25) we need a plot of phase shift versus frequency. This can be obtained by measuring the transfer function S_{21} of the device. Results of such measurement using Agilent 8714E5 RF Network Analyzer are shown in Fig. 41. In this figure the upper plot is the magnitude

and the lower plot is the phase angle S_{21}. For an ideal device, the phase plot will be perfectly linear. For our device, we find that the plot is very close to linear, but shows some ripples. These are due to the small spurious signals observed in Fig. 40. From the phase plot, we find the following, $\phi_1 = 179.2^o$ at $f = f_1 = 0.926$ MHz, $\phi_2 = -177.3^o$ at $f = f_2 = 0.965$ MHz, $\phi_3 = 178.59^o$ at $f = f_3 = 1.004$ MHz. Taking slope between f_2 and f_1, we get $t_d = 25.38$ μs; and taking slope between f_3 and f_2 we get $t_d = 25.12$ μs. This compares to the calculated value of 23.54 μs.

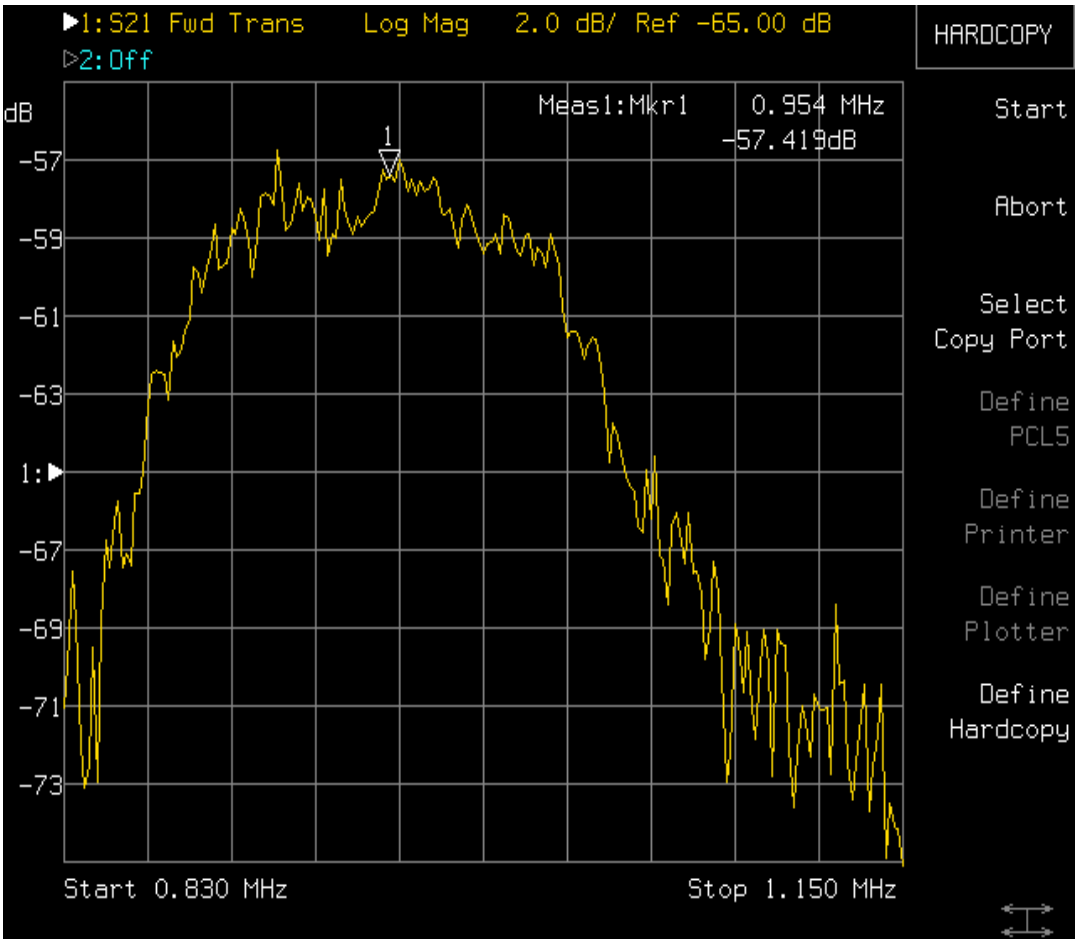

Figure 41(a): Magnitude plot of transfer function S_{21} of device D5.

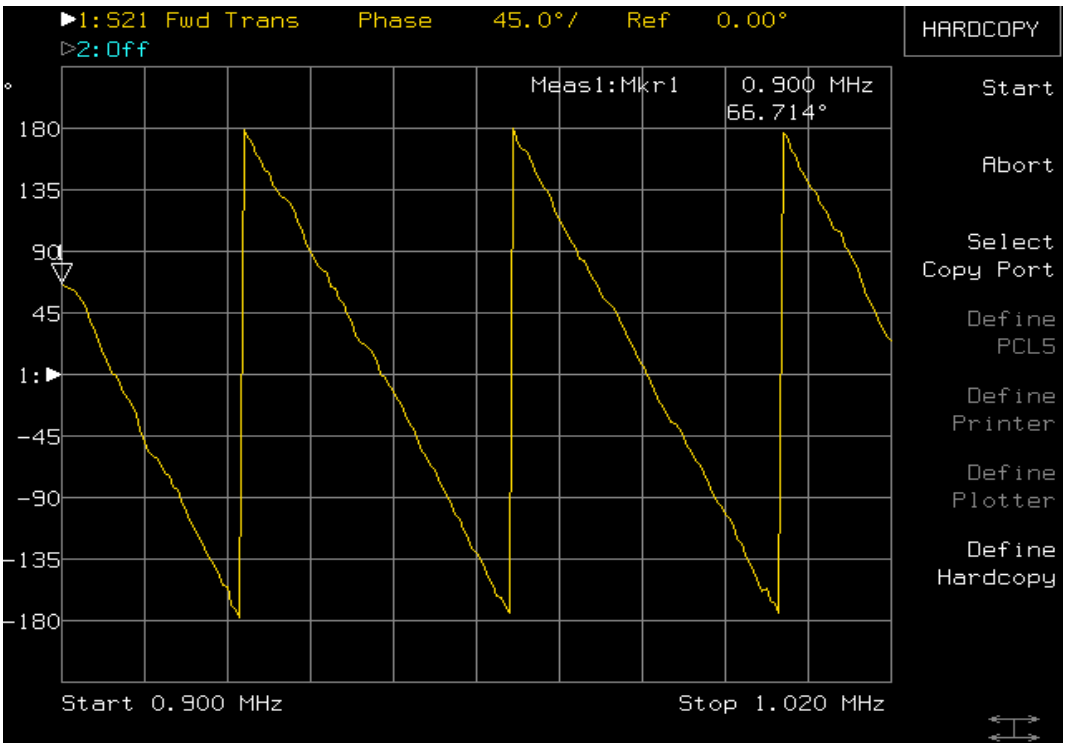

Figure 41(b): Phase angle plot of transfer function S_{21} of device D5.

Next let us consider the insertion loss of the device. In this device the transduction process takes place in four steps. First, the input signal applied to transducer T_1 gets converted into plate acoustic wave travelling on a delay line A. Second the plate acoustic wave converts into bulk acoustic wave in the fluid. Third, the bulk acoustic wave converts back into plate acoustic wave on delay line B and finally, the plate acoustic energy is converted into electric signal by transducer T_2. Therefore the insertion loss will consist of four different parts. The overall insertion loss (in decibel) of this device can be written as

$$\text{Insertion loss IL} = L_1 + L_2 + L_3 + L_4 \qquad (26)$$

where L_1 = insertion loss of the input transducer T_1, L_2 is the mode conversion loss in delay line A converting PAW to BAW, L_3 is the mode conversion loss in delay line B for

converting BAW back into PAW, and L_4 is the insertion loss of the output transducer T_2. Measuring each of these losses individually is very difficult. For example to measure L_1 we need to measure the acoustic power generated by transducer T_1, which is very difficult. To measure L_2 we need to measure plate and bulk acoustic powers which are also very difficult. Nevertheless, we can find the total mode conversion loss L_M by rearranging Eq. (26). This can be done as

$$IL = L_T + L_M \tag{27}$$

where $L_T = (L_1 + L_4)$ = insertion loss due to two IDTs, and $L_M = (L_2 + L_3)$ = total mode conversion loss incurred in going from PAW to BAW and back from BAW to PAW.

The loss L_T was measured by fabricating a delay line having input and output IDTs identical to those used in devices A and B. The delay line was operated in air therefore there was no mode conversion taking place. L_T was measured as 51dB as shown in chapter 2. From Fig. 41, we note that the total insertion loss of our device is 58 $\pm$ 1dB. Therefore the mode conversion loss $L_M = I_L - L_T = 7 \pm 1$dB. These characteristics of the flow cell have been described in one of our recent publications [17].

The fact that the total mode conversion loss is only 7dB indicates that the plate wave to bulk wave and bulk wave to plate wave mode conversion is taking place fairly efficiently. However we wished to investigate if the conversion efficiency can be improved further. For this purpose we revisit the transducer arrangement used in our flow meter. The essential parts of this arrangement are shown in Fig. 42 below.

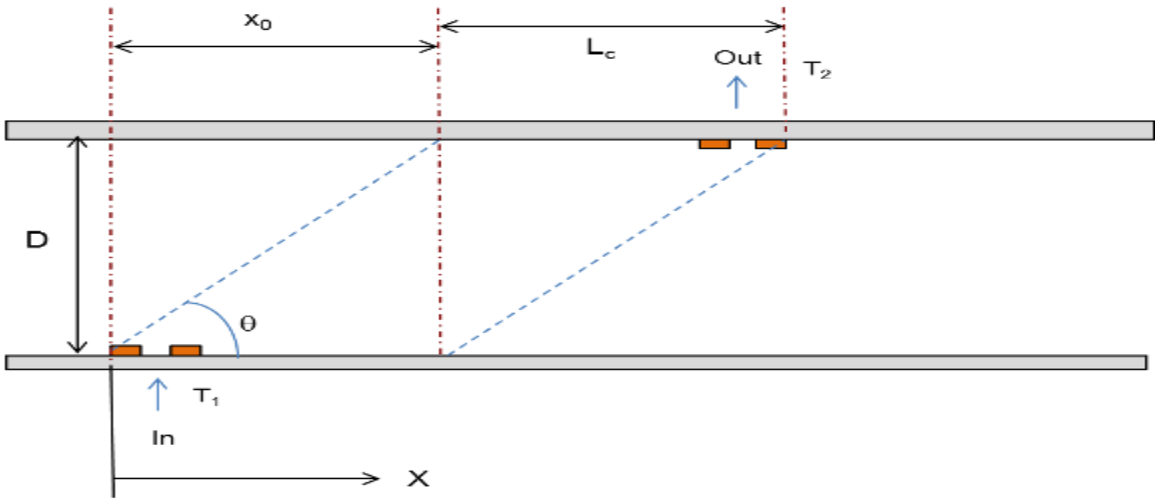

Figure 42: Experimental arrangement used to study output variation as a function of coupling length.

Here plate wave to bulk wave conversion takes place in delay line A while bulk wave to plate wave conversion takes place in delay line B. The bulk wave radiated by the first finger of transducer T_1 intersects delay line B at the point $x = x_0$. From Fig. 42 we note that $x_0 = D/\tan\theta$, where θ is the angle with which bulk wave is radiated into the fluid. In our experiments $\theta = 45$, so $x_0 = D$. Fig. 42 defines a length L_c. This is the length over which the plate and bulk waves are coupled with each other. We call this the coupling length. On delay line A as L_c increases, more and more plate wave energy will convert into bulk energy. So from this point of view, one would like to keep increasing L_c. The situation at delay line B is however different. The reason is as follows. The bulk wave converts its energy into plate wave energy at the point where it intersects the surface of delay line B. The generated plate wave travels to the right towards the output transducer T_2. However, as it travels along the plate surface, it re- radiates a bulk wave back into the fluid. This is shown in Fig. 42. at delay line B, if the coupling length L_c is small, not enough bulk wave energy will get converted into plate wave. If L_c is too large then lot of

plate wave energy will re-radiate into bulk wave. So there must be some value of L_c where the conversion of bulk wave energy to plate wave energy becomes maximum.

Now in order to see if this theory holds, we performed the following experiment. Two identical PAW delay lines A and B were fabricated. Next a fixture was designed such that the delay lines could be held parallel to each other as shown in Fig. 43. This fixture had dimensions 150 mm x 110 mm x 100 mm. The distance between the delay lines was 12.7 mm. Delay line A was kept fixed while delay line B could be moved along the x- direction. Input signal was applied to transducer T1 on delay line A and output on transducer T2 was observed as delay line B was moved. The delay line was moved along positive x-direction, starting at x = 0 as in Fig. 42.

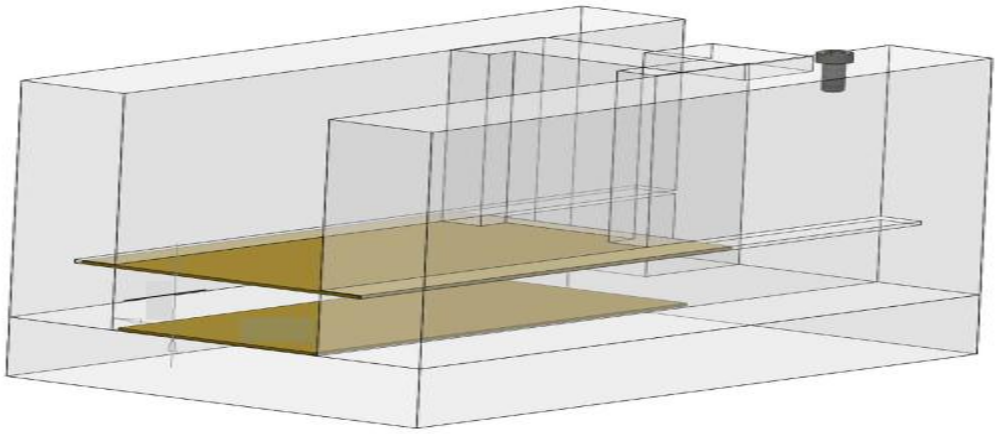

Figure 43: Three-dimensional view of fixture used in experiment shown in Fig. 42.

First we noted that there was no output until its right most electrode reached the point x = x_0. This is as expected. As we moved past the point x = x_0, the output on T_2 increased, reached a maximum and then started to decrease. This can be seen from the oscilloscope

pictures shown below in Fig. 44 (a) through (c). The pictures are taken at coupling length L_c of 7.93 mm, 15.0 mm and 25.4 mm.

(a)

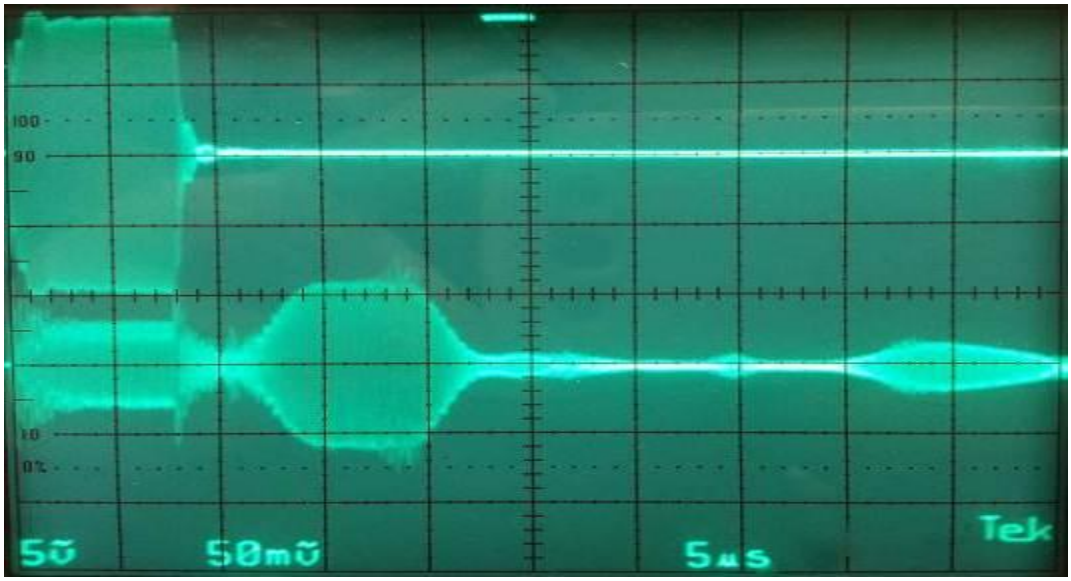

(b)

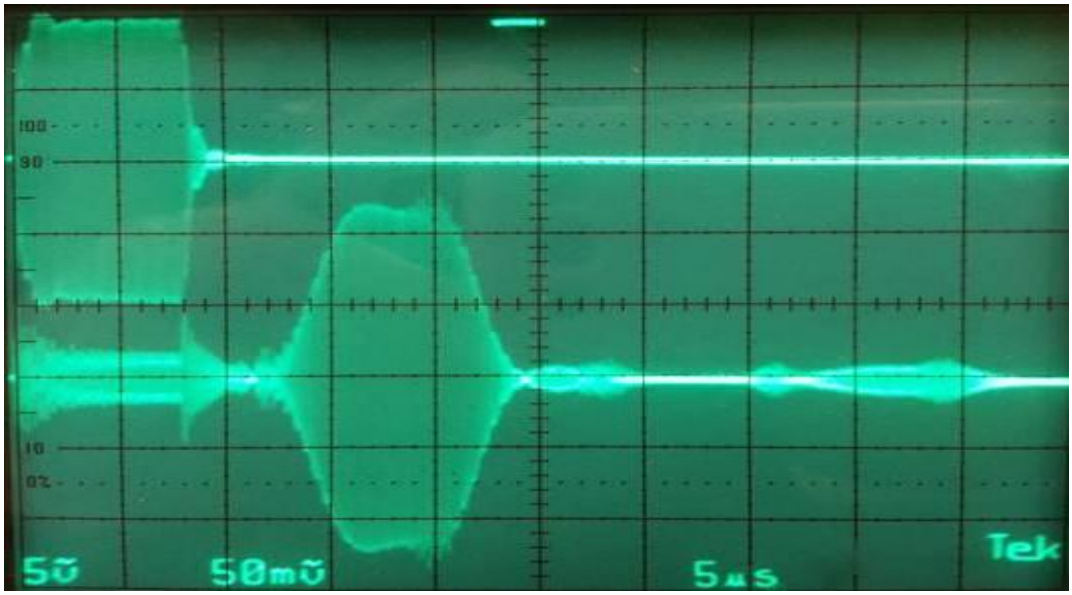

(c)

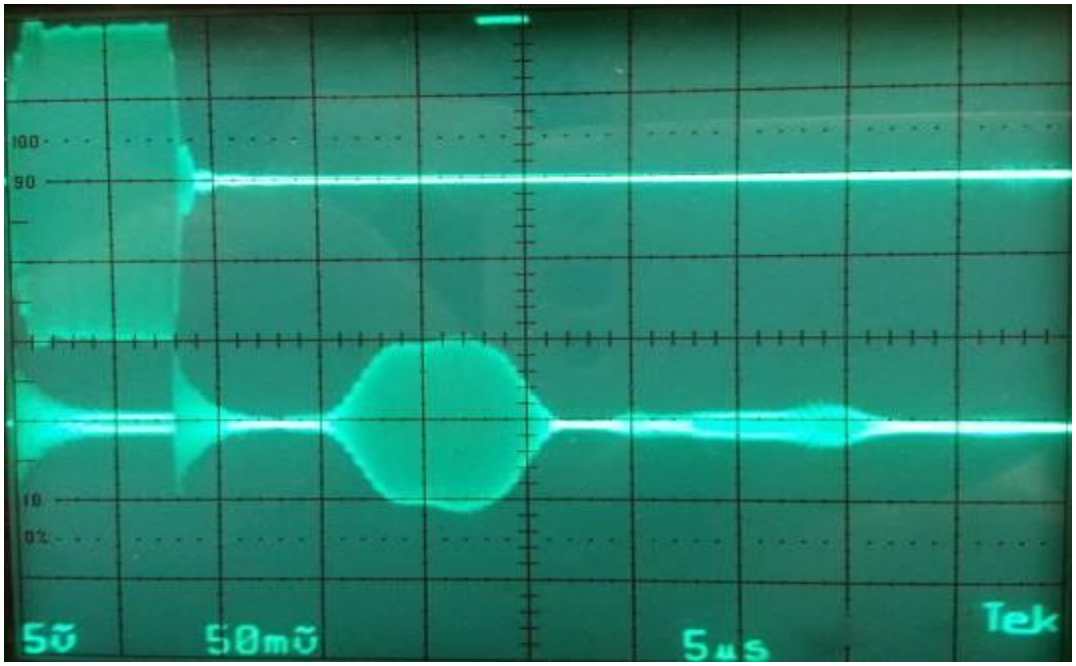

Figure 44: Oscilloscope pictures showing output obtained for different coupling lengths L_c; (a) 7.93 mm, (b) 15.0 mm, and (c) 25.4 mm.

A plot of output voltage obtained on T_2 versus the coupling length L_c is shown in Fig. 45. The plot is similar to what was expected in our theoretical analysis. The output becomes maximum at L_c = 15mm. We also note that as L_c increases the time delay between T_1 and T_2 also increases. This is also an agreement with theory. From Fig. 42 we note that the path length traveled by wave is independent of L_c but the length traveled by the wave on the crystal increases as L_c increases. Therefore the time delay between input and output will increases as L_c increase. The time delay through the fluid is same in all cases but the path length on the delay line B increases as L_c increases accounting for increase in time delay. We note that the conversion of energy becomes maximum at L_c = 15mm. In the design of our flow cell device D5, we had used L_c = 20 mm. From Fig. 45 we note that the output on T_2 will increase by a factor of 1.33 if we chance L_c from 20 to 15 mm. This

corresponds to improvement in efficiency of 2.5 dB. Thus with optimal design we can reduce the total mode conversion loss from 7 dB to 4.5 dB.

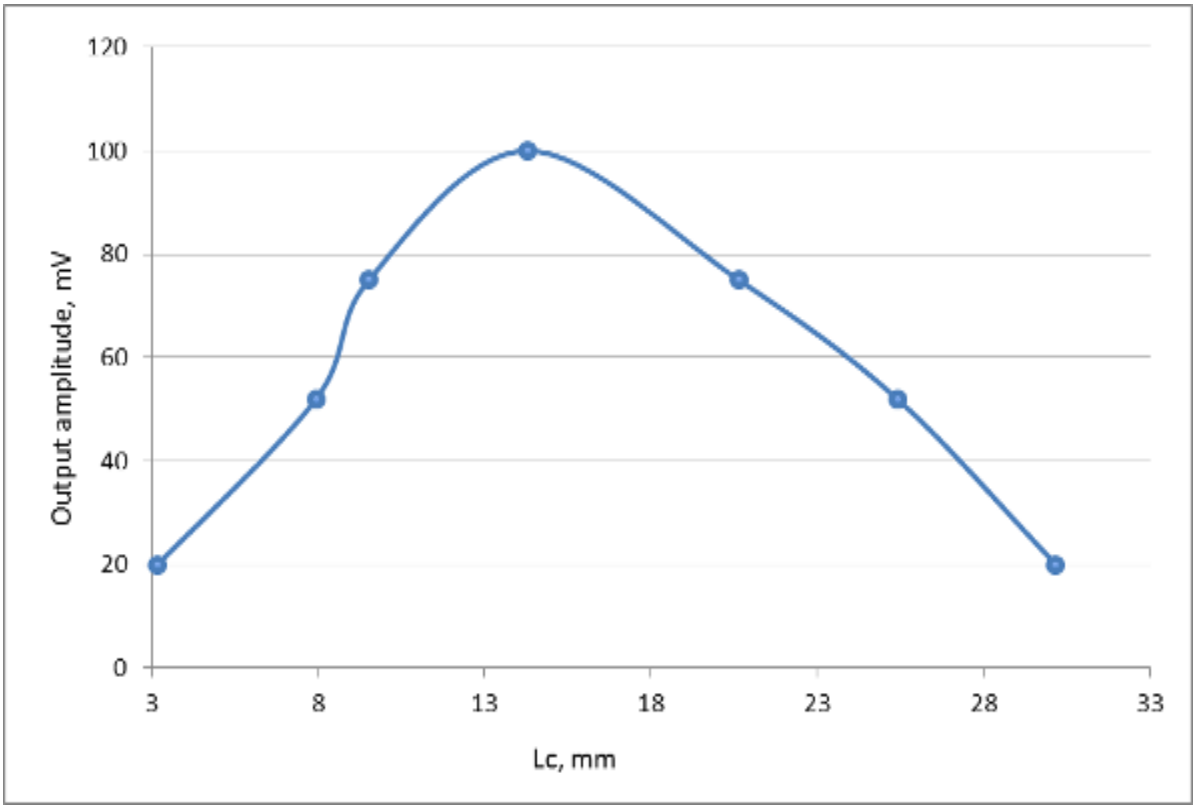

Figure 45: Output in mV versus coupling length in mm.

3.3 Performance of the device under flow

Now we study the performance of our device under conditions of water flowing through the device. Fig. 46 shows the setup we had for performing experiments under water flow. A rectangular tank was taken and filled with water. A small mechanical pump was used for pumping the water through the flow cell. The flow rate could be varied from 0 to 7.5 liters per minute (LPM). A reference flow meter was attached which showed us the different flow rates. The valve enabled us to vary the flow rate. Water tubes are

connected to both ends of the flow meter and water is then flown in the direction as shown in Fig. 46.

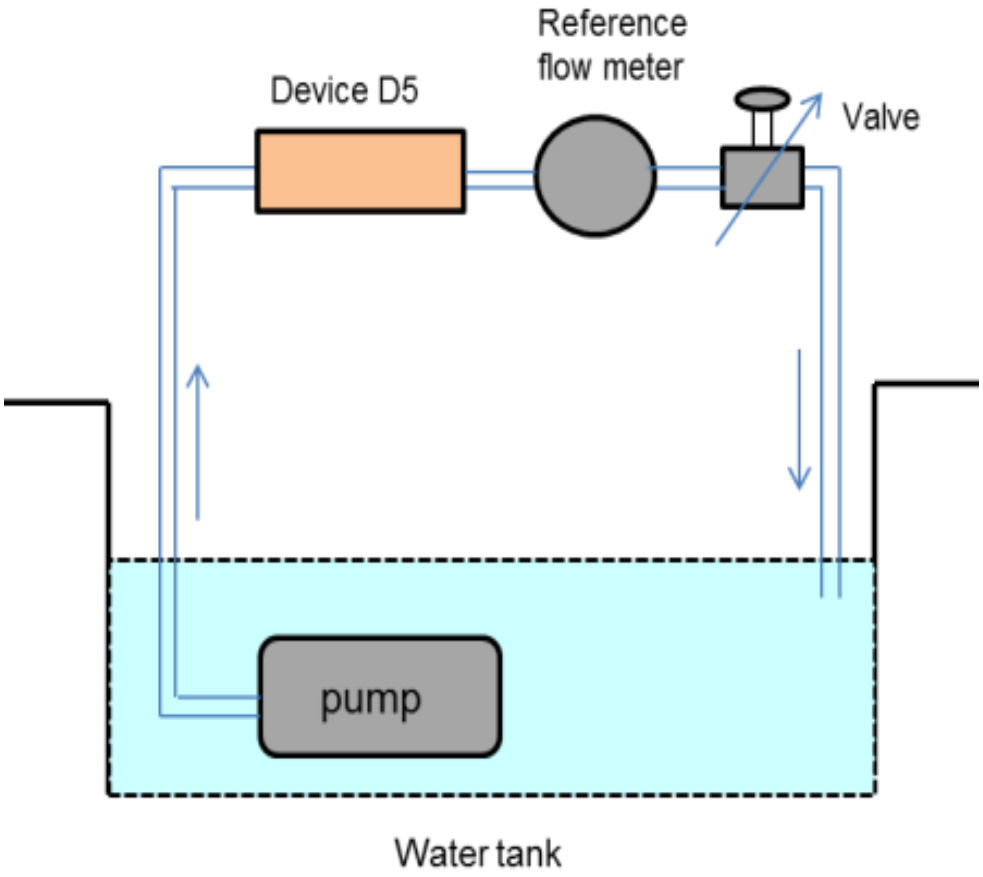

Figure 46: Block diagram of the flow set up used.

When water begins to flow the time delay of the device will change. We note that the change in time delay is very small. For example let us calculate the change in time delay as flow rate changes from 0 to 1 LPM. The volume flow rate, U and the flow velocity, V are related by the equation

$$V = U/A \tag{28}$$

where A is the cross section area of the channel through which the fluid is flowing. For our device the channel cross section is 5/8" x 5/8" = 2.52 x 10^{-4} m^2. Therefore for U = 1 LPM = 1.66 x $10^{-5}$$m^3$/s, we get V = 6.58 10^{-2} m/s. Therefore for V = 6.58 10^{-2} m/s, we get change in time delay, Δt_d to be 0.56 ns. This is calculated by taking the difference of time delay when there is a fluid flow of 1 LPM and 0 LPM. Time delay is given by by ($L / (v_B + V \cos\theta)$) where L is 0.0269 m, v_B is 1500 m/s, V = 6.58 10^{-2} m/s and θ is 45°. At 0 LPM, time delay becomes (L / v_B) and therefore when we take the difference in time delay we get the Δt_d to be 0.56 ns. In a practical flow meter, one is typically required to resolve changes in flow rates of the order of 0.1 LPM. This will correspond to change in time delay of less than 0.06 ns. Measuring such small changes can be quite challenging.

We tried to measure this change in time delay using the phase method. The change in phase through our device is given by Eq. (29)

$$\phi = - 2\pi f t_d, \qquad (29)$$

therefore a change in time delay will give a corresponding phase shift. The phase shift can be measured by using a vector voltmeter. The experimental arrangement is shown in Fig. 47. The device is excited by CW signals from the signal generator. The output of the signal generator is connected to channel A (reference channel) of the reference volt meter. The output of the device is connected to the channel B of the vector voltmeter. The vector voltmeter measures the phase shift through the device. The output of the vector voltmeter was connected to the strip chart recorder. Fig. 48 shows the results of our experiment. The figure shows that the phase does indeed change when flow rate is changed. However we observed large ripples (noise) in the output of the phase meter.

Also there is constant upward drift in the phase meter output. The reasons for this behavior are not clear but we conclude that the phase meter method is not suitable for measuring the small changes in time delay.

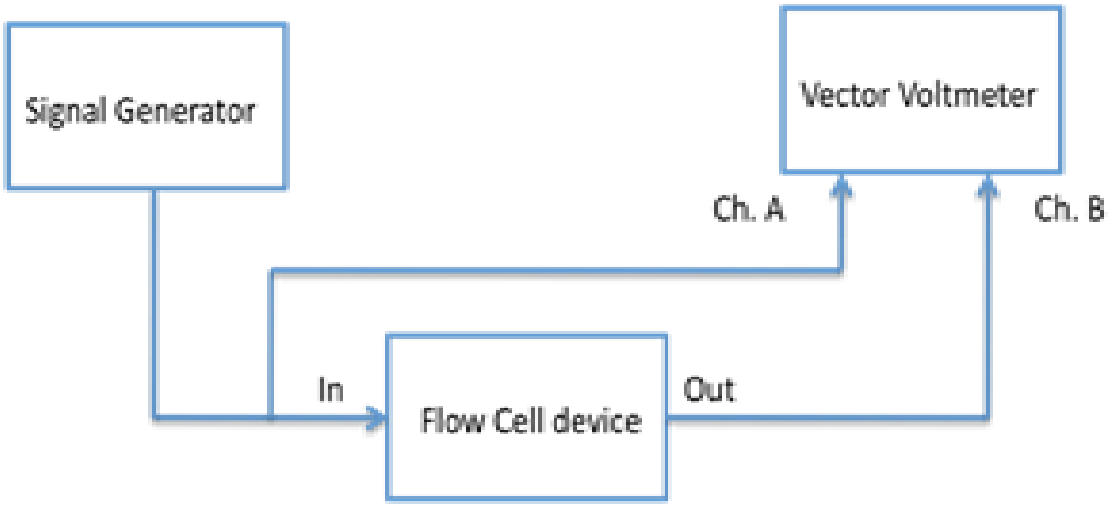

Figure 47: Experimental arrangement used for time delay measurement using phase shift method.

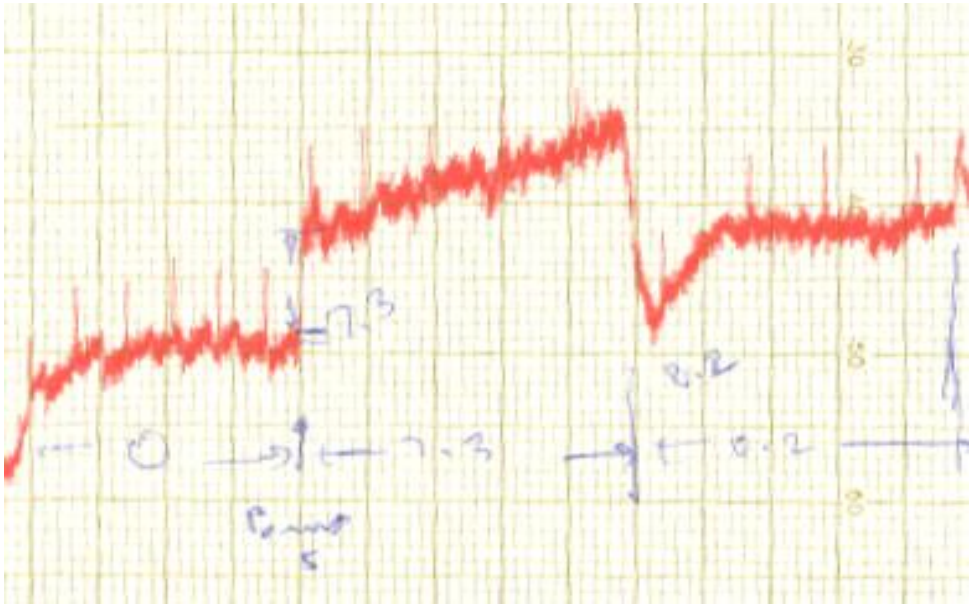

Figure 48: Chart recorder results.

Fortunately we were able to get a flow meter instrument from Dynasonics Inc., (series DXN, model 2800), which allowed us to measure these small changes in time delay in our application. The principle of operation of this instrument is as follows. First input signal is applied to transducer T_1 and the output waveform received on T_2 is digitally stored. Next, input is applied to transducer T_2 and the output waveform received on transducer T_1 is stored. One then performs cross correlation of the signal waveforms received on the two transducers. If the fluid is at rest, the flow velocity V = 0 and $t_{21} = t_{12}$. So the output waveforms on T_1 and T_2 will be in phase and the cross correlation is maximum at $\tau = 0$. On the other hand when the fluid begins to flow, $t_{21} \neq t_{12}$ and the two waveforms are slightly shifted with respect to each other. The time shift τ at which the cross correlation becomes maximum is Equal to $(t_{21}-t_{12})$. Thus the instrument is able to precisely measure the very small time shift $\Delta td = (t_{21} - t_{12})$.

The flow rate was varied and the change in time delay was noted. Fig. 49 shows the experimental results for Δt_d versus flow rate. We note that the time delay changes by 8.47 ns when the flow rate varies from 0 to 7.5 LPM. Fig. 49 shows that Δt_d has a non-zero value of 1.5 ns for zero flow. This is mainly due to the fact that the co-axial cables going from the Dynasonics instrument to the transducers T_1 and T_2 are not equal in length. This problem can be easily corrected by choosing exactly equal length cables or in software.

The calculated plot of Δt_d versus flow rate is shown in Fig. 50. For comparison the experimental plot (with the zero-offset removed) is also shown in this figure. We see that experimental plot is fairly close to the calculated plot.

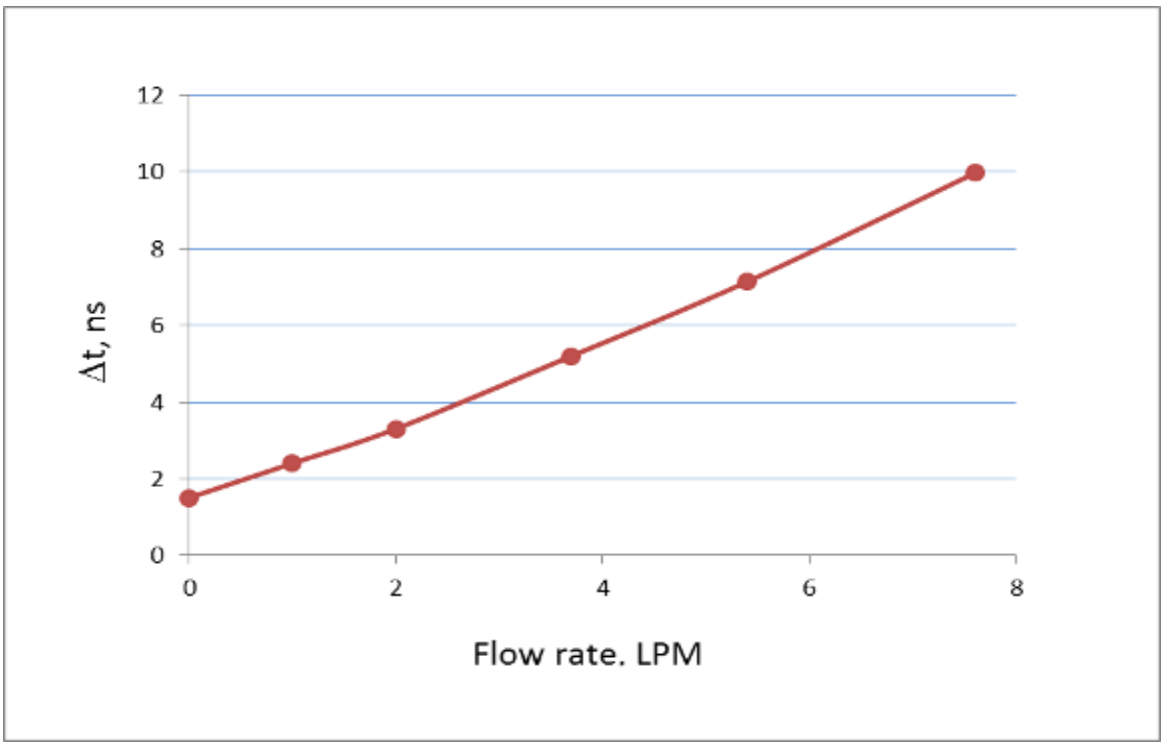

Figure 49: Change in time delay in μs versus flow rate in liters per minute (LPM).

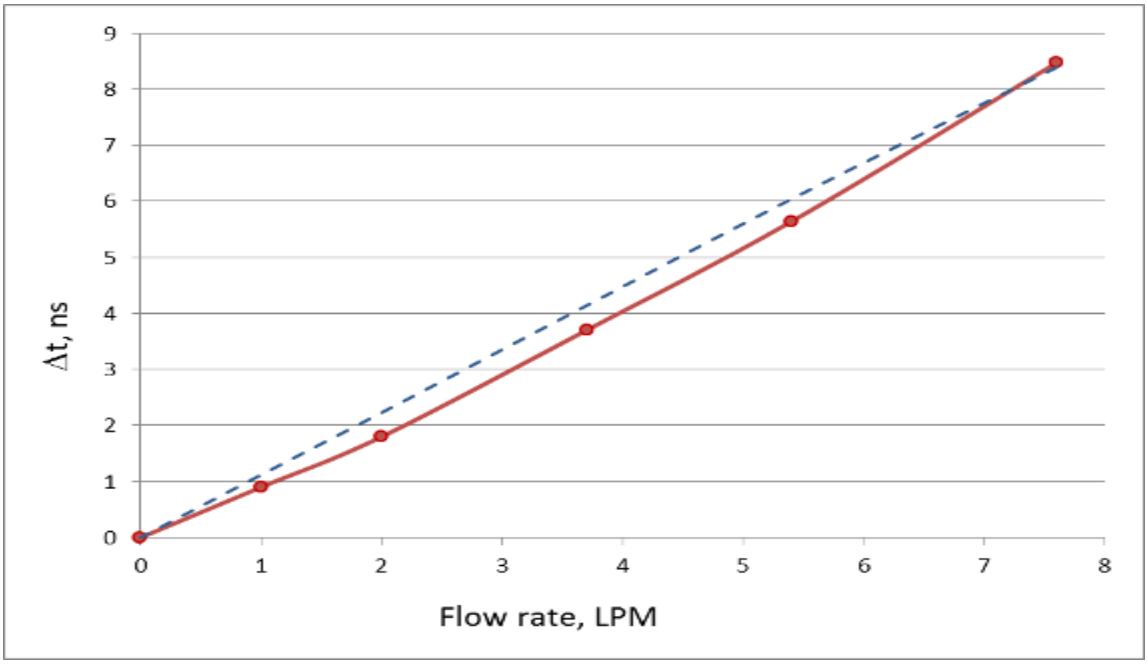

Figure 50: Plot showing measured and calculated values of time delay change versus flow rate. Blue trace: calculated and red trace: measured with offset removed.

3.4 Use of backing plate

The results presented above show that the new mode coupling transducer works well in an ultrasonic flow meter. However, there is one problem in the flow cell arrangement shown in Fig. 39. In many cases of interested the fluid flowing through the pipe would be under high pressure. The pressure inside the pipe will exert a force on the piezoelectric plates. Since our plates are very thin, they may rapture due to this force. One way to overcome this force is to attach a thick backing plate of a suitable material to the crystal. This is shown in Fig. 51. The backing plate will help the crystal to withstand the pressure inside the pipe. However attaching the backing plate could cause a problem. The cross-sectional view of the piezoelectric crystal mounted on the backing plate is shown in Fig. 52. From this figure one can see that it is possible that the plate acoustic wave can radiate its energy into bulk acoustic wave in the backing plate. Fortunately this problem doesn't arise here. The reason for this is as follows. The backing plate is much thicker than the acoustic wavelength, so the acoustic wave that can propagate in the backing plate are bulk longitudinal and shear wave. The plate wave being used in our device is the A_0 plate wave mode. The velocity of the A_0 mode we used in our work is v_p = 2120 m/s. the velocity of bulk acoustic waves in most solids are 3000 m/s or higher. Since v_p is less than this value, the plate wave will not radiate into bulk wave in the backing plate. This fact was experimentally confirmed by attaching backing plates of brass to one of our PAW delay lines. The backing plates were attached both on the top and bottom surfaces of the piezoelectric plate. The presence of the backing plate had virtually no effect on the performance of the delay line. This can be seen from Fig. 53.

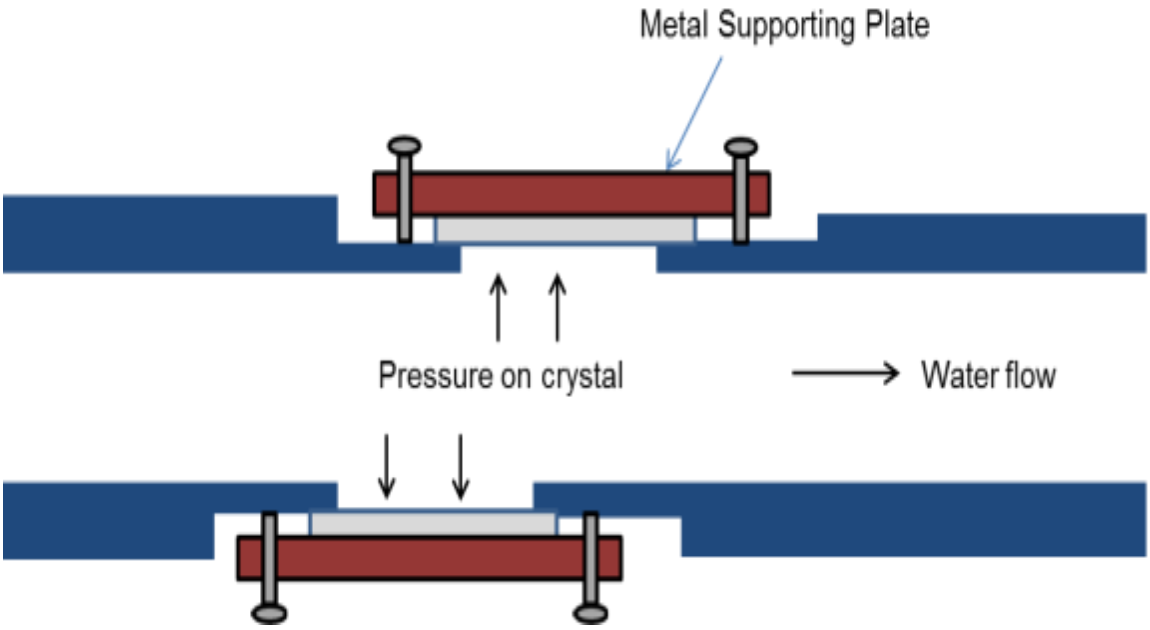

Figure 51: Top view of flow cell with backing plates.

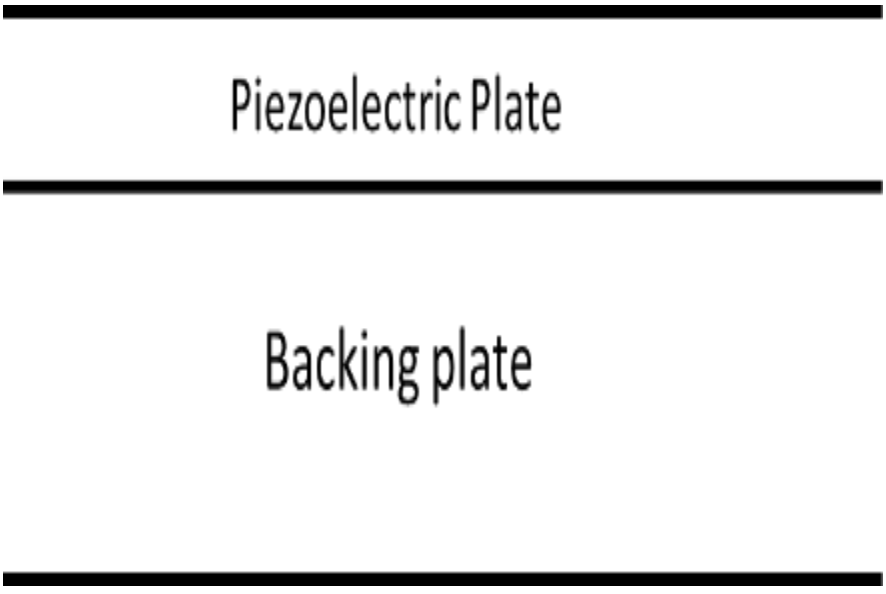

Figure 52: Cross-sectional view of piezoelectric plate mounted on backing plate.

(a)

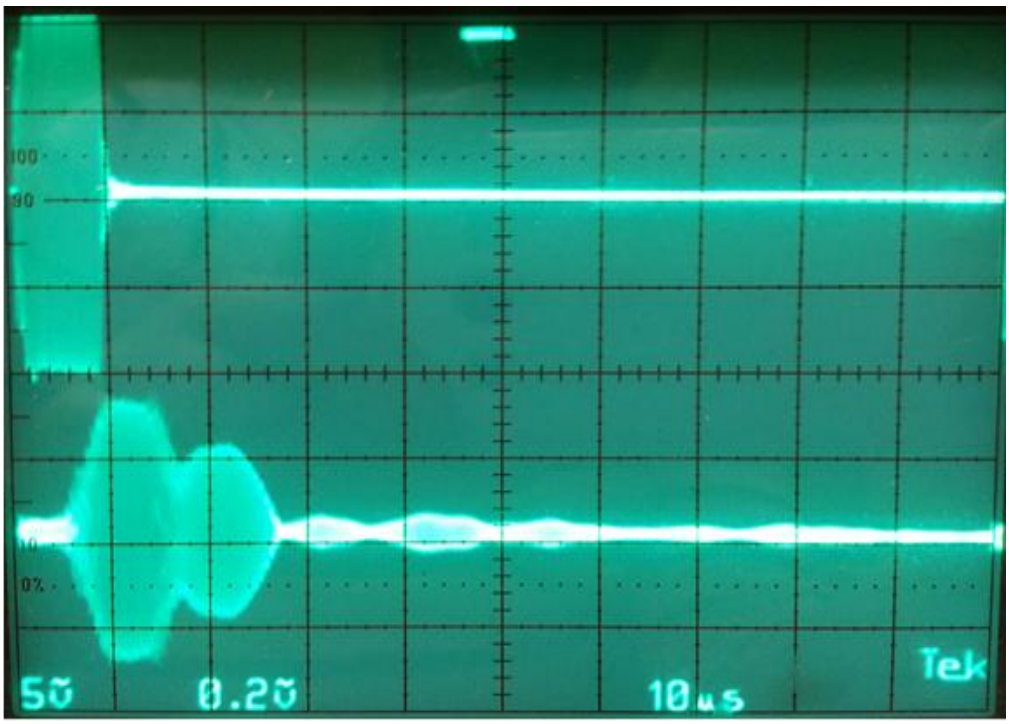

(b)

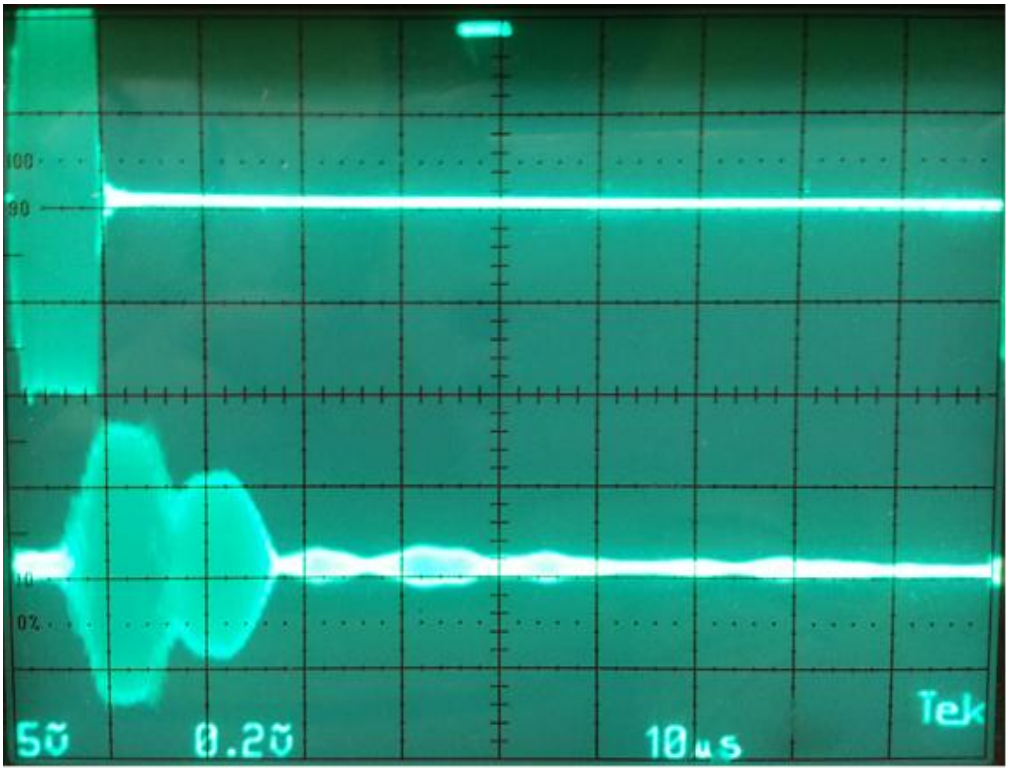

Figure 53: Oscilloscope pictures of output obtained from a PAW delay line. (a) Without backing plate and (b) With backing plate.

This chapter has shown that one can use the mode coupling principle to realize an efficient transducer for use in ultrasonic flow meters. The mode coupling transducer developed here has two main advantages over the bulk wave transducer. First, the new transducer is a thin, flat plate of piezoelectric material which can be mounted flush with the walls of the pipe through which fluid is flowing. Thus the transducer will cause minimal disruption to the fluid flow. The second factor is cost. In the conventional transducer the layers shown in Fig. 31(b), have each got to be made separately by lapping and polishing and then the individual layers have to be acoustically bonded together. Therefore the fabrication tends to be expensive. On the other hand the fabrication of mode coupling transducer involves the simple steps of thin film deposition and lithography. So it can be mass produced at very low cost. It should also be noted here that the transducer based on coupling of energy between SAWs and BAWs have been developed in our laboratory previously [18, 19]. The transducer developed here uses a coupling between PAWs and BAWs. The use of PAWs provides the following advantages. Since the energy of plate acoustic wave is available on both plate surfaces, the IDT can be located in the surface opposite from that which is in contact with the fluid. For the flow cell experiments described in this thesis, the IDTs were located on the surface opposite to the fluid flow. This prevents the IDT electrode from coming in contact with the fluid. It also simplifies the job of making electrical connections to the IDT. The second advantage of using PAW has to do with the choice of piezoelectric substrate material. Using the SAW approach, one is restricted essentially to using only one substrate material, namely, lead zirconate titanate (PZT). Using the SAW approach,

we need a substrate whose SAW velocity will be approximately 2120 m/s. Most of the commonly used SAW materials such as quartz, lithium noibate etc. have SAW velocity 3000 m/s or higher. Lead zirconate titanate (PZT) is the only material whose SAW velocity is close to required value of 2120 m/s. This material has significant acoustic loss and is also difficult to handle. On the other hand, using PAW approach, one can use any of the widely used substrate material such as lithium niobate, lithium tantalate, quartz, etc.

Chapter 4

Summary and Conclusions

The main theme of this thesis is the development of miniature, high efficiency transducers for use in ultrasonic flow meters. The idea for this thesis originated from the theoretical work that was carried out in our laboratory about three years ago. That work had shown that a plate acoustic wave propagating in a piezoelectric substrate can couple its energy efficiently into a bulk acoustic wave propagating in an adjoining fluid medium. This suggested to us that this coupling of energy between plate acoustic waves and bulk acoustic waves can be exploited to realize transducers for use in ultrasonic flow meters. This thesis is a description of how that theoretical concept has been developed into a device useful for practical applications.

The following is a summary of the main topics covered in the individual chapters. Chapter 1 provides brief introduction to the subject of plate acoustic waves and summarizes the prior theoretical work on coupling of energy from plate waves into bulk waves. Chapter 2 describes detailed investigations that have been carried out to study conversion of energy from plate acoustic waves into bulk acoustic waves and back from bulk acoustic waves into plate acoustic waves. The experiments performed in this chapter indeed confirm the theory presented in ref [1], thus verifying that PAW converts into BAW and vice-versa under suitable conditions. The use of this coupling to develop

transducers for use in ultrasonic flow meters is described in chapter 3. Based on the results of the experiments conducted in Chapter 2, a prototype flow meter was designed and tested using suitable transducers. This confirms that the theory of conversion of energy from PAW to BAW and vice versa under suitable conditions can indeed be applied to ultrasonic flow meters. However, it must be noted that this prototype flow meter must be further improved to meet commercial needs. For example, in our experiments testing was done for flow rate range of 0-7.5 LPM. To make this flow meter ready for practical applications, testing should be done for flow rate range 0 – 150 LPM [20]. Powerful pumps can be used to achieve this higher flow range. The support of transducers used in the flow meter need to be improved further such that it can withstand higher pressures up to 200 psi [20]. This is left for future investigation.

It should be pointed out here that while the focus of this thesis has been on ultrasonic flow meters, the research described here has application to several other areas. For example, the mode coupling transducer developed here can be used to efficiently generate ultrasonic waves in fluids. Such transducers are very useful in the field of ultrasonic nondestructive evaluation (NDE). Another possibility is that these transducers may also be useful for generating ultrasonic waves in air. If so, then they will be useful in the field of noncontact or air coupled ultrasonics.

While developing this transducer idea it was realized that our transducer has another attractive property, namely that it can be potentially used to develop flow meters with wireless capability. This is briefly discussed below. The basic principle of a wireless sensor is shown in Fig. 54. A radio frequency interrogating signal is sent from a

transmitter to the sensor. The signal is sent back from the sensor, which is received by the receiver. The received signal contains information about the parameter that is being sensed. The use of SAW devices as passive, wireless sensors is well known since the last 15 – 20 years [21-23]. These devices typically operate in the 300 MHz to 3 GHz frequency range. However, the transducers used in ultrasonic flow meters (and several other acoustic wave sensors) operate in the low MHz frequency range. The SAW methods cannot directly be used with these transducers, but will have to be modified.

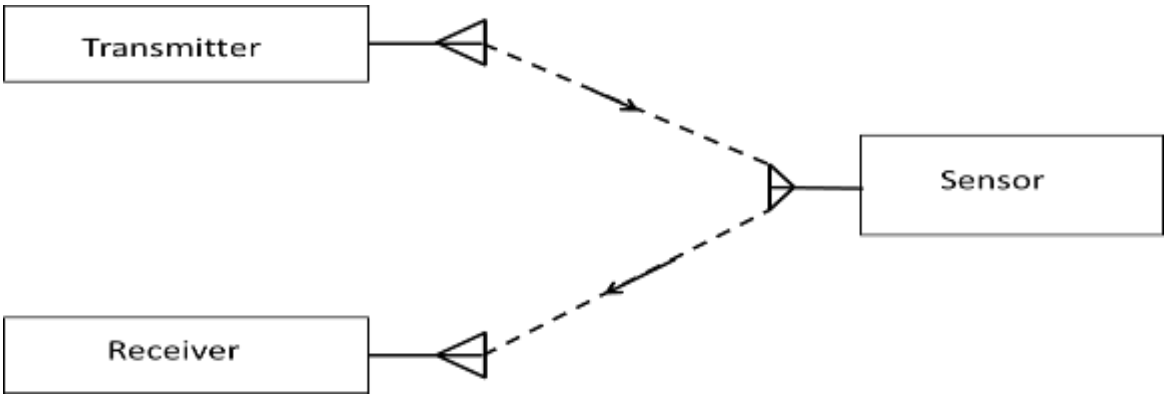

Figure 54: Block diagram showing basic operation of a wireless sensor.

This topic is discussed below. In order to build wireless capability into this flow meter, one should be able to excite transducer T_1 and read the output from transducer T_2 in a wireless fashion, that is, without connecting any wires to the transducers. The techniques used to achieve these objectives can be explained by means of Fig. 55 through 57 shown below. Fig. 55 shows that a low frequency signal that is required to excite transducer T_1, is modulated onto a high frequency carrier wave and then transmitted by the transmitter.

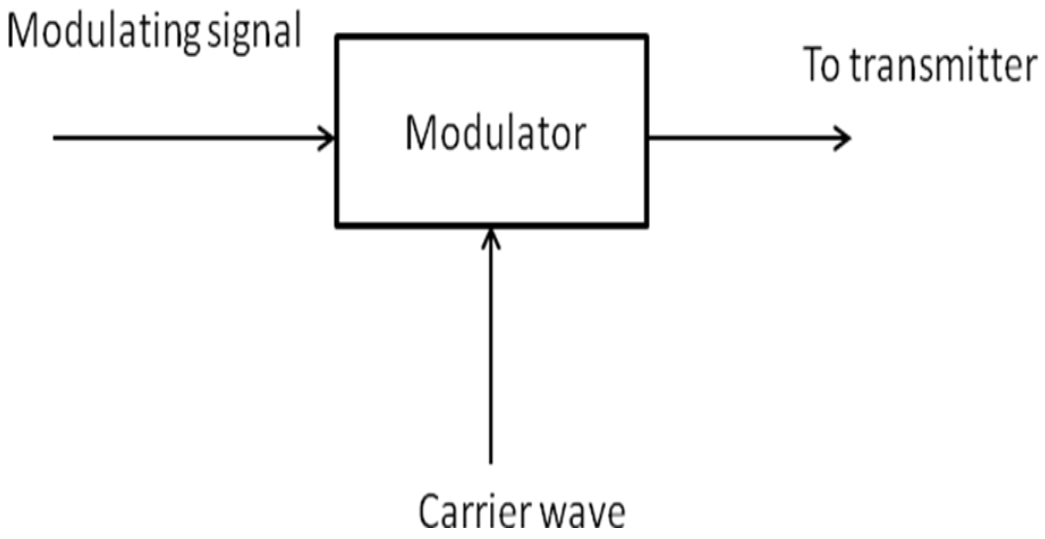

Figure 55: Low frequency signal required to excite transducer T_1 is modulated on to a high frequency carrier wave before transmission to the flow meter.

At the sensor end, this signal is picked up by a suitable antenna; demodulated to recover the original low frequency signal, and the demodulated signal is applied to transducer T_1 (Fig. 56). After a certain time delay this signal will be received at transducer T_2. Now one needs to send this signal back to the receiver. But this cannot be done directly, because this is a low frequency signal. So the idea is to modulate this signal onto the high frequency carrier wave, and then transmit it to the receiver. Using a suitable modulator circuit one can do this. But one needs to have the carrier frequency signal available for this purpose. One possible way is by using a suitable storage device, such as a high quality factor SAW resonator, to store the carrier frequency signal. As shown in Fig. 56, the original transmitted signal is also used to excite a SAW resonator, which will be able to store it for a long time.

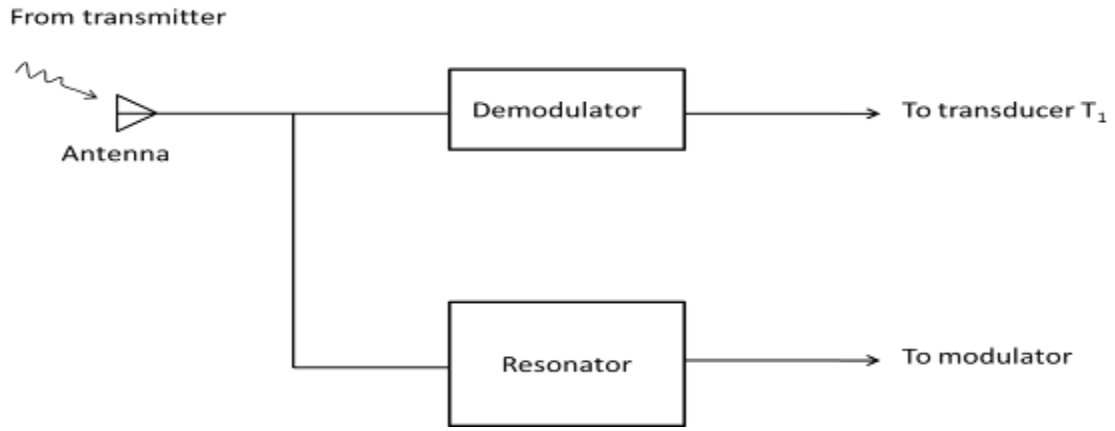

Figure 56: Demodulator extracts the low frequency signal and applies it to transducer T_1. The carrier wave signal is stored in a SAW resonator for later use for modulating the output of transducer T_2.

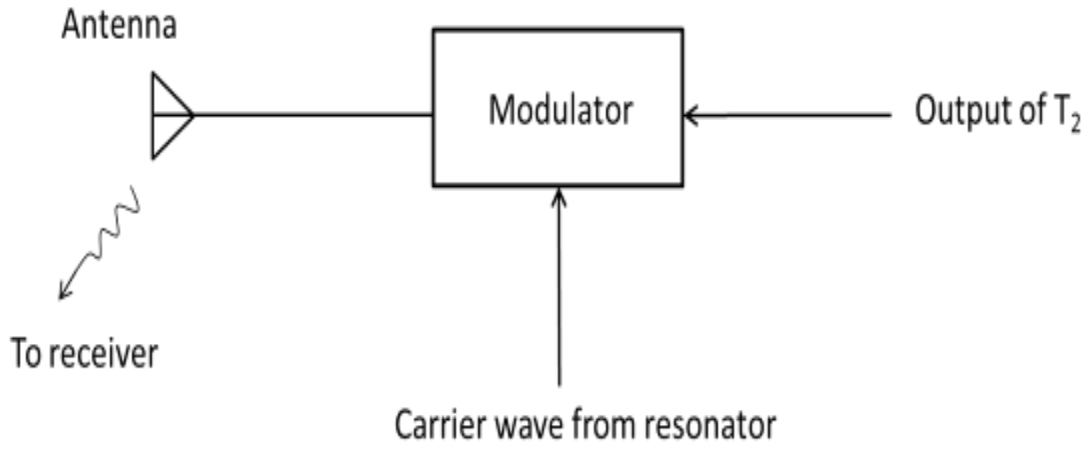

Figure 57: The output of transducer T_2 is modulated on to the high frequency carrier wave and sent back to the receiver.

The signal from the resonator is then taken and used in the modulator (Fig. 57). By using the methods outlined above, we see that transducers T_1 and T_2 work at their normal low frequency, while all the antennas work at the high carrier frequency, so that their size does not become too large. This wireless idea is left for future investigation.

REFERENCES

1. N. G. Suraji, “Propagation of plate acoustic waves in contact with fluid medium”, MS thesis, Marquette University, May 2011.

2. H. Lamb, “On waves in an elastic plate,” Proc. Roy. Soc. London, Series A, vol. 93, pp. 114-128, 1917.

3. I.A. Viktorov, “Rayleigh and lamb waves: physical theory and applications,” Plenum, New York, 1967.

4. S. G. Joshi and Y. Jin, “Propagation of ultrasonic Lamb waves in piezoelectric plates,” J. Appl. Phys., vol. 70, pp. 4113-4120, Oct. 15, 1991.

5. W. R. Smith, H.M. Gerald, J.H. Collins, T.M. Reeder, and H.J.Shaw, “Analysis of interdigital surface wave transducers by use of an equivalent circuit model,” IEEE Trans. Microwave Theory and Tech., Vol. MTT-17, pp.856-864, Nov 1969.

6. C. K. Campbell, “Surface acoustic wave devices for mobile and wireless communications,” Academic Press, New York, 1998.

7. I.E. Kuznetsova, B.D. Zaitsev, S.G. Joshi, and I.A. Borodina, “Investigation of acoustic waves in thin plates of Lithium Niobate and Lithium Tantalate,” IEEE Trans. Ultrasonics, Ferroelectrics, and Freq. Control, vol 48, pp. 322-329, Jan 2001.

8. S.G. Joshi and P. Sudhakar, “Scattering parameters of interdigital surface acoustic wave transducers,” IEEE Trans. Sonics and Ultrasonics, vol. SU-24, pp.201-206, May 1977.

9. L. C. Lynnworth, “Ultrasonic Measurements for Process Control,” Academic Press, New York, 1989.

10. L. C. Lynnworth and Y. Liu, “Ultrasonic flowmeters: half century progress report, 1995 - 2005,” Ultrasonics, vol. 44, pp. e1371-e1378, 2006.

11. http://www.shenitech.com, last accessed April 2013.

12. http://www.sensorland.com, last accessed April 2013.

13. T.G. Beckwith, N. L. Buck, R.D. Marangoni, “Mechanical measurements,” Addison-wesley publishing company, Massachusetts, 1982.

14. http://www.efunda.com/designstandards/sensors/flowmeters/flowmeter_tbn.cfm, last accessed June 2013.

15. http://www.omega.com/ppt/pptsc.asp?ref=hhf42, last accessed June 2013.

16. http://www.omega.com/prodinfo/magmeter.html, last accessed June 2013.

17. M. Saikia and S. G. Joshi, "Miniature, low cost, high efficiency transducers for use in ultrasonic flow meters," in Proceedings of the 2013 International Congress on Ultrasonics (ICU 2013), Singapore, 2013, pp. 390- 395.

18. S. G. Joshi and B. D. Zaitsev, "Low Profile Transducer for Flow Meters", U. S. Patent 6,609,430.

19. S. G. Joshi, B. D. Zaitsev, and I. E. Kuznetsova, "Miniature, high efficiency transducers for use in ultrasonic flow meters," J. Appl. Phys., vol. 105, 034501, 2009.

20. http://www.badgermeter.com/Water-Utility/Meters/E-Series-Ultrasonic-Meters.htm, last accessed July 2013.

21. L. Reindl, G. Scholl, T. Ostertag, H. Scherr, U. Wolff, and F. Schmidt, "Theory and application of passive SAW radio transponders as sensors," IEEE Trans. Ultrason., Ferroelec., Freq. Control, vol. 45, pp. 1281 – 1292, Sept. 1998.

22. A. Saitoh and T. Nomura, "Wireless sensor system using surface acoustic wave devices," ICROS-SICE International Joint Conference, pp. 2359-2363, Aug. 2009.

23. F. Li, D. Xiang, S Chiang, B.R. Tittmann and C. Searfass, "Wireless surface acoustic wave radio frequency identification (SAW-RFID) sensor system for temperature and strain measurements," Proc. IEEE Ultrason., symp, pp. 822-825, 2011.